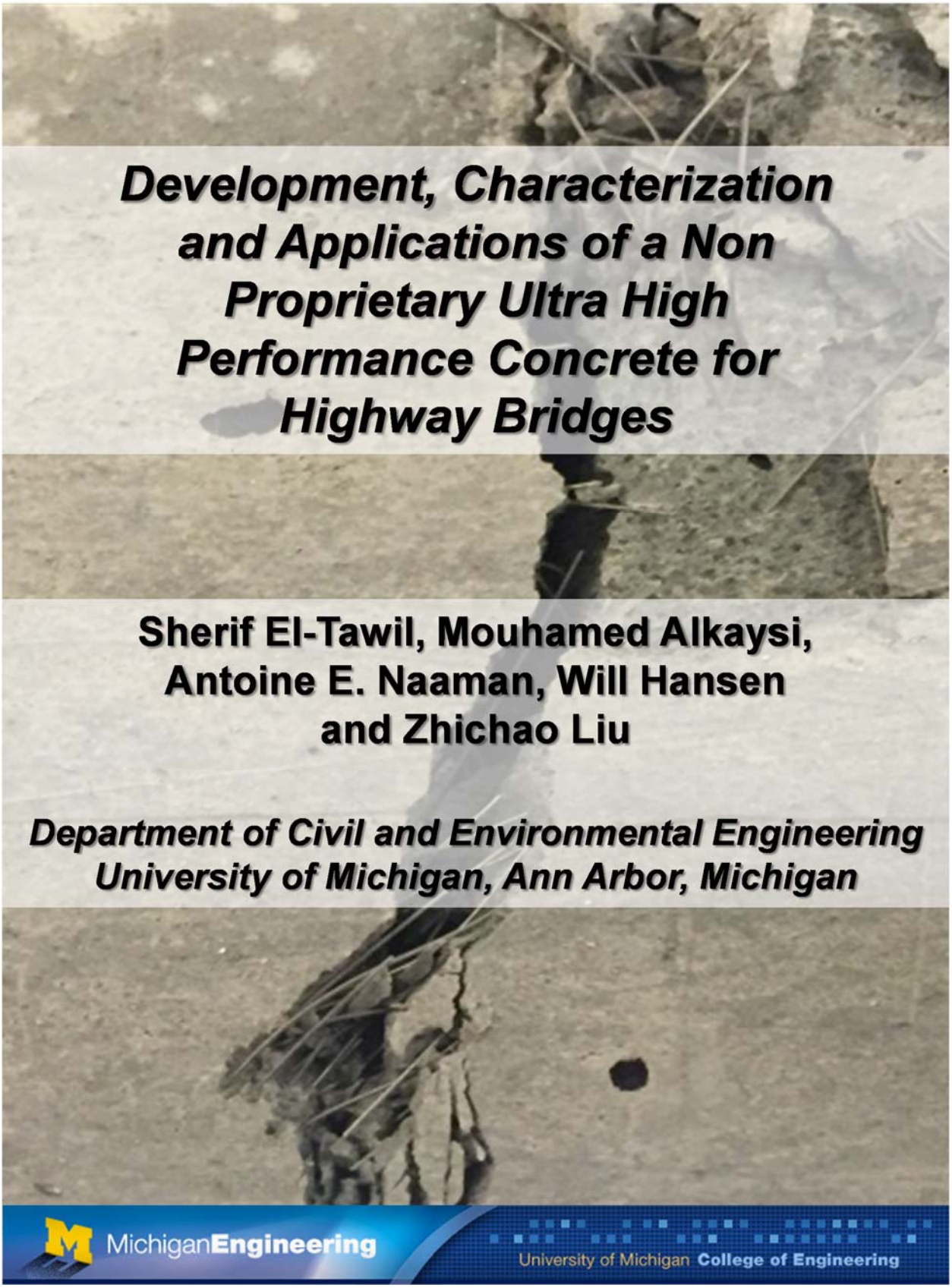

Development, Characterization and Applications of a Non Proprietary Ultra High Performance Concrete for Highway Bridges

Sherif El-Tawil, Mouhamed Alkaysi, Antoine E. Naaman, Will Hansen and Zhichao Liu

Department of Civil and Environmental Engineering
University of Michigan, Ann Arbor, Michigan

MichiganEngineering
University of Michigan College of Engineering

Intentionally left blank

1. Report No. RC-1637	**2. Government Accession No.** N/A	**3. MDOT Project Manager** Steve Kahl
4. Title and Subtitle Development, Characterization and Applications of a Non Proprietary Ultra High Performance Concrete for Highway Bridges		**5. Report Date** 03/14/2016 **6. Performing Organization Code** N/A
7. Author(s) Sherif El-Tawil, Mouhamed Alkaysi, Antoine E. Naaman, Will Hansen and Zhichao Liu		**8. Performing Org. Report No.** N/A
9. Performing Organization Name and Address University of Michigan Room 1038 Wolverine Tower 3003 South State Street Ann Arbor, MI 48109		**10. Work Unit No. (TRAIS)** N/A **11. Contract No.** 2013-0068 **11(a). Authorization No.** Z1
12. Sponsoring Agency Name and Address Michigan Department of Transportation Research Administration 8885 Ricks Rd. P.O. Box 30049 Lansing MI 48909		**13. Type of Report & Period Covered** Final Report 3/30/2013 – 3/14/2016 **14. Sponsoring Agency Code** N/A
15. Supplementary Notes N/A		

16. Abstract

Ultra-high performance concrete (UHPC) is a new class of cementitious materials that have exceptional mechanical and durability characteristics. UHPC is commercially available. However, its cost for construction of highway structures is prohibitive. Based on an extensive testing program, a new family of non-proprietary UHPC materials with excellent characteristics in compression and tension, as well as exceptional resistance to freeze-thaw and chloride ion penetration were developed. The most cost effective of these deviates from traditional UHPC mixtures in that it uses a 50:50 mix of Portland Type I and Ground Granulated Blast-Furnace Slag (GGBS) as a binder, lacks any silica powder (inert filler) and requires no post-placement treatment. The use of GGBS improves the material's 'greenness' making it a more sustainable cementitious product. Specifications for making the new UHPC were proposed. The developed UHPC blend was then used to conduct a comprehensive study on bond between UHPC and deformed steel bars to facilitate and enable future structural applications. Bond pull out tests showed the developed UHPC requires significantly reduced development lengths in order to attain steel bar yield compared to traditional concrete. Models to characterize the bond strength were proposed and a UHPC joint consisting of two pre-cast bridge deck elements was developed and tested at full scale. It was shown that a 6'' (150 mm) joint made of the developed UHPC was sufficient to successfully transfer loading between the decks.

17. Key Words Ultra-high performance concrete, non-proprietary, durability, strength, bond, joints, precast concrete, bridge, freeze-thaw	**18. Distribution Statement** No restrictions. This document is available to the public through the Michigan Department of Transportation.

19. Security Classification - report Unclassified	**20. Security Classification - page** Unclassified	**21. No. of Pages**	**22. Price** N/A

Intentionally left blank

DISCLAIMER

This publication is disseminated in the interest of information exchange. The Michigan Department of Transportation (hereinafter referred to as MDOT) expressly disclaims any liability, of any kind, or for any reason, that might otherwise arise out of any use of this publication or the information or data provided in the publication. MDOT further disclaims any responsibility for typographical errors or accuracy of the information provided or contained within this information. MDOT makes no warranties or representations whatsoever regarding the quality, content, completeness, suitability, adequacy, sequence, accuracy or timeliness of the information and data provided, or that the contents represent standards, specifications, or regulations.

Intentionally left blank

ACKNOWLEDGEMENT

This project was funded by the Michigan Department of Transportation. The authors would like to acknowledge the support and efforts of Mr. Steve Kahl and Mr. David Juntunen for initiating and directing this research. The authors also wish to acknowledge the continuing assistance of the Research Advisory Panel (RAP) members in contributing to the advancement of this study. The authors acknowledge the help and ideas of Prof. Kay Wille of the University of Connecticut, Storrs, who served as a consultant on this project. Parts of this work were conducted by the second author in fulfillment of his PhD dissertation requirements at the University of Michigan.

Intentionally left blank

Table of Contents

List of Figures

Intentionally left blank

List of Tables

Intentionally left blank

EXECUTIVE SUMMARY

Introduction:

Ultra-high performance concrete (UHPC) is a cementitious material that achieves a compressive strength of at least 22 ksi (150 MPa) and has self-consolidation properties. It is comprised of component materials with particle sizes and distributions carefully selected to maximize packing density. The high packing density, which means that constituent particles are arranged as compactly as possible, is the reason for the extremely high mechanical and durability properties of the material.

UHPC is commercially available at the present time. However, its cost for construction of highway structures is prohibitive. A non-proprietary version of UHPC was recently developed at the University of Michigan (UM). While significantly cheaper than the cost of commercial products, the cost of the UM version is still relatively high and can be substantially reduced through optimization of its constituent components while still maintaining the extraordinary properties that make UHPC such an exceptional building material.

Objectives:

The primary objective of this project is to develop a cost-optimized version of non-proprietary UHPC and characterize its mechanical and durability properties. Another key objective is to investigate the possibility of using UHPC for field-cast joints that commonly occur in precast construction. Specific objectives include:

- Identify a low cost, non-proprietary UHPC mix design through cost-optimization of the constituent components while still maintaining the exceptional properties of UHPC.

- Characterize the strength and durability properties of the optimized mixture, focusing specifically on tensile and compressive strengths, freeze-thaw resistance and rapid chloride penetration resistance.
- Quantify the bond between UHPC and deformed steel bar reinforcement for a range of parameters and loading scenarios associated with feasible bridge applications.
- Investigate the use of UHPC bridge field joints between precast regular concrete decks.

Summary of Research:

Some of the component materials of UHPC are substantially more expensive than those used in regular concrete. To optimize cost, research was conducted to investigate the relationship between material performance and the type or amount of the most expensive components, i.e. cement, silica fume and silica powder. Short-term material performance was assessed via tensile and compressive tests and durability properties were evaluated based on freeze-thaw and chloride ion penetration testing as well as quantification of the presence and distribution of air voids. The test results were used to optimize cost versus performance characteristics of the UHPC blends considered. At the structural level, a comprehensive study investigating the bonding between UHPC and deformed bars was carried to investigate the effect on bond of bar size, type, embedded length, fiber content, fiber orientation and curing age. Using this data, new joints making use of UHPCs superior bond characteristics were constructed and tested in order to prove a quick and simple method for the assembly of precast bridge elements.

Summary of Results:

From the material testing program, a low cost UHPC material with excellent characteristics in compression and tension, as well as exceptional resistance to freeze-thaw and chloride ion

penetration was developed. The proposed mix deviates from traditional UHPC mixtures in that it uses a 50:50 mix of Portland Type I and Ground Granulated Blast Furnace Slag (GGBS) as a binder, lacks any Silica Powder (inert filler) and requires no post-placing treatment. The cost of the cementitious material ingredients was reduced by half compared to available non-proprietary UHPCs available at the onset of this research. The use of GGBS improves the material's 'greenness' making it a more sustainable cementitious product. Specifications for making the new UHPC were proposed.

The developed UHPC blend was then used to conduct a comprehensive study on bond between UHPC and deformed steel bars to facilitate and enable future structural applications. Bond pull out tests showed the developed UHPC requires significantly reduced development lengths in order to attain steel bar yield compared to traditional concrete. Models to characterize the bond strength were proposed and a UHPC joint consisting of two pre-cast bridge deck elements was developed and tested. It was shown that a 150 mm (6 inch) joint was sufficient to successfully transfer loading between the decks.

The Promise of UHPC - An Opportunity for the State of Michigan:

UHPC derives its unique properties from its high packing density and the presence of steel fibers. The special constituents of UHPC make it more expensive than regular concrete. However, they also give it its exceptional short- and long-term properties. In particular, the extremely high freeze-thaw resistance, negligible chloride penetration, and ability to mobilize the material's strain hardening response in tension to limit crack width, suggests that UHPC structures can be extremely long-living and low maintenance at the same time. Such structures will have inherently low life cycle costs, in spite of relatively higher initial costs.

UHPC is currently in its infancy and this project is an important early step. Additional research on fiber optimization, mixing technology and structural testing is needed to fully realize the material's promise. These research topics represent an opportunity for the State of Michigan to take leadership in steel fiber production, a key component of UHPC. The State, with its focus on vehicle manufacturing, is well suited to be major fiber industry hub given that steel fibers are made from chopped high strength wires that are used in steel-belted tire products.

1. INTRODUCTION

1.1. Ultra-High Performance Concrete (UHPC)

Ultra-high performance concrete is a new class of cementitious materials that achieve a compressive strength of at least 22 ksi (150 MPa) (Wille et al. 2014, Graybeal 2014, Wille et al. 2012, Wille et al. 2011). When properly reinforced with steel fibers, UHPCs can achieve strain hardening behavior and display compressive and direct tensile strengths as high as 35 ksi (242 MPa) and 2 ksi (14 MPa), respectively (Graybeal, 2003). Changes in the type and quantity of steel fibers directly affect the ductility, durability and strength of the material (Wille et al. 2011; Kim et al. 2011, 2010a, 2010b, 2010c, 2008a, 2008b, 2008c, 2008d, 2007). UHPC also exhibits exceptional energy absorption prior to crack localization (Pyo et al. 2015a, 2015b, 2013a, 2013b, 2013c) and self-consolidation properties (Graybeal, 2006).

Recent developments in UHPC at the University of Michigan have led to new, non-proprietary formulations that are cheaper than the patented versions (Wille et al, 2011). The new formulation described in Wille et al. (2011) is made up of components readily available on the US open market, does not require any special mixing or placing equipment and has a higher ductility than other commercially available products (Rigaud et al., 2012). Relative to traditional concretes, the price of the non-proprietary UHPC in Wille et al. (2011) remains high, but still it is substantially less than its patented commercial equivalent.

1.2. Research Objectives

With strengths in compression approaching that of mild steel, finding new uses for UHPCs is intriguing many practitioners, who want to use the material in their projects. However, broad usage

is hindered by the high cost of the material and lack of test results, and understanding in general, of UHPCs behavior at the structural level. With these issues in mind, the objectives of this research project are:

- Survey and identify potential applications for non-proprietary UHPC particularly for Accelerated Bridge Construction (ABC) and Precast Bridge Element Systems (PBES).
- Investigate whether a family of new UHPC materials can be made using locally available components and optimize the cost by tailoring of the mix, while still maintaining ultrahigh performance characteristics.
- Characterize the properties of the new family of UHPCs, focusing on tensile strength, compressive strength, modulus of elasticity, and durability by laboratory testing.
- Conduct pullout tests of steel reinforcing bars from UHPC to investigate the bond strength between steel bars with various coatings and the surrounding UHPC matrix.
- Investigate using computational and experimental methods to simulate the behavior of UHPC field joints (closure pours).
- Develop detailed guidance (special provisions) for making the proposed UPHC on a construction site.
- Assess the life cycle performance of UHPC in light of the experimental results.
- Propose future research efforts using the developed UHPC.

1.3. Organization of the Report

The main body of the report is preceded by detailed contents including lists of figures and tables. This is followed by an introduction giving briefly the scope and objectives of the study and importance of the topic.

- Chapter 2 outlines the previous works involving UHPC that are of interest to the topics covered in this report.
- Chapter 3 covers an investigation into how material properties change as a result of variations in the amount and/or type of individual components. The chapter aims to optimize the cost of UHPC with respect to its strength.
- Chapter 4 investigates the durability of select UHPC mixes identified in chapter 3 through freeze-thaw testing, rapid chloride penetration testing and air void characterization.
- Chapter 5 gives an in depth study into the factors affecting bond between UHPC and reinforcing steel.
- Chapter 6 studies the use of UHPC in precast bridge construction via experimental testing and finite element analysis.
- Chapter 7 provides a summary of the research, the most important conclusions and future work.

All chapters are preceded by a brief synopsis of the chapter. References which have been used for certain inputs are listed at the very end of the report.

Intentionally left blank

2. BACKGROUND AND LITERATURE REVIEW

2.1. Strength of UHPCs

2.1.1. Compressive and Tensile Behavior of UHPC

The high compressive strength of UHPC is well known and established (Graybeal, 2014). Larrard and Sedran (1994) produced a concrete mortar with a compressive strength of 35 ksi (236 MPa). Wille, Naaman and El-Tawil (2011) were able to prepare UHPCs with 28-day compressive strengths in excess of 30 ksi (200 MPa) without requiring the use of expensive post treatment techniques. Graybeal (2006) has shown that UHPC reaches a peak stress of around 22 ksi at 0.003 strains (0.3%). Wille and Namaan (2011) showed that when reinforced with steel fibers, UHPC mixes were able to achieve 0.6% strain capacity in tension prior to strain softening. More information regarding the tensile and compressive behavior of UHPCs can be found in the works by Wille (2011) and Graybeal (2003, 2006, and 2014).

UHPC not only has a higher tensile strength than conventional concrete, it can also exhibit strain hardening response after initial cracking when properly reinforced with steel fibers. The typical stress strain curve for ultra-high performance concrete is shown in Figure 2-1. Following the definitions set forth by Naaman (Naaman & Reinhardt, 2007), the first part of the material's tensile behavior is elastic, which continues up until the specimen develops an initial crack at what is known as the first cracking strength point (σ_{cc}, ε_{cc}) in Figure 2-1. Following this, the material then exhibits strain hardening up until its peak point (σ_{pc}, ε_{pc}). The strain hardening behavior of segment II is typically characterized by multiple crack development in the gauge length of the specimen. Following the strain-hardening region, the material then begins to exhibit crack localization (segment III). This segment of the curve is best represented by a stress versus crack opening

response but many researchers continue to describe the region as a stress versus strain relationship, based on the nominal gage length of the specimen, as is done herein.

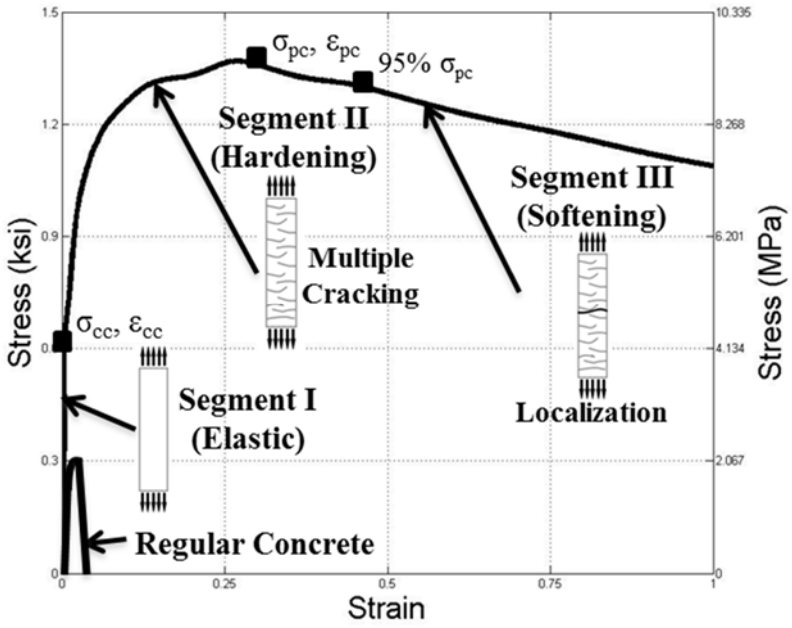

Figure 2-1 Typical Tensile Strain Response in UHPC

2.1.2. Effect of Silica Fume

Most UHPCs contain silica fume and silica powder. Silica fume is a reactive powder with pozzolonic properties. Silica powder is an inert powder, used primarily to increase the density of the cementitious matrix. Several research studies have investigated the effects of silica fume (SF) on the behavior of UHPCs. Rong, Xiao and Wang (2014) investigated the effects of SF on the hydration and microstructure of UHPCs, concluding that SF dominated the hydration process at lower water-binder ratios. Rong et al. (2015) also partially replaced cement with SF in UHPCs and determined the flexural and compressive strengths were highest when the content of SF was approximately 3% to binder, and decreased at higher contents due to the agglomeration of SF particles. Brouwers et al. (2014) similarly investigated the effect of SF on the UHPC hydration

process and material behavior, concluding that an optimal ratio of 3.74% SF to binder yields the highest mechanical properties of UHPC. Oertel et al. (2013) reported that the nearer the dispersion of silica particle sizes match to those in the primary mixture particle sizes, the further the compressive strengths increase in UHPCs. Wille (2015) studied the effects of various SFs on the compressive behavior in UHPCs, and reported compressive strengths ranging from 20 ksi to 26 ksi. To the authors' knowledge, no work has been done on the effect of silica fume on the direct tensile properties of UHPCs.

2.1.3. Effect of Silica Powder

To date, little work has been done to investigate the effects of Silica Powder (SP) on the tensile and compressive performance of UHPCs. Wille (2011) researched the effects of SP on UHPCs ranging from 0 SP-binder to 0.5 SP-binder ratios, finding a ratio of 0.3 SP to cement yielded the highest compressive strength. As with silica fume, to the knowledge of the authors, no work has been done evaluating the effect of different silica powder quantities in UHPCs under direct tension.

2.1.4. Effect of Cement

Additionally, little work has been done to investigate the effects of various cements on the material behavior of UHPC. Yu and Brouwers (2015) used fly ash (FA), ground granulated blast-furnace slag (GGBS) and limestone powder (LP) to replace cement in UHPC mixes, determining UHPCs with the GGBS has higher mechanical properties at 28 and 91 days than with other cements they considered. Wille (2015) investigated the compressive strengths for UHPCs substituting several different cements, yielding strengths between 19 ksi (130 MPa) and 32 ksi (221 MPa). To date, no work quantifies the effects of cement type on the tensile response of UHPCs.

2.1.5. Effect of Fiber Type and Quantity

Several papers currently discuss the effects of fiber content, shape, size and topology on ultra-high performance concretes. The addition of steel fibers into the ultra-high performance concrete matrix leads to enhanced material performance such as a high tensile capacity, ductility, reduced crack spacing, and high energy dissipation capability. The magnitude of these effects is a direct result of the fiber material strength, cementitious matrix – fiber bond ability, fiber aspect ratio (length: diameter), fiber volume content and fiber surface topology. Pyo (2015) investigated the strain rate dependent tensile properties of UHPCs with different fibers and fiber volume contents. Wille (2011) investigated the tensile performance of UHPCs with fiber contents as low as 1%. Yu and Brouwers (2015) investigated hybrid fiber UHPCs containing a combination of hooked, short and long straight fibers, at 2% volume contents. They concluded that the combination of several fiber types yields ultra-high performance while using fewer fibers. To date, no work has been done investigating the effect of low fiber contents (<1%) on the compressive and tensile performance of UHPC.

2.2. DURABILITY OF UHPCs

2.2.1. Freeze-Thaw Resistance

Tests investigating UHPCs resistance to freeze-thaw have been limited. Ahlborn et al. performed freeze-thaw cycling tests in accordance to ASTM C 666 (2008), procedure B, showing that after 32 freeze-thaw cycles, ultra-high performance concrete specimens showed no degradation. Acker and Behloul (2004) similarly reported that after 300 freeze-thaw cycles, UHPC showed no degradation. Pierard et al. (2012) reported that specimens achieving strength between 20.3 ksi (140 MPa) and 23.2 ksi (160 MPa) also showed no degradation after 112 cycles. Graybeal (2006)

performed air void analyses on Ductal©, finding UHPC void numbers to be between 0.2 and 7.5 voids/in (0.008 and 0.30 voids/mm), corresponding to an air content of 5.7% to 7.3% with no vibration.

To date, no research has been done to investigate the durability parameters for a non-proprietary blend of UHPC. Further, no testing has been done to investigate the effects of various material parameters on the durability of UHPC. Yazici (2008) looked into the effect of silica fume and high-volume Class C fly ash on the durability of self-compacting concretes, determining that a 10% by volume inclusion of silica fume resulted in enhanced freeze-thaw resistance, accompanied by increased compressive strengths. Work by Alexander and Magee (1999) evaluated the durability of concretes containing condensed silica fumes and ground granulated blast furnace slag (GGBS), determining blends containing these materials outperformed regular concretes in durability testing of water absorption.

2.2.2. Chloride Ion Penetration Resistance:

Performing rapid chloride permeability tests, Ahlborn (2008) showed that UHPC was capable of achieving permeability values less than 100 coulombs for both air-cured and steam-cured specimens. Materials with coulomb values less than 100 are generally considered to have negligible chloride ion penetration. Testing two different types of reactive powder concretes, Bonneau (1997) showed that specimens were able to achieve 6 to 9 coulombs. Graybeal (2006) reported that untreated specimens achieved coulomb values of 360 and 76 at 28 days and 56 days respectively. Most of the existing chloride permeability studies pertain to proprietary materials and data for non-proprietary blends is lacking at present.

2.3. Bond Development in UHPCs

2.3.1. Bond Development of Steel Bars Embedded in UHPC

There is limited published data on the bonding behavior between UHPCs and steel reinforcement bars. Graybeal (2010, 2014) performed pull out tests for #4, #5, and #6 bars embedded 3, 4 and 5 inches (75, 100 and 125 mm) respectively into UHPC cylinders, with all of the steel bars fracturing before bond failure. Graybeal (2014) recently has shown that under static conditions, UHPC specimens are capable of developing a bond stresses of approximately 2.9 - 5 ksi (20 – 35 MPa) in bar pull out specimens and are largely dependent on bar spacing, concrete cover, and development length and bar size. In a different study, Swenty and Graybeal (2012) performed pull out tests on #4 bars embedded into 6 in (150 mm) concrete cubes. Two different UHPC mixes were used, one achieving bar fracture and the other achieving bar yield. Performing pull out tests on 12 mm diameter bars, varying concrete cover and embedment lengths, Fehling et al. (2012) determined that increasing cover widths and embedment lengths increased the bond stress, reaching those sufficient for bar yield. Holschemacher et al. (2004) reported achieving bond stresses up to 8.7 ksi (60 MPa) using 12 mm bars in UHPC cylinders. Saleem et al. (2013) investigated the development length requirements for high strength steel bars in UHPC, concluding that 10 mm and 22 mm (#3 and #7 U.S. sizes) bars require 12 d_b and 18 d_b to develop adequately. Jungworth et al. (2004) performed tests on 20 mm and 12 mm diameter bars, reaching bond stresses of 5.5 ksi (38 MPa) and 9.5 ksi (66 MPa). Of the literature currently available on bond, data only exists on testing performed using Ductal® or Ceracem®, both proprietary concretes No published data currently exists for non-proprietary UHPCs. As discussed later on, there is much discrepancy in existing data regarding the maximum achieved bond stress during the pull out tests, with some

studies reporting values as high as 9.5 ksi (66 MPa), or as a low as 1.4 ksi (9.8 MPa) (Graybeal, 2010).

2.3.2. Lap Splice & Component Tests with UHPC

Component level testing with UHPC remains largely confined to highway infrastructure projects. The Federal Highway Administration has released several reports on test installations on existing structures. UHPC was used in concrete waffle slab decks in an accelerated bridge construction in Wapello County, Iowa showing that UHPC is a viable material for infrastructure redesign (Wipf et al, 2011). New York D.O.T. also tested a live installation of a UHPC joint using hooked bars and a small joint width, also concluding exceptional joint performance for the UHPC (FHWA, 2014).

Steinberg et. al. (2010) investigated the structural reliability of pre-stressed UHPC flexure models for bridge girders showing that acceptable levels of reliability can be obtained using typical AASHTO procedures. Graybeal (2014) released a series of tests evaluating the joint force transfer capacity of UHPC under various parameters, including type of bars, size of bars etc. He concluded that UHPC was able to act as a closure pour joint between two precast decks more efficiently than traditional grouts and concretes at splice lengths as little as 6 inches (150 mm). Of these tests performed so far, all of them have made use of Ductal.

Few studies have investigated the splice length requirements for UHPC joints. Graybeal recently investigated the splice length of pre-stressing strands in field cast UHPC connections, concluding that 12 mm and 15 mm diameter strands require 20 inches (510 mm) and 24 inches (610 mm) to fully develop (Graybeal, 2015). Hoonhee and Park (2014) investigated the lower limits of contact splice lengths in precast, steam-cured UHPC beams under flexure, determining a lap splice length

greater than 6 in. (150 mm) was required to cause yield in the bars. Both of these studies were performed using Ductal, i.e. no studies currently exist for non-proprietary UHPCs, as provided herein. Furthermore, to the author's knowledge no studies exist investigating the UHPC's performance in non-contact lap splices between two precast beam elements, as done herein.

3. MATERIAL PERFORMANCE AND CHARACTERIZATION

3.1. OVERVIEW

This chapter investigates the performance of several new UHPC mix designs with a focus on minimizing cost. Performance parameters include compressive strength and full tensile stress-strain characterization. The experimental variables are four different quantities of silica fume, three different quantities of silica powder, three different cement types (white cement Type I, Portland cement Type V, GGBS/Portland cement Type I blend) and three different fiber volume contents (0.5%, 1.0%, and 1.5%) of straight, smooth, high strength steel fibers. Experimental results showed minor differences in mechanical behavior due to variations in the quantity of silica fume. Silica powder changes led to little difference in material behavior, suggesting that silica powder can be removed due to its high cost. UHPCs containing white cement Type I exhibited the best performance in almost all aspects of behavior including load carrying capacity, energy absorption capacity and multiple cracking behaviors, but carried the highest cost. Specimens containing the GGBS/Portland cement Type I binder showed lower performance, but at decreased cost. UHPC specimens containing 0.5% fibers exhibited some strain hardening behavior, which became more pronounced as the fiber volume fraction increased. The results suggest that fiber volume contents of 1.0% or 1.5% could significantly reduce the chance for crack localization under dead load or working conditions, respectively, in structural applications.

3.2. EXPERIMENTAL PARAMETERS AND PROCEDURE

3.2.1. UHPC Material Properties and Cost

UHPC, depending on the types and quantity of reinforcing fibers added to the cementitious mixture, carries a high cost. Currently, commercially available proprietary blends cost \$2,000/yd^3 (\$2615/m^3) and includes 2% steel fibers by volume (Ahlborn, 2008). This is 15 - 20 times higher than the cost of conventional concrete. Using current prices, the UHPC recently developed at the University of Michigan (Wille, 2011) carries a lower cost of materials (\$516/yd^3 without fibers, \$1,029/yd^3 with 2% fibers).

The cement used in the initial development of the UHPC in Wille et al. (2011) was a Portland Type I white cement. This cement has a high C_3S content (74%), and a moderate fineness (3930 cm^2/g Blaine Value) as well as a low C_3A content (less than 5%). The particle sizes and costs for each UHPC constituent is listed in Figure 3-1 shows the grain size distributions for the two types of sands, F12 and F100 used in this research. The materials are obtained from reputable suppliers and the costs specified are valid for 2013 when the bulk of the research was conducted.

In Wille et al. (2011), the optimal cement to silica fume to silica powder ratio was determined to be 1 C: 0.25 SF: 0.25 SP, with a w/c ratio of 0.22 and a compressive strength of 27.8 ksi (192 MPa). Maintaining the w/c ratio established in the previous work, Table 3-2 lists the mix proportions and associated costs (without fibers) for all of the mixes considered in this work. Cost is listed as a cost index in order to simplify the discussion later on. The cost index is simply the ratio of the mix's cost compared to the starting mixture published in Wille (2011), based on current prices in the US. The index is a relative indicator of cost, since actual costs will vary in time and by location. The first entry, W-25-25, represents the original mix ratio in (Wille, 2011).

`	Median	10% of Particles	90% of Particles
Cement	10 – 20 μm	3 μm	40 μm
Silica Fume	0.1 – 1 μm	0.1 μm	10 μm
Silica Powder	10 – 20 μm	1 μm	40 μm
F12 Sand	500 μm	Larger than 300 μm	Smaller than 1000 μm
F100 Sand	100 μm	Larger than 50 μm	Smaller than 300 μm
Silica Fume		Silica Powder	
SiO_2	Minimum 85%	SiO_2	Maximum 90%
H_2O	Maximum 3%	H_2O	Maximum 1%
Pozzolonic Activity	Minimum 105%	Pozzolonic Activity	N/A

Table 3-1: Chemical and Physical Properties of Materials

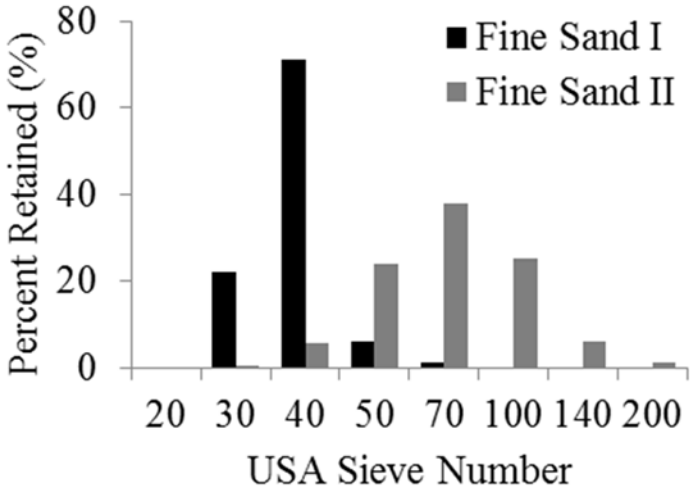

Figure 3-1 Grain Size Analysis for Sand

Cement quantity was held constant at 1306 lbs/yd^3 throughout all mixes. Additionally, the admixture Advacast 575 high range water reducer was again used at a ratio of 1.35% to cement for all mixes. All mixes use the same, low w/c ratio of 0.22. Cement, silica powder, and silica fume

carried the highest costs per cubic meter. In order to lower this cost, 2 additional types of cement were identified for their reduced cost, Portland Type V and a Ground Granulated Blast Furnace Slag (GGBS) / Portland I cement blend. Table 3-3 lists the properties for the three cements used in this study. The Type I / GGBS cement blend was identified as a candidate for its exceptional long-term performance (Cheng et al., 2005).

Name	White Cement Type I	Silica Fume	Silica Powder	Cost ($/yd^3)	Cost Index*
W-25-25	1.00	0.25	0.25	513	1.0
W-30-20	1.00	0.30	0.20	502	0.98
W-35-15	1.00	0.35	0.15	492	0.96
W-25-20	1.00	0.25	0.20	487	0.95
W-25-15	1.00	0.25	0.15	461	0.90
W-25-00	1.00	0.25	0.00	369	0.72
	Portland Type V				
PV-25-15	1.00	0.25	0.15	364	0.71
PV-25-10	1.00	0.25	0.10	338	0.66
PV-25-05	1.00	0.25	0.05	307	0.60
PV-30-05	1.00	0.30	0.05	338	0.66
PV-35-05	1.00	0.35	0.05	348	0.68
PV-25-00	1.00	0.25	0.00	282	0.55
PV-25-25	1.00	0.25	0.25	420	0.82
	Portland Type I / GGBS Cement				
GG-25-00	1.00	0.25	0.00	266	0.52
GG-25-15	1.00	0.25	0.15	353	0.69
GG-25-25	1.00	0.25	0.25	405	0.79

*Matrix only, without fibers.

Table 3-2: Mixture Proportions by Weight with Cost Index

Type	C_2S %	C_3S %	C_2S + C_3S %	C_3A %	C_4AF %	Blaine m^2/kg
White Cement Portland Type I	13	74	87	5	1	395
Portland Type V Cement	17	59	76	4	15	430
Type I / Slag Cement Blend	13	58	71	8	10	600

Table 3-3: Cement Properties

The cost for silica powder and silica fume was reduced through reductions in material quantities. Ratios for SF ranged from 0.25 SF: C to 0.35 SF: C. Ratios for SP ranged from 0.00 SP: C to 0.25 SP: C. Reduction in the amount of SP was of particular interest due to its high material cost. In some mix designs, when SP was reduced, the amounts of SF were increased since SF and SP have similar particle sizes along their particle size distribution.

3.2.2. Steel Fibers

Steel fiber reinforced concretes resist post-cracking tensile stress through the composite action between the concrete and fibers, including chemical and mechanical bonding at the interface between the two. In this study, all UHPC mixes contain 1.5% steel fibers by volume of the wet concrete. The steel fibers (Figure 3-2) used are brass coated, smooth fibers. Each fiber is 0.75 in (19 mm) long with a diameter of 0.0078 in (0.2 mm) and has a minimum tensile strength of 285 ksi (1965 MPa).

Figure 3-2: Example of the Steel Fibers Used in this Study

3.2.3. Mixing Procedure

Mixing was done using a large Hobart food-type mixer with a 2.65 gal. (10 liter) capacity (Figure 3-3). First, silica fume and the two silica sands were added into the mixer and were dry mixed for approximately 5 minutes at 136 rpm. Silica powder (if any) and cement were then added into the pan and mixed for an additional 5 minutes at 136 rpm. After this, water and the high range water reducer was gradually dispensed into the pan while the mixer was spinning. The blend was allowed to mix for approximately 1-2 more minutes at 136 rpm. Then the mixing speed was increased to 281 rpm for approximately 5 min, or until the concrete reached an acceptable consistency. Once an adequate mixture consistency was achieved, the high strength steel fibers were added into the mixer and allowed to mix at 136 rpm until the fibers were sufficiently dispersed.

Figure 3-3 Mixing process (photos courtesy of Prof. Kay Wille)

3.2.4. Tensile Strength Testing:

For the purpose of this study, a direct tension test based on AASHTO T 132-87 (2009) was chosen to test the specimens. In this test procedure, precast specimens were made and then tested under

direct tension. As shown in Figure 3-4, the specimens are supported by plates ensuring anchored and rotation-capable boundary conditions.

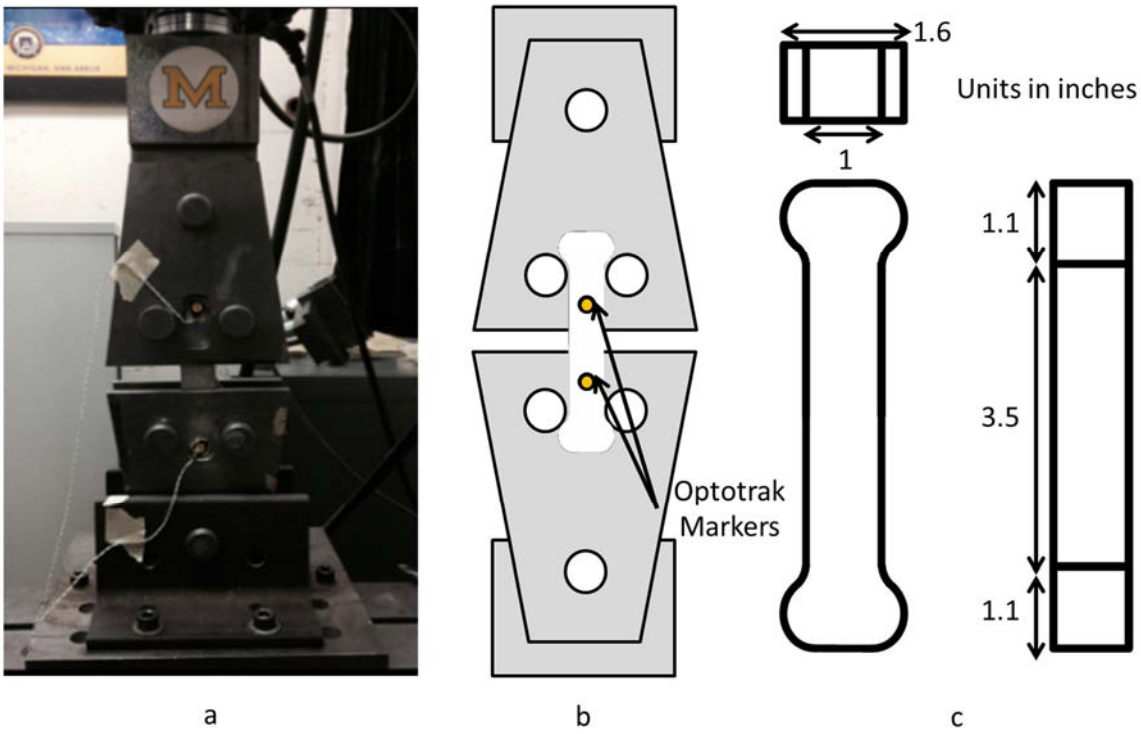

Figure 3-4 (a) Tensile test set up, (b) Instrumentation, (c) Specimen dimensions

Each specimen has a constant cross sectional area of 1 in^2 (25 mm^2) and a gauge length of 3.14 in (80 mm). The long gauge length used enables careful observation for multiple crack development. The UHPC specimens were first mixed in accordance with the procedure prescribed above. They were then poured in layers into dog-bone shaped molds to full capacity. No vibration was used. After initial casting, the specimens were covered and stored at room temperature for 24 hours. Following this, the specimens were removed from the molds and stored in a water tank at 68° F (20° C) for 28 days. Specimens were then given time to dry (approximately 12 hours) and then

tested. For each of the mixes, at least 6 dog-bone tensile specimens were tested and the stress and strain data recorded. Figure 3-5a shows a tested specimen.

Each tensile specimen was carefully loaded into the MTS testing machine. A small preload (20% of the matrix cracking strength) was applied to the specimen, which was then manually moved into the best-aligned position to insure uniaxial tension stress. The loading rate was set to 0.003 in/min those results in an estimated strain rate of $\dot{\varepsilon} = 0.0001\ \text{s}^{-1}$. Following the tensile tests, the specimen crack distribution was observed and quantified. Isopropyl alcohol 99.9% was sprayed onto the specimens followed by a blue dye. The contrast in color between the dye and specimen enables a clear visualization of the crack formations.

3.2.5. Compression Testing:

The UHPC specimens were first mixed in accordance with the ratios prescribed above. Compression specimens were poured at once into 2 in. (50 mm) cubed molds. At least 6 compression specimens were tested for each mix and their post cracking strength recorded. The cube specimens were placed into the center of the testing machine and tested in accordance to ASTM C109 (2009). Some specimens were initially precision ground in order to provide a flat surface for testing, however this was later stopped, as it did not yield noticeable differences in strengths between ground and non-ground specimens. Figure 3-5b shows a tested specimen.

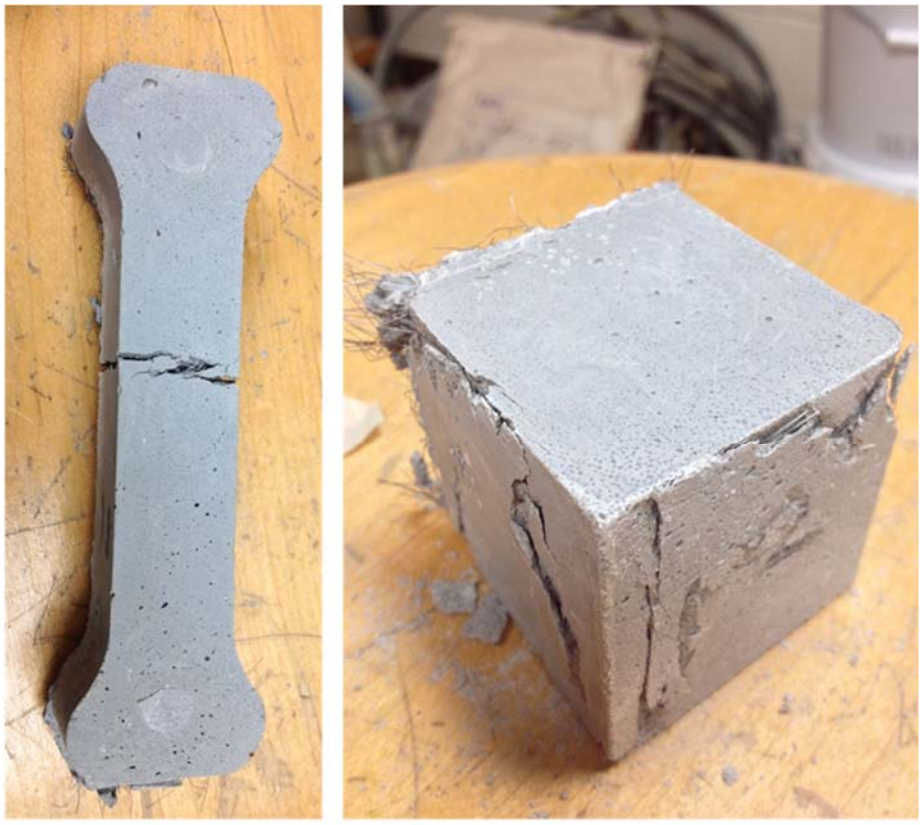

Figure 3-5: Tensile and Compression Specimens Post Test

3.3. RESULTS AND DISCUSSION

3.3.1. Analysis of Data

The following naming scheme was used in order to simplify the discussion of the results. The first number corresponds to the cement type used in the mix design as discussed earlier, W for White Cement Type I, PV for the Portland V and GG for the Portland I / GGBS mix. The second letter refers to the quantity of silica fume present in the mix. The third number corresponds to the quantity of silica powder, and the fourth number corresponds to the steel fiber volume fraction of the UHPC mix design. For example, W-25-25-1.5 would indicate white cement, with 25% silica fume and 25% silica powder, containing 1.5% steel fibers by volume.

For compression, only the maximum compressive strength was considered. For the tensile testing, the test curve was broken down into the three distinct regions as discussed earlier. Adopting the characterization scheme from Naaman (1996), the following parameters were determined: first cracking strength, σ_{cc}, post cracking strength, σ_{pc}, strain capacity, ε_{pc}, energy absorption capacity, $_{g}$, elastic modulus, E_{cc}, and stress in the fibers, σ_{fpc}. Also, the average number of cracks in the gauge length of the specimen was found. The energy absorption capacity, *g*, represents the energy absorption capacity prior to tension softening. This graphically corresponds to the total area under the curve up until 95% of σ_{pc}. Experience and experimental data showed that consistent softening behavior occurred in samples beyond this point. E_{cc} represents the elastic modulus of the material and is determined by the slope of the tensile curve prior to initial cracking. The value of σ_{fpc} represents the average fiber tensile stress as determined using the equation proposed by Naaman (1996) and is simply the total post cracking strength divided by 90% of the fiber volume content. This 90% factor is recommended to account for the statistical variability in the experimental procedure. For each set of tensile tests, at least 3 specimen tensile plots are averaged in order to produce a single tensile response curve. The plots are averaged at each point along the strain range. The result is then processed through a moving average filter to account for minute changes due to the sensitivity of the equipment. The average number of cracks is observed visually.

3.3.2. Overview of Results

The tensile and compressive test results produced by the experimental procedure are shown in Table **3-4**. The average values between the six specimens tested per experiment were used.

Test Series	Compressive Strength	Post Cracking Strength σ_{pc}	Energy Absorption Capacity G	Strain Capacity ε_{pc}	Fiber Tensile Stress σ_{fpc}	Average Number of Cracks	Cost Index ($/$ Original Mix)*
	ksi (MPa)	ksi (MPa)	kcal/yd^3 (KJ/m^3)	%	ksi (MPa)	#	
W-25-25-1.5	28.0 (192.7)	1.4 (9.48)	5.5 (30.2)	0.19	101.3 (698)	7.8	1.0
W-30-20-0.5	21.0 (144.7)	0.9 (6.1)	0.6 (3.3)	0.05	196.5 (1354)	1.7	
W-30-20-1.0	23.7 (163.5)	1.2 (8.1)	2.7 (14.9)	0.11	131.2 (904)	5.2	0.98
W-30-20-1.5	28.3 (195.2)	1.4 (9.4)	10.0 (54.7)	0.64	100.9 (695)	8.3	
W-35-15-0.5	20.9 (144.1)	0.8 (5.7)	0.5 (2.6)	0.01	182.7 (1259)	2.2	
W-35-15-1.0	24.0 (165.6)	1.4 (9.7)	3.7 (20.3)	0.16	155.7 (1073)	6.2	0.96
W-35-15-1.5	28.4 (195.4)	1.3 (8.8)	4.3 (23.7)	0.07	94.9 (654)	7.8	
W-25-20-0.5	25.8 (177.6)	0.7 (5.1)	0.7 (4.1)	0.08	164.4 (1133)	2.2	
W-25-20-1.0	27.3 (187.8)	1.0 (7.2)	2.7 (14.9)	0.18	116.5 (803)	4.3	0.95
W-25-20-1.5	28.3 (195.3)	1.6 (10.9)	3.2 (17.5)	0.10	117.3 (808)	7.7	
W-25-15-0.5	26.3 (181.0)	1.1 (7.7)	1.4 (7.6)	0.07	246.9 (1701)	2.3	
W-25-15-1.0	25.8 (177.8)	1.4 (9.6)	5.6 (30.5)	0.10	154.7 (1066)	5.2	0.90
W-25-15-1.5	28.0 (192.7)	1.3 (9.2)	5.3 (29.2)	0.16	99.0 (682)	7.5	
W-25-00-1.5	25.2 (173.8)	1.2 (8.2)	4.0 (21.7)	0.18	88.2 (608)	11.0	0.72
PV-25-15-0.5	20.9 (143.7)	0.9 (6.1)	1.7 (9.4)	0.06	197.7 (1362)	2.5	
PV-25-15-1.0	25.0 (172.1)	1.4 (9.5)	3.2 (17.3)	0.13	152.5 (1051)	6.4	0.71
PV-25-15-1.5	26.6 (183.1)	1.6 (10.7)	6.5 (35.6)	0.11	115.4 (795)	8.3	
PV-25-10-1.5	25.3 (174.4)	1.2 (8.5)	10.5 (57.2)	0.33	91.6 (631)	10.5	0.66
PV-25-05-1.5	26.4 (182.0)	1.2 (8.1)	7.6 (41.6)	0.50	86.5 (596)	10.7	0.60
PV-30-05-1.5	25.0 (172.4)	1.2 (8.2)	7.0 (38.5)	0.27	87.8 (605)	11.0	0.66
PV-35-05-1.5	25.7 (177.2)	1.0 (7.2)	3.7 (20.2)	0.24	77.5 (534)	10.5	0.68
PV-25-00-0.5	22.2 (152.9)	0.6 (4.1)	1.4 (7.4)	0.15	132.8 (915)	2.4	
PV-25-00-1.0	23.5 (161.7)	1.1 (7.6)	6.4 (35.1)	0.11	122.9 (847)	5.6	0.55
PV-25-00-1.5	25.3 (174.0)	1.3 (9.0)	6.4 (35.1)	0.11	96.7 (666)	8.1	
PV-25-25-1.5	27.6 (190.0)	1.3 (8.8)	3.4 (18.7)	0.15	94.5 (651)	10.0	0.82
GG-25-00-1.5	25.2 (173.8)	1.2 (8.0)	3.2 (17.6)	0.15	86.4 (595)	9.0	0.52
GG-25-15-1.5	26.2 (180.6)	1.2 (8.6)	4.4 (24.2)	0.21	91.9 (633)	10.5	0.69
GG-25-25-1.5	26.9 (185.5)	1.4 (9.4)	7.4 (40.5)	0.28	101.5 (699)	11.3	0.79

*Matrix only, no fibers.

Table 3-4: Cost and Performance Summary

3.3.3. Cement Type

Three different cements were tested with three different mix ratios. Figure 3-6 shows the effects of cement types on various performance parameters for mixes with 1.5% volume fiber fraction. From Figure 3-6a, it can be seen that the compressive strength of the material varies slightly with differences in cement type. In general, the mixes containing the Portland Type V mixes perform the worst, averaging 25.9 ksi (179 MPa). Slightly better, those containing the GGBS / Portland Type I cement achieved on average 26.1 ksi (180 MPa) in compression. Those containing the White cement performed the best, averaging 27.7 ksi (191 MPa). All three cements performed above the minimum required compressive strength to qualify as UHPC, i.e. 22 ksi (150 MPa).

In tension, the average post cracking strength for each mix was also considered. From Figure 3-6b, White Cement mixes exhibited the highest tensile strength, averaging a max post cracking strength of 1.3 ksi (9.3 MPa). Portland Type V mixes averaged the lowest strengths, 1.2 ksi (8.4 MPa) and those containing GGBS / Portland Type I mixes achieved average post crack strengths of 1.3 ksi (8.9 MPa). All specimens showed at least 8 cracks in the gage length (Figure 3-6c), while specimens containing the GGBS / Portland Type I cement exhibited the most cracking. All specimens exhibited strain hardening and had a strain capacity, ε_{pc} , ranging from 0.21 to 0.24 (Figure 3-5d). Similarly, the energy absorption capacity (Figure 3-6e) and fiber tensile stress (Figure 3-6f) for all three cement types showed little variation and no clear trend between the three cement types. While specimens containing white cement performed the best in compression, all three cements showed good performance under tension and compression indicating they are all suitable for UHPC.

3.3.4 - Silica Powder

Figure 3-7 shows the effects of SP on various performance parameters for all mixes with 1.5% volume fiber fraction. From Figure 3-7a, it's seen that compressive strengths ranged from 25.1 ksi (173 MPa) at 0% SP up to 27.1 ksi (187 MPa) at 25% SP. Compressive strengths increased as SP increased up to 20%, dropping slightly as SP increased further to 25%. In tension, post cracking strengths (Figure 4b) showed little variation, with specimens containing 0% SP achieving 1.2 ksi (8 MPa) up to 1.4 ksi (9.5 MPa) for those containing 25% SP. Similarly, the average number of cracks formed showed little change from 0% SP to 25% SP. Energy absorption capacity decreased slightly from 0% SP to 20% SP, though 25% SP showed the greatest energy absorption capacity. Fiber tensile stresses essentially remained unchanged, indicating SP did not affect the ability of the fibers to transfer load. Figure 3-7 shows that significant changes in SP content resulted in minor changes in all the performance parameters.

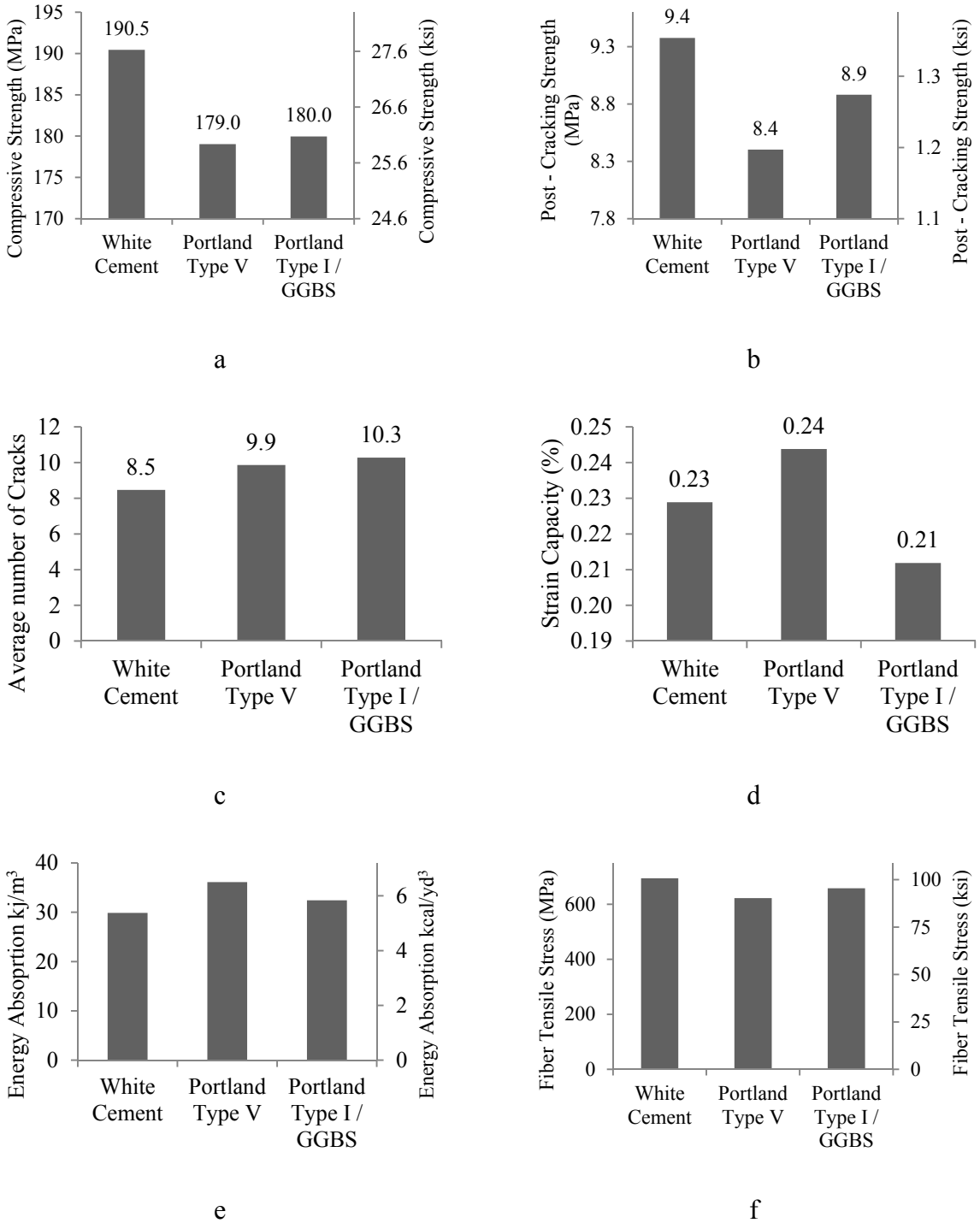

Figure 3-6: Effects of Different Cements on UHPC for Mixes with 1.5% Volume Fiber Content

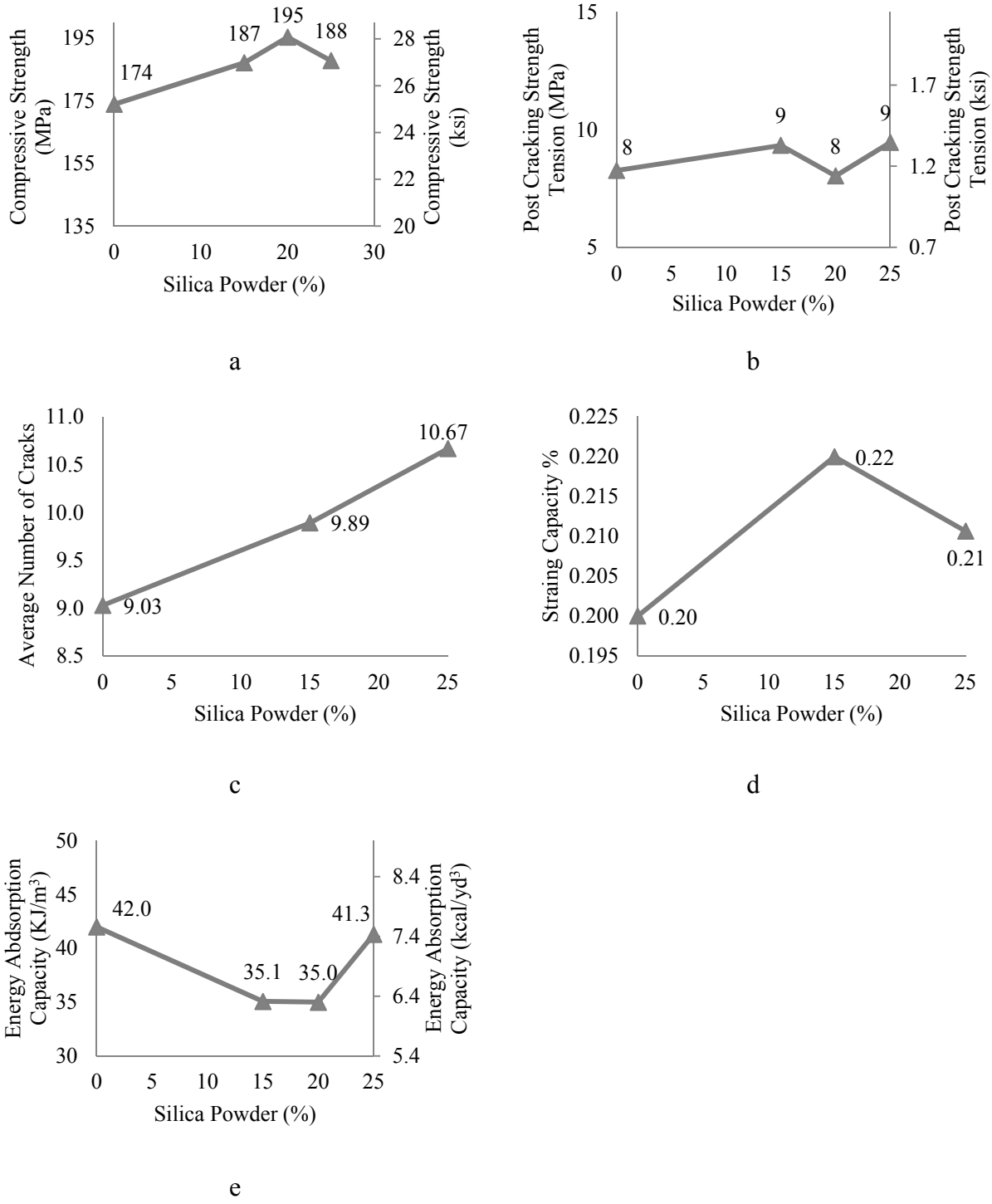

Figure 3-7: Effects of Silica Powder Content on UHPC for Mixes with 1.5% Volume Fiber Content

3.3.4. Silica Fume

Three different ratios of silica fume were tested. Figure 3-8 shows the effects of silica fume on various performance parameters for all mixes with 1.5% volume fiber fraction. In Figure 3-8a, the compressive strength of the material varies slightly with variation in silica fume. Mixes containing 25% SF averaged 26.7 ksi (184 MPa), increasing up to 27 ksi (186 MPa) for those containing 35% SF. This accounts for less than a 1.5% variation in compressive strength at increases in SF up to 15%.

Similarly, in tension, the results showed slight changes with variations in silica fume. Post cracking strengths (Figure 3-8b) for mixes containing 25% SF averaged 1.3 ksi (9 MPa) decreasing with additional SF; 35% SF averaged 1.2 ksi (8 MPa) in tension. This accounted for an 11% difference in strengths for a 15% increase in SF. The average number of cracks for all mixes was above 8 (Figure 3-8c), again indicating good strain hardening behavior. Strain capacity for all SF percentages ranged from 0.2% to 0.24%. Energy absorption (Figure 3-8e) decreased somewhat as SF content increased. While the changes in compressive strength were minimal, increased SF content led to lower performance under tension, and a reduction in fiber tensile stress indicated a decrease in the ability of the steel fibers to carry tensile forces.

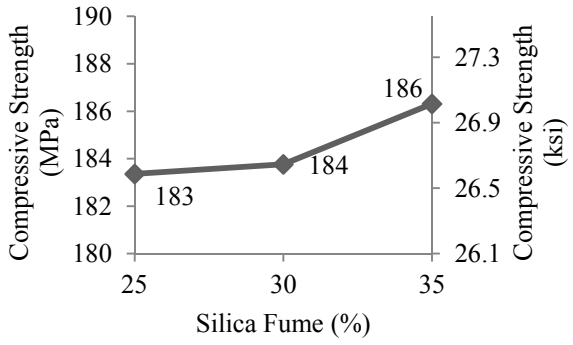

a

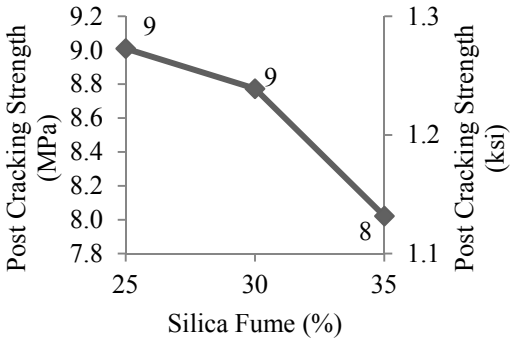

b

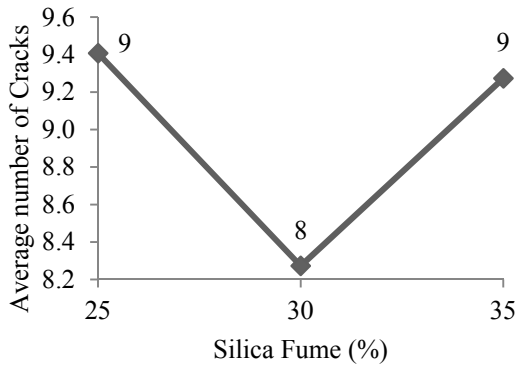

c

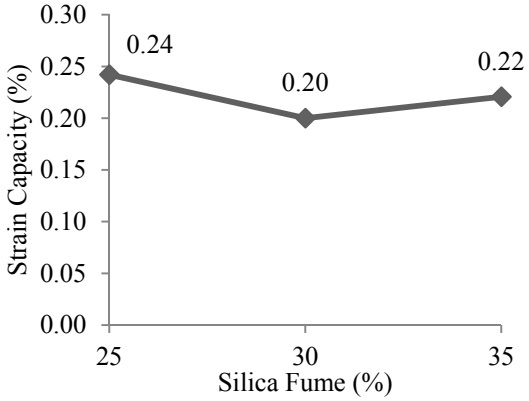

d

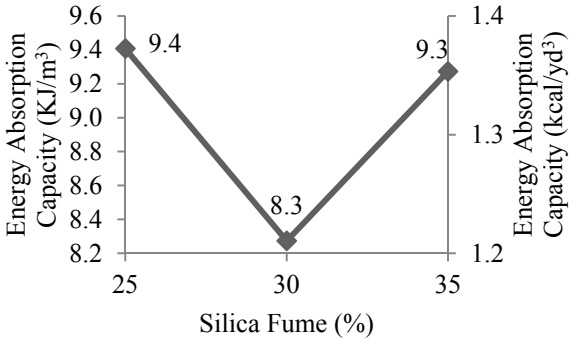

e

Figure 3-8: Effect of Silica Fume Contents on UHPC for Mixes with 1.5% Volume Fiber Content

3.3.5. Fiber Content

Figure 3-9 shows the effect of fiber volume fractions averaged across all performance parameters for the various mixes. As seen in Figure 3-9a, compressive strength ranges from 22.7 ksi (157 MPa) at 0.5% fibers by volume to 26.5 ksi (183 MPa) at 1.5% fibers by volume, a difference of 15% in strength capacity. Compressive strength of the specimens increased linearly with increases in fiber content. In tension, specimens containing 1.5% fibers yielded the highest average post cracking strength (Figure 3-9b) averaging 1.3 ksi (9.0 MPa), while those containing 0.5% fibers were the lowest at 0.8 ksi (5.8 MPa). Similarly, the strength increases linearly with respect to increasing fiber content. The remaining tensile properties also increased almost linearly with an increase in the steel fiber content (Figure 3-9c, d, e). The fiber tensile stress decreased with increasing fiber content, as more fibers were available to transfer the load. The decreased stress in the steel fibers is also likely affected by the fiber-group effect, which reduces the matrix's ability to resist the bond. These results are in line with what has been observed in other fiber reinforced concretes (Wille et al, 2012).

Figure 3-10 shows the average tensile stress-strain response for specimens containing 0.5%, 1.0% and 1.5% steel fibers by volume, while Figure 3-11 shows the data in another format for clarity. The average tensile response curve was calculated taking the mean value of the stress for each strain value for each of the tests performed in the series. It is clear that strain hardening is achieved for all fiber contents studied in this work. At 0.5% steel fibers, the strain capacity is 0.07%. This almost doubles to 0.13% as the fiber volume fraction increases to 1%. At 1.5% volume fraction, the strain capacity is 0.23.

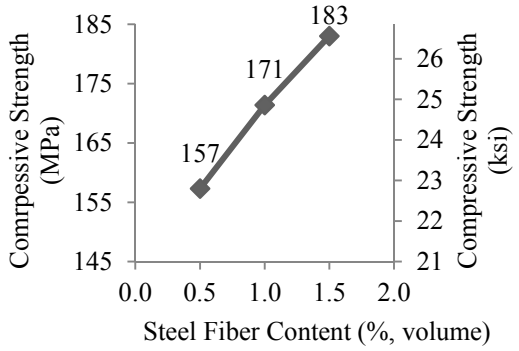

a

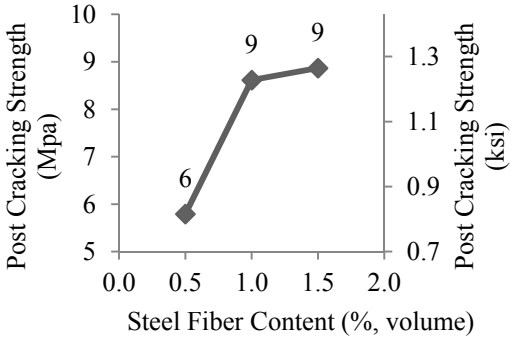

b

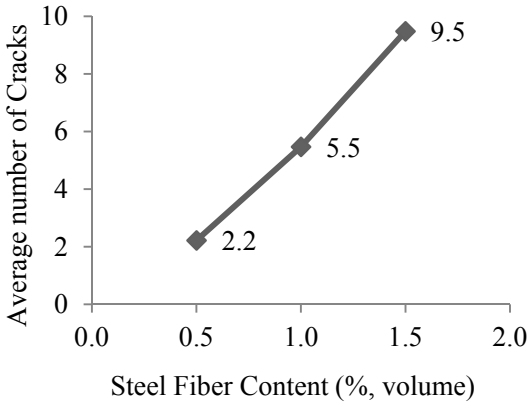

c

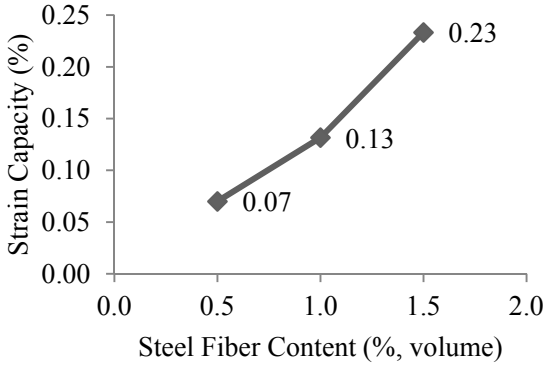

d

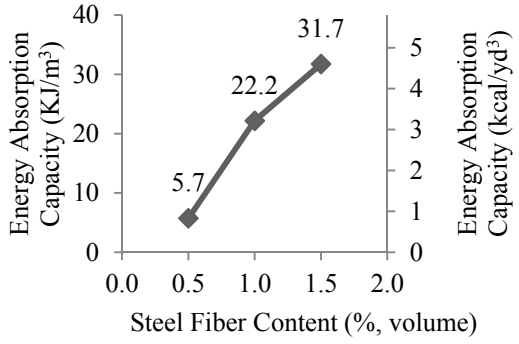

e

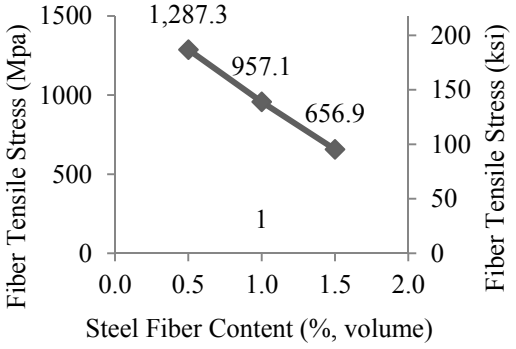

f

Figure 3-9: Effects of Lower Steel Fiber Volume Contents on UHPC

In most structural applications, construction grade reinforcing steel yields at 0.2% strain. Assuming that the live and dead loads on a structure are equal, load factors for them to be 1.4 and 1.7 according to ASCE7 (2010) respectively, and the only forces on a structure, the strain in steel bars can be estimated to be 0.09% under dead loads alone and 0.13% under working conditions. Using a tensile strain hardening material that has a strain capacity that is at least one of these values will limit crack localization and protect the steel from moisture and ingress of chlorides.

It appears from the test results provided that using UHPC with 0.5% volume fiber content could come close to the lower bound (0.09%). However, the tensile coupons conducted in this work tend to align fibers preferentially along the load direction. In a real structure, the fibers will be randomly oriented, resulting in a lower effective volume fraction in any particular direction. Hence it is unlikely that UHPC with 0.5% volume fraction can provide sufficient strain hardening to eliminate crack localization under dead loads. However, UHPC with 1% fibers likely is able to do so, and with 1.5% fibers, the protection likely extends beyond just dead loading and into working conditions. Clearly, the observations pertaining to structural behavior must be evaluated through full-scale structural tests.

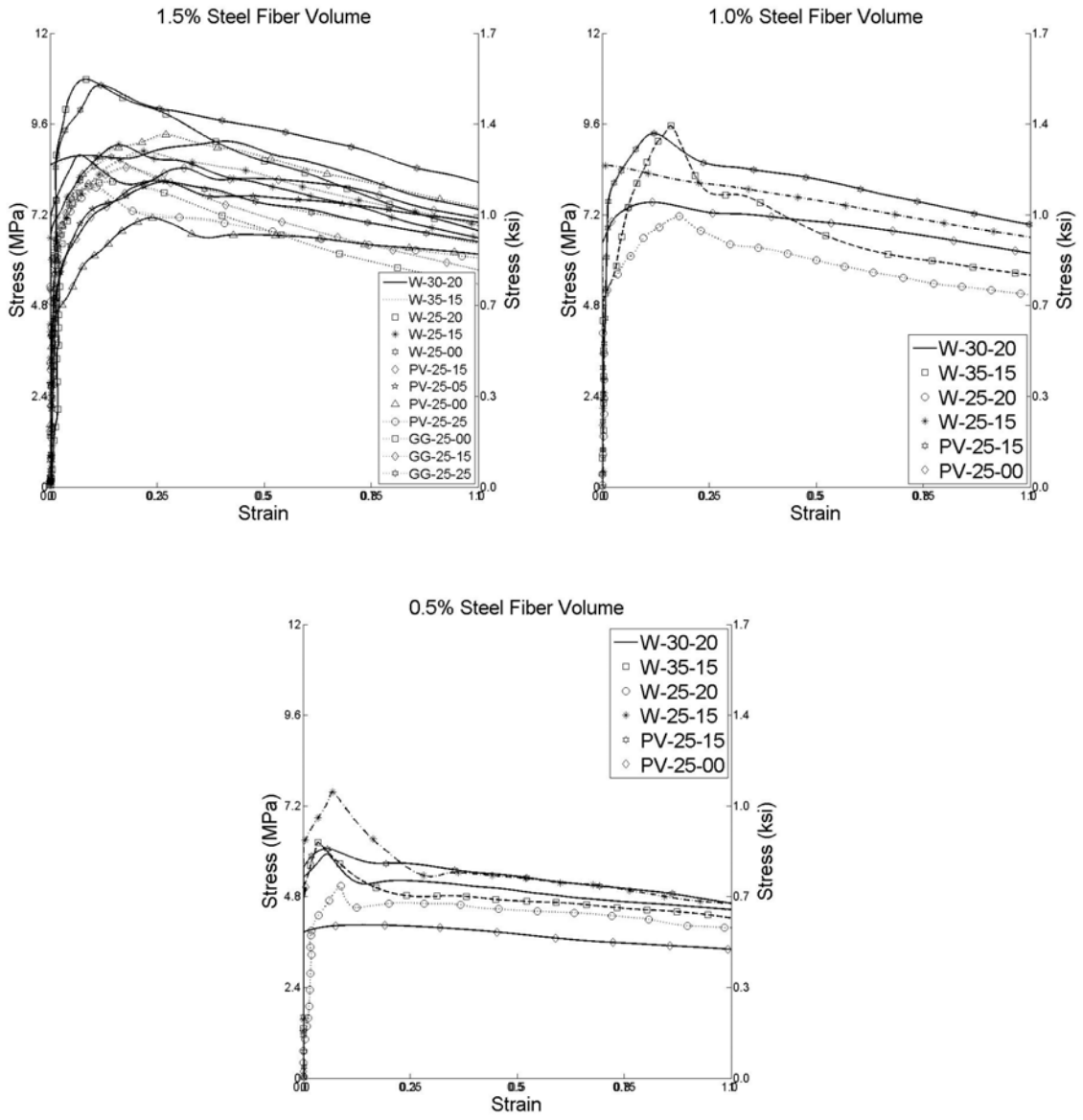

Figure 3-10: Strain Response for UHPC Specimens in Tension

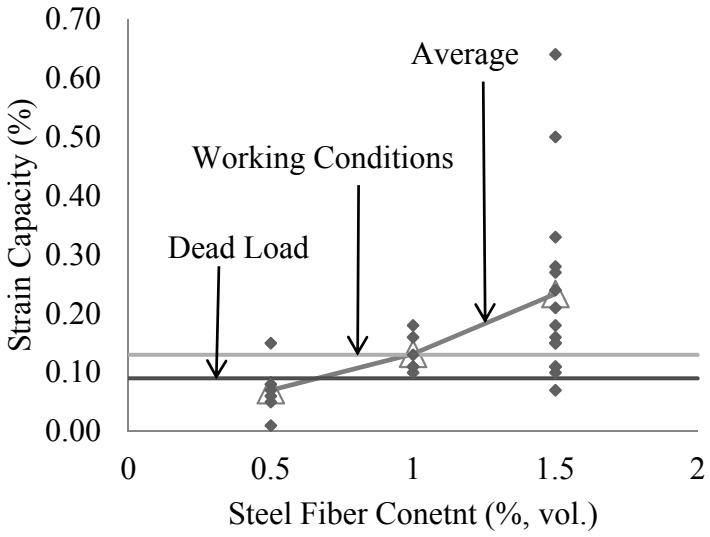

Figure 3-11: Strain (%) Capacity as function of Steel Fiber Content

3.3.6. Cost Analysis

The cost indices for each of the UHPC mixes tested are listed in Table 3-4. All of the costs used to calculate the cost index are for the cementitious materials alone, excluding the cost of steel fibers. Steel fibers, produced and sold in the US, would add an additional cost of approximately \$516/yd^3 for every 1% increase in fiber content by volume, or increase the cost index by 1.0. Figure 3-12 shows the compressive strengths for all the specimens tested vs. cost index. As can be seen, compressive strength increases linearly with increased cost. In general, cost was the highest in specimens containing the white cement, and lowest in those containing the Portland Type I / GGBS mix, as is consistent with their material costs. The least expensive mix, GG-25-00, contained 0% silica powder and used the Portland Type I / GGBS blend. Its cost index of 0.52 represents a 48% reduction in cost compared to the starting mix (5), W-25-25. Considering its lowered cost, and overall good performance, GG-25-00 presents the most optimal performance vs. cost mix of those tested. Details of this mix can be found in Table 3-5.

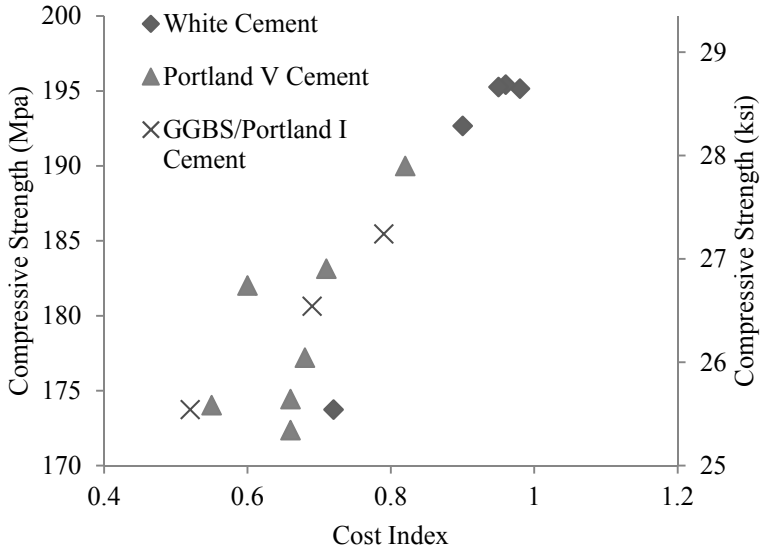

Figure 3-12: Compressive Strength as a function of Cost Index

Type	UHPC Ratio	kg/m^3
Cement	1	775
Silica Fume	0.25	194
Water	0.22	165
High Range Water	0.0054	10
Fine Sand I	0.26	245
Fine Sand II	1.03	975

Table 3-5: UHPC Mix Design and Ratios

3.4. CONCLUSION

The objective of this study was to optimize a UHPC mixture through modification of the material's constituents. Several parameters were considered, and designs were created and tested. Each design was assigned a cost index value, and ultimately a recommendation was made. The conclusions of this study are as follow:

- All of the mixes tested achieved sufficient strengths in compression for them to be labeled as UHPC.
- All three cements tested performed comparably well in tension and compression. White cement yielded the high compressive strengths, but the Portland Type I / GGBS Cement blend carried the lowest cost, thus making it a good, cost-effective choice for future UHPC mixes.
- Changes in silica powder content yielded little variation in the performance parameters examined. In particular, specimens containing no silica powder were all within 5% of the strength in tension and compression. Due to its high cost and minimal beneficial effects, silica powder could be eliminated from UHPC mixes to reduce cost.
- Changes in silica fume led to minimal changes in compressive strength. Increased SF content led to somewhat lower performance under tension, and a reduction in fiber tensile stress indicating a slight decrease in the ability of the steel fibers to carry tensile forces.
- The results suggest that fiber volume contents of 1.0% or 1.5% could significantly reduce the chance for crack localization under dead load or working conditions, respectively, in structural applications.
- Mix GG-25-00 had the lowest cost index, while still maintaining ultra-high performance, making it the recommended mix from this study. Additionally, the availability of GGBS and Portland Type I cement make it an appealing choice for use in further UHPCs.

Intentionally left blank

4. DURABILITY PERFORMANCE OF UHPC

4.1. OVERVIEW

The dense matrix of UHPC promotes exceptional durability properties and is arguably the biggest benefit of the material. A durable concrete enables structures to last longer, reduces the cost of maintenance and helps achieve a significantly more sustainable infrastructure. To assess the durability of UHPC, the performances of several non-proprietary blends are investigated by assessing the materials' resistance to freeze-thaw cycles, ingress of chlorides as well as the presence and distribution of air voids. The main experimental variables are cement type and the quantity of silica powder, which varies from 0% to 25% of the cement weight. All mixes display negligible chloride ion penetration and high resistance to freeze-thaw with mass loss well below the limit in over 60 cycles of freeze-thaw. Analysis of the test data indicates that the silica powder content has little influence on performance.

4.2. EXPERIMENTAL PARAMETERS

4.2.1. UHPC Mix Designs

UHPC blends from Chapter 3 identified as potential, lower cost mixes, were selected for durability testing in this chapter. Three different cements are considered, the previously mentioned White Cement, Portland Type V and the Ground Granulated Blast Furnace Slag. The last cement was selected due to its reduced cost and the known high durability of GGBS cements (Cheng, 2005). GGBS also has the added benefit of being a sustainable material as it is currently produced as a byproduct of the iron manufacturing process and therefore its use in concrete is an efficient method of recycling.

The quantity of cement and silica fume was held constant for all of the mixes, but the amount of silica powder was changed from 0% (none) to 25% of the total amount of cement. The water to cement ratio was held constant for all mixes, at 0.22 w/c. The admixture Advacast 575 high range water reducer was again used at a ratio of 1.35% to cement for all mixes. All of the blends tested in this chapter contain 1.5% smooth steel fibers by volume fraction. Particle sizes for each material can be found in Table 3-1. The chemical properties of Silica Fume and Silica Powder used in the testing are presented in Table 3-1. Additionally, the grain size distribution for the silica sand filler can be seen in Figure 3-1. Table 4-1 lists the mix constituents of the 9 mixes highlighted in this study. The naming scheme follows the same convention as in Chapter 3.

Name	White Cement Type I	Silica Fume	Silica Powder	Fiber (%)	F100	F12
W-25-25-1.5	1.00	0.25	0.25	1.50%	0.26	1.06
W-25-15-1.5	1.00	0.25	0.15	1.50%	0.29	1.14
W-25-00-1.5	1.00	0.25	0.00	1.50%	0.31	1.26
	Portland Type V					
PV-25-25-1.5	1.00	0.25	0.25	1.50%	0.26	1.05
PV-25-15-1.5	1.00	0.25	0.15	1.50%	0.28	1.14
PV-25-00-1.5	1.00	0.25	0.00	1.50%	0.31	1.26
	Type I / GGBS					
GG-25-25-1.5	1.00	0.25	0.25	1.50%	0.26	1.06
GG-25-15-1.5	1.00	0.25	0.15	1.50%	0.28	1.14
GG-25-00-1.5	1.00	0.25	0.00	1.50%	0.31	1.26

Table 4-1: Mix Proportions for tested UHPCs

4.2.2. Experimental Procedure

Freeze-Thaw Resistance

The resistance of concrete to the combined attack of de-icing salt and frost is evaluated by a modified CIF (Capillary suction, Internal damage and Freeze-thaw) test, where the surface scaling, moisture uptake and the internal damage were measured simultaneously. Cylindrical specimens of 6 inches (150 mm) in diameter and 12 inches (300 mm) in height were made. After 24±2 hours of curing the specimens were removed from the mold and submerged in tap water at 68 °F (20 °C) for 28 days. After storage in the water, the specimens were cut into rectangular prisms of 4.75 inches (120 mm) by 4.25 inches (107 mm) by 2.75 inches (70 mm). The cut section was away from the two ends of the cylinder to avoid surface in-homogeneity associated with a cast surface and is parallel to the finishing surface. After air drying at 68 °F (20 °C) and 65% relative humidity for 24 hours, the lateral surfaces of the specimens were sealed by the aluminum foil with butyl rubber. The freeze-thaw machine, as shown in Figure 4-1, contains fifteen stainless steel bowls, each containing one specimen. The specimen sits on four spacers so that the bottom test surface is in contact with the test liquid (Figure 4-2).

A freeze-thaw cycle duration is 12 hours. The temperature profile is as follows (Figure 4-3): the start temperature for the freeze-thaw test is 68 °F (20 °C); the temperature of the stainless steel bath with liquid (3% NaCl solution in this case) is lowered at a linear rate of 50 °F (10 °C) /hour for 4 hours; the specimens are kept at -68 °F (-20 °C) for 3 hours, then brought back up to room temperature at the same constant rate of 50 °F (10 °C) /hour as used for cooling; the temperature is maintained for 1 hour at 68 °F (20 °C) before the commencement of the next freeze-thaw cycle. During the one-hour isothermal period at 68 °F (20 °C), the amount of surface scaling, the moisture

uptake and the internal damage were measured after a specific number of freeze-thaw cycles. A total of two specimens were tested for each of the material parameters.

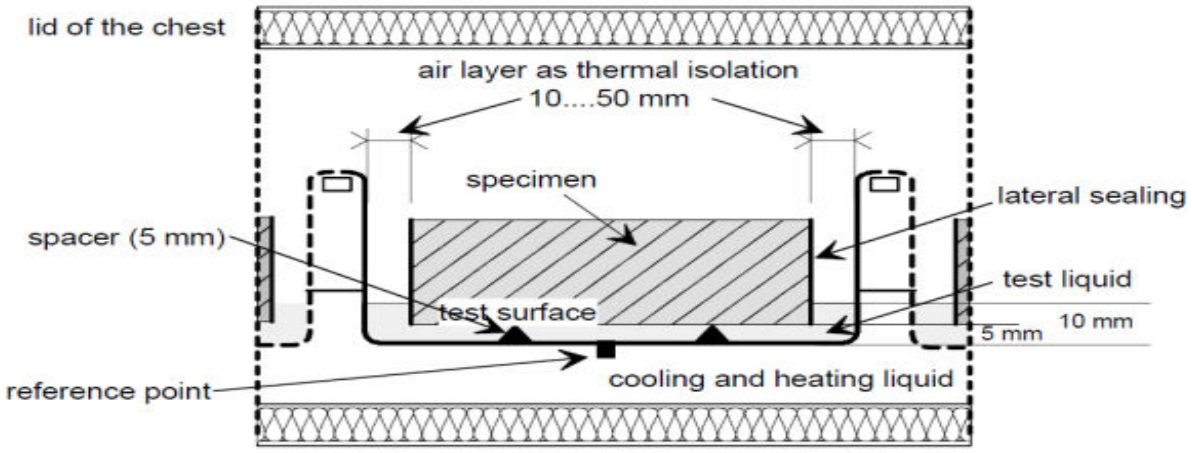

Figure 4-1: Freeze Thaw Test Close-Up (17)

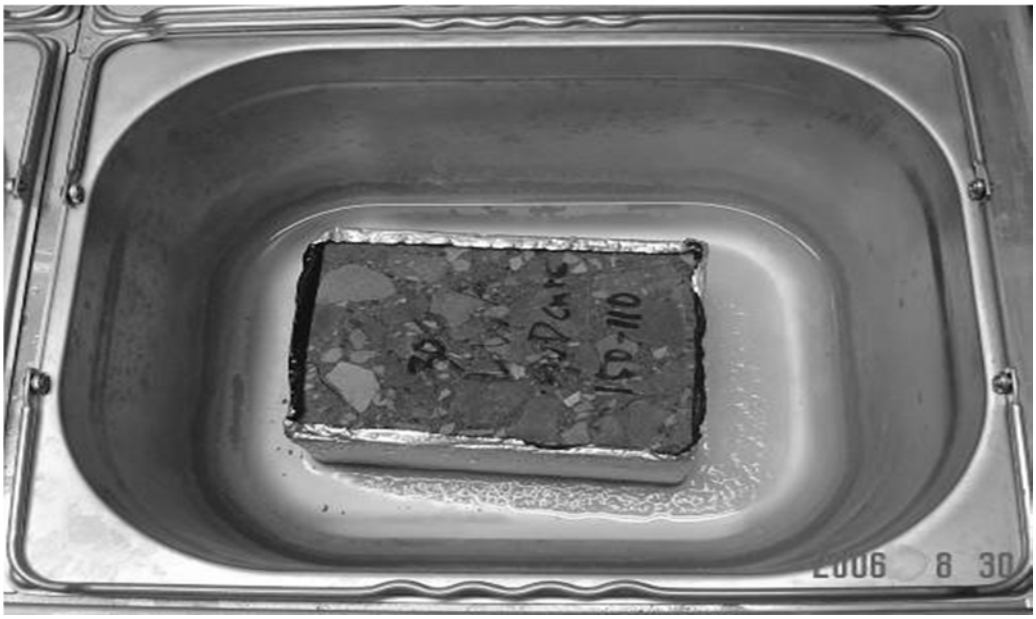

Figure 4-2: Specimen with Test Surface Facing the Bottom under Frozen Condition

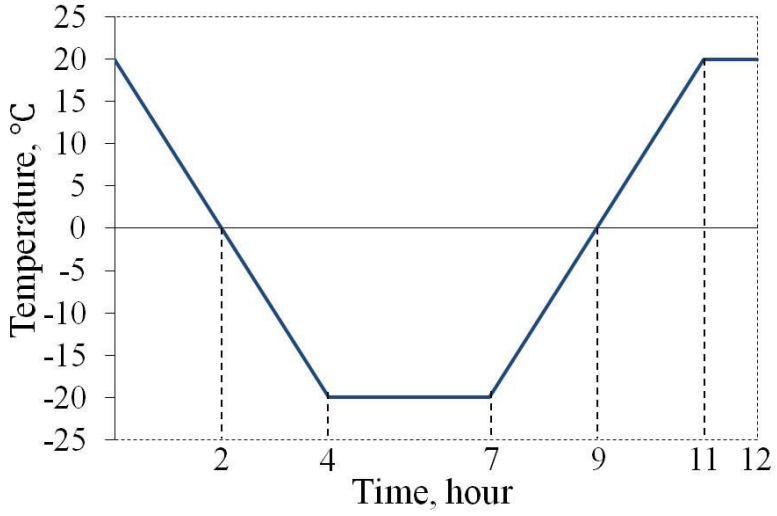

Figure 4-3: Temperature Profile of Freeze-Thaw Test

4.2.3. Air Void Analysis

The air void analysis of the concrete was measured using ASTM C457, "Standard Practice for Microscopical Determination of Parameters of the Air-Void System in Hardened Concrete". Square specimens of 4 inches (100 mm) by 4 inches (100 mm) were cut from the mid-depth portion of 6 inch (150 mm) diameter cores with the testing surface parallel to the finishing surface. Specimens were carefully polished with silicon carbide abrasives to obtain a smooth surface with undamaged paste and clearly defined air voids. Then the point count method was used to determine the fractions of air void, paste and aggregate and also the percentage of air voids with infillings. This step provides information on the quality of air void and the input to the computation of the spacing factor in the next step. After the point count procedure, the polished surface was pretreated by filling all the air voids with a white powder (barium sulfate) and the rest of the surface was darkened by a permanent marker to produce a sharp contrast (Figure 4-4). Then, the linear traverse method was used to measure the chord length distribution and the total length of the traverse line

over air void, based on which, the air void parameters can be calculated. A total of two specimens were tested for each of the material parameters.

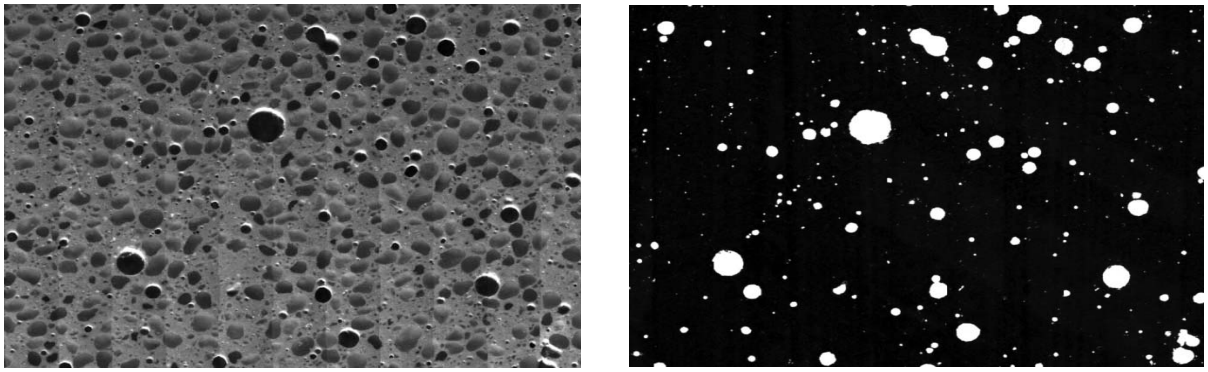

(a) Untreated Surface (b) Coated Surface

Figure 4-4: (a) Polished surface for point count measurement and (b) coated surface for linear traverse measurement.

4.2.4. Rapid Chloride Penetration Test

Evaluation of chloride ingress resistance was tested according to ASTM C1202-12, "Standard Test Method for Electrical Indication of Concrete's Ability to Resist Chloride Ion Penetration". A commercially available device, PROOVE'it, was used in order to complete the testing. Specimens of 4" (100 mm) in diameter and 2" (50 mm) in width were positioned into the measuring cell. Each cell contains a fluid reservoir at each face of the specimen. One reservoir is filled with a sodium chloride solution (3.0% NaCl). The other reservoir is filled with a sodium hydroxide solution (0.3 M NaOH).

The reservoir containing the NaCl is connected to a negatively charged terminal, the NaOH reservoir is connected to the positively charged terminal of the device's microprocessor-controlled power unit. Once started, the test automatically measures the total electrical current passing

through a concrete specimen for a standard period of 6 hours, with a direct current voltage of 60 V. A total of two specimens were tested for each of the investigated parameters.

4.2.5. Compressive Strength Testing

For each of the mixes, at least 6 cube specimens were cast. Each cube measured 2" x 2" x 2" (50 mm x 50 mm x 50 mm) and was placed into the molds without any vibration. Previous research has shown that compression test results using cubes vs. cylinders in UHPC yield 4.6 % to 6.1% higher results in the cubed specimens (Graybeal, 2006). The specimens were tested for each mix and peak compressive strength recorded. Each cube specimen was subjected to a loading rate of 0.25 kip/sec until the specimen began to strain soften in compression.

4.3. EXPERIMENTAL RESULTS

Table 4-2 shows a summary of all the test results, which are discussed in more detail in the following sections.

4.3.1. Freeze-Thaw Resistance

The freeze-thaw resistance of the ultra-high performance concrete specimens was tested in accordance with RILEM TC 176-IDC. The specimens were subjected to at least 60 freeze-thaw cycles and the mass loss of the specimens was recorded. For all of the different mixes tested, it was clear that no internal damage occurred, as evidenced by an almost unchanged relative dynamic modulus (RDM). The RDM provides a reliable measure for evaluating internal frost damage, and is calculated as follows (Equation 4-1):

$$RDM\% = \frac{n_c^2}{n^2} x100$$

Equation 4-1: Relative Dynamic Modulus

where c is the number of cycles of freezing and thawing, n_c is the resonant frequency after c cycles, and n is the initial resonant frequency (at zero cycles). For all 9 specimens, the RDM remained at 100%.

	Rapid Chloride Penetration	Air Void Analysis	Freeze-Thaw Test		Compressive Strength	
UHPC	Total Charge Passed (Coulombs)	Air Content (%)	Total Mass Loss after 28 cycles oz./yd^2 (g/m^2)		ksi (MPa)	
W-25-25-1.5	89	5.8	2.9	(98.8)	28.3	(195.0)
W-25-15-1.5	295	7.9	0.6	(20.7)	27.4	(188.8)
W-25-00-1.5	637	6.6	0.5	(17.7)	25.2	(173.6)
PV-25-25-1.5	939.5	6.1	0.5	(18.2)	25.3	(174.3)
PV-25-15-1.5	488.5	6.5	0.5	(18.0)	27.2	(187.4)
PV-25-00-1.5	57	4.5	1.2	(42.2)	25.8	(177.8)
GG-25-25-1.5	137.5	5.7	0.6	(20.5)	25.1	(172.9)
GG-25-15-1.5	229	4.8	0.7	(24.2)	26.3	(181.2)
GG-25-00-1.5	137.5	5.8	1.3	(44.7)	27.7	(190.9)

Table 4-2: Summary of Test Results

Additionally, as can be seen in Figure 4-5, mass loss for all of the specimens fell significantly below the 44.2 oz./yd^2 (1500 g/m^2) limit defined by the testing standard. This limit for mean scaling after 28 cycles measures surface scaling resistance of the specimens. For all nine specimens, this value remained consistently low, despite changes in cement types used and ratios of silica powder included. For comparison, Figure 4-5 also shows some typical results for regular concretes.

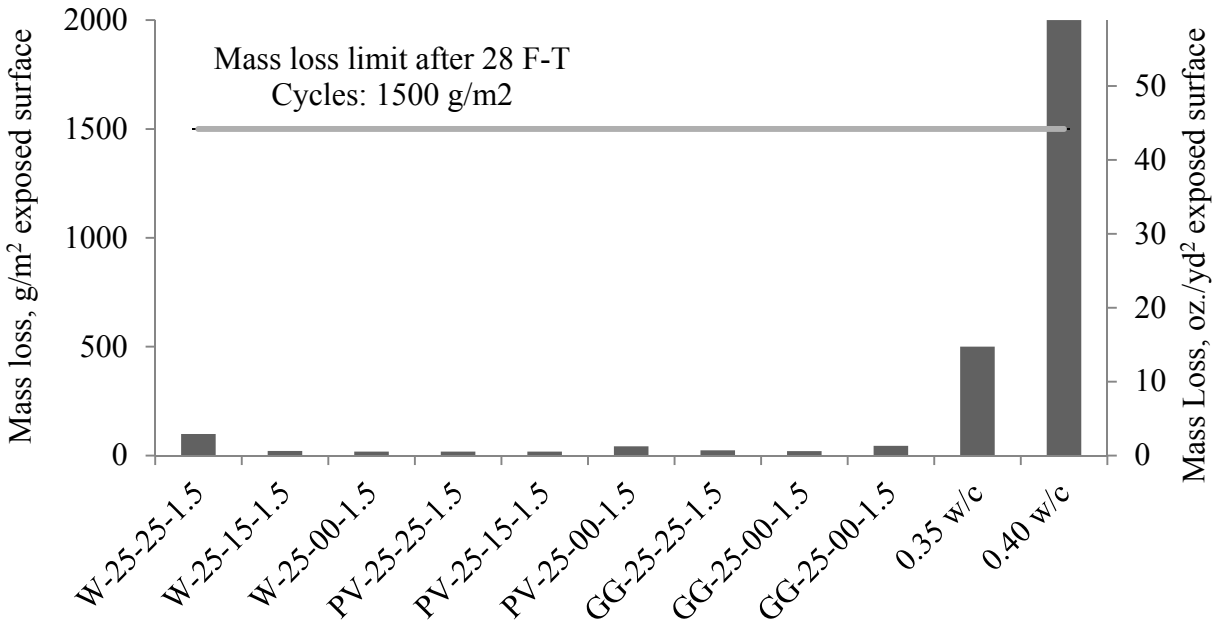

Figure 4-5: Mass Loss of UHPC Mixes after at Least 60 Cycles

From Figure 4-5, the best performing mix in terms of the least total mass loss was W-25-00-1.5, with a total loss of 0.5 oz./yd^2 (17.7 g/m^2). The worst performing mix was W-25-25-1.5, with a total loss of 2.9 oz. /yd^2 (98.8 g/m^2). Generally, there are no distinct differences in the freeze-thaw resistance of UHPCs with 0% SP, 15% SP and 25% SP. The values are all so low compared to the acceptable mass loss limits for concretes that the differences exhibited by W-25-25-1.5 are considered to be within statistical tolerances. Figure 4-5 shows that, with the exception of W-25-25-1.5, all of the mixes are within 15% of each other, and less than 3.3% of the acceptable mass losses limit for concrete, despite varying the level of silica powder and cement type.

As seen in Figure 4-6a, all specimens performed well for freeze-thaw resistance, with those containing Portland Type V performing marginally better than the other two. When averaged across all cement types, (Figure 4-6b), specimens containing 15% silica powder outperformed

those containing 25% silica powder by 40% and those containing 0% silica powder by 54%. Figure 4-7 compares the effects of cement type on the total mass loss for the UHPCs averaged for all silica powder contents. Specimens containing Portland V cement experienced 12% less mass loss than its Portland I / GGBS counterpart and 43% less mass loss than those containing white cement. Although the variations may appear large, it should be noted that all the mass loss values are small to start with and well below acceptable mass loss limits.

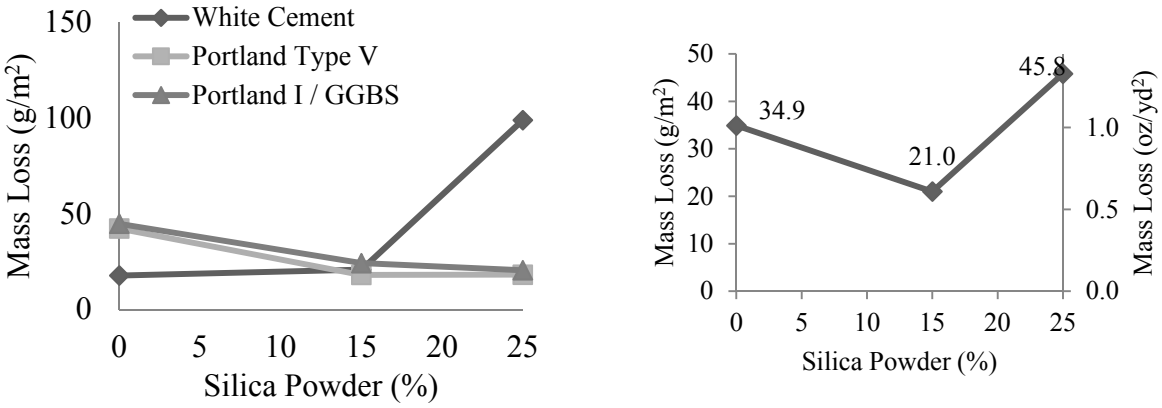

a b

Figure 4-6: a. Effect of Silica Powder on Mass Loss; b. Average Mass Loss as a Function of Silica Powder Quantity

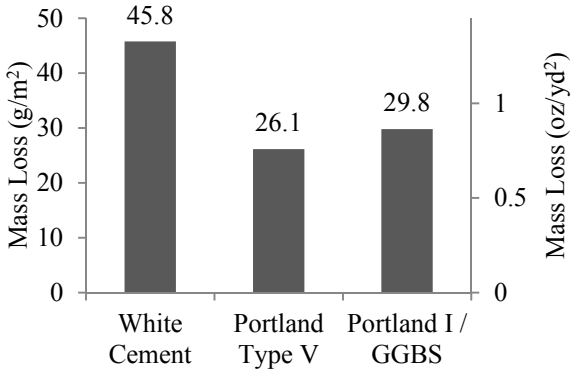

Figure 4-7: Average Mass Loss as a Function of Cement Type

4.3.2. Air Void Analysis

All of the UHPCs tested in this study tested well for freeze thaw resistance using both the linear traverse method and the point count method. The linear traverse method counts the number of voids along a single line, or chord length, while the point count method determines the number of voids within an area. Figure 4-8 shows the measured air contents using the two methods. From the chart, it can be seen that there is good agreement between the two methods.

Figure 4-8 shows that the total hardened air contents for the mixes range between 3.0% - 7.5%. These values correspond to an equivalent air content of 1.8% - 4.0% in normal concrete. Unlike regular concretes, UHPCs have a much large paste content, i.e. approximately 60% versus 30% for regular concretes. For freeze thaw, paste is the frost susceptible component, where the air-voids are embedded. In practice, air content is expressed as the air void volume as a percentage of the concrete volume. In order to accurately compare UHPC and regular concrete, the measured air content in UHPC must therefore be converted to an equivalent for regular concrete, hence the 1.8% - 4.0% range mentioned above.

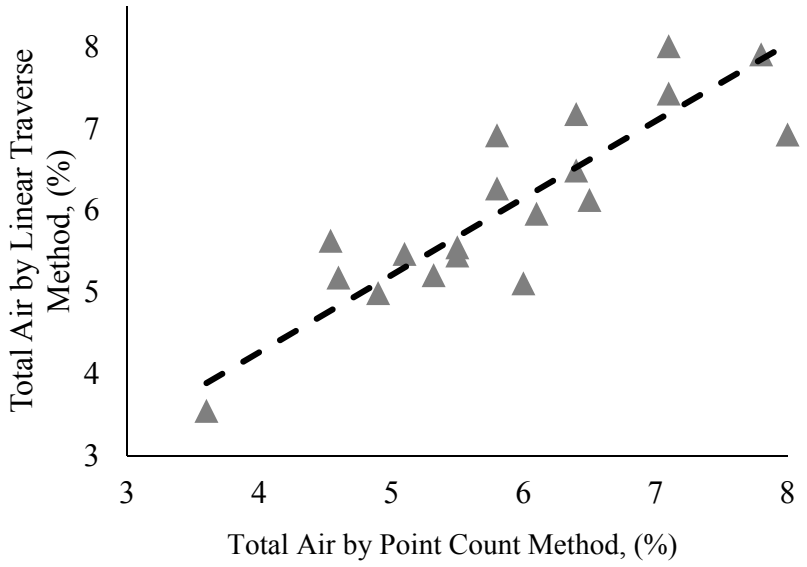

Figure 4-8: Air Content by LTM and PCM

Figure 4-9 shows the total air content as a function of the powers' spacing factor. The spacing factor here refers to the paste-void proximity; the fraction of paste within some distance of an air void. For all of the UHPC specimens tested, both air contents and spacings range from 5.9 E-4 inches to 0.02 inches (0.15 to 0.51 mm), with an average of 0.01" (0.29 mm). For normal concrete (dotted box), air-void systems with a powers spacing factor 0.0078" (0.20 mm) or less depending on conditions and 6% (+/- 1) total air content will typically provide good freeze-thaw protection (Tanesi, 2007). Though the UHPC used in this study had spacing factors higher than those of conventional concrete, it exhibited excellent freeze thaw resistance. These values also fall in line with those reported by other studies (Graybeal, 2006). Thus, the air content and/or powers spacing factor may not be a suitable metrics by which to judge the freeze-thaw resistance in UHPC.

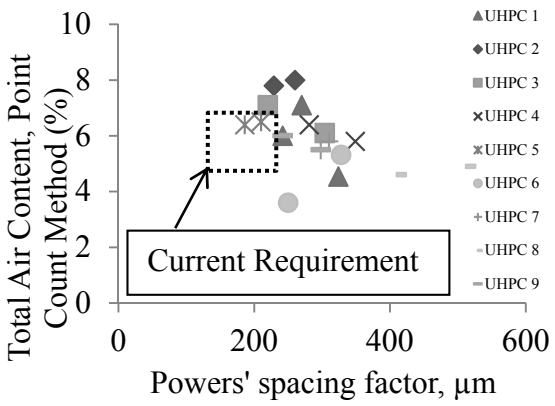

Figure 4-9: Air Content as a Function of Power's Spacing Factor

Figure 4-10a shows the air content percent as a function of silica powder for the three different cement types. The differences in air content percent between specimens containing 0%, 15% and 25% silica powder are small. When averaged across all cement types (Figure 4-10b), the air content measures are within 13% of the other specimens' air content. Figure 4-11 shows the average air content for each of the cement type used. From the data, mixes containing the Portland I / GGBS cement mix showed the least total air content percent at 5.4% when averaged across all silica powder contents. Mixes containing White cement showed air content percentages 20% higher (6.8%), and those containing Portland V cement were only 5% higher (5.7%), again when averaged across all silica contents.

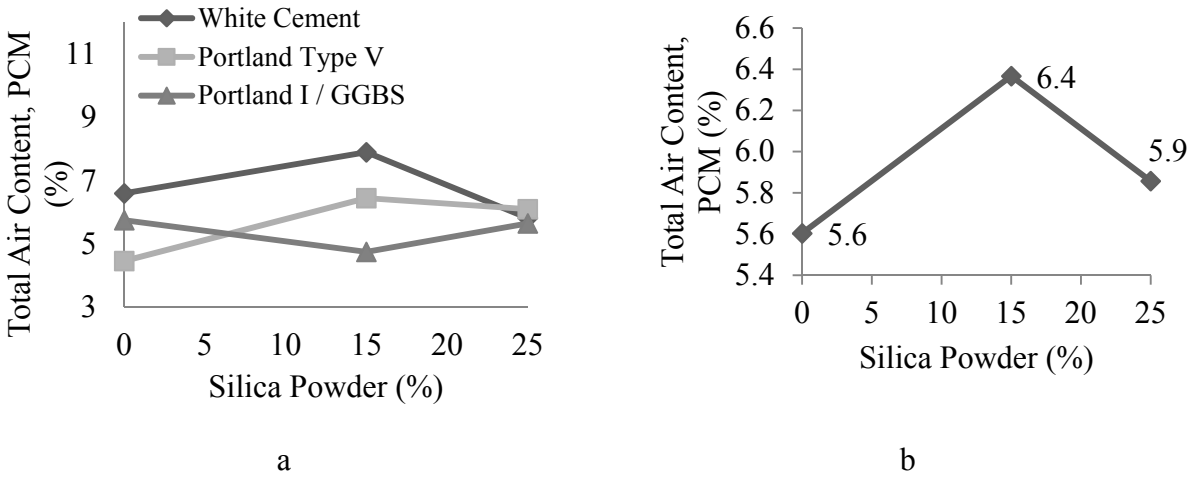

Figure 4-10: a. Air Content as a Function of Silica Powder Percent, b. Average Air Content as a function of Silica Powder

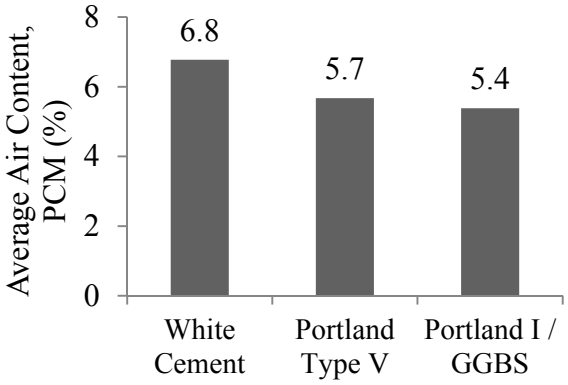

Figure 4-11: Average Air Content as a Function of Cement Type

4.3.3. Rapid Chloride Permeability

A summary of results is shown in Figure 4-12 for the nine mixes. The chloride permeability rating is illustrated based on Table 4-3. Also shown are some typical results for regular concrete.

`

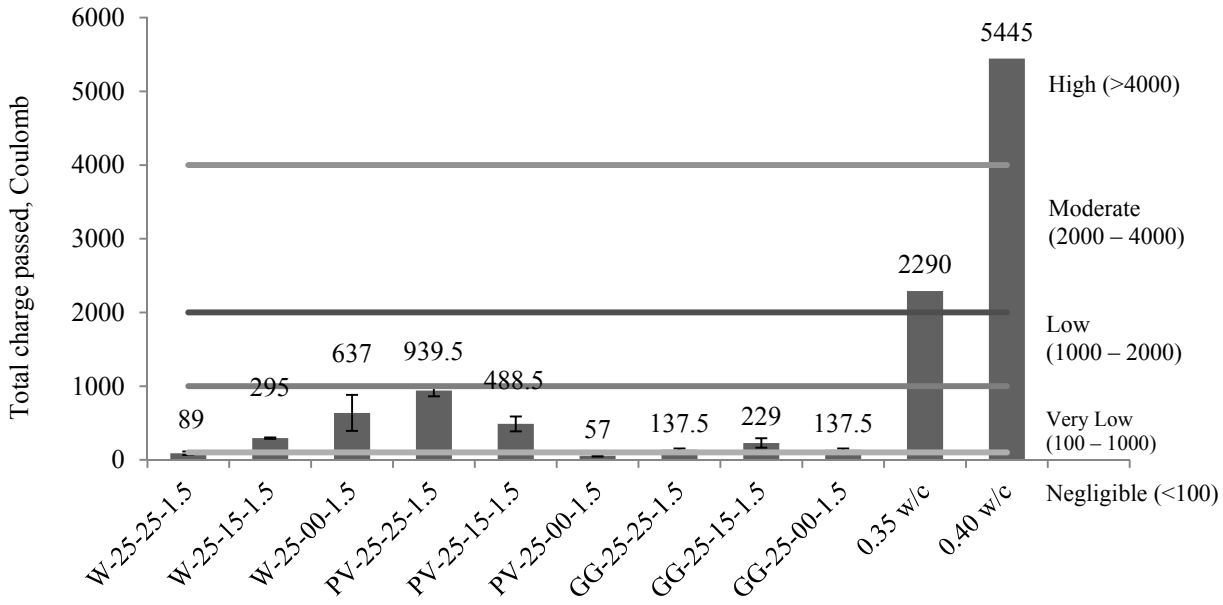

Figure 4-12: Total Charge Passed for UHP C and RC Mix

Chloride permeability	Charge (Coulomb)	Typical concrete
High	> 4000	High w/c ratio (> 0.6)
Moderate	2000 - 4000	Moderate w/c ratio (0.4 - 0.5)
Low	1000 - 2000	Low w/c ratio (< 0.4)
Very low	100 - 1000	Latex-modified concrete, internally sealed concrete
Negligible	< 100	Polymer impregnated concrete, polymer concrete

Table 4-3: Chloride Permeability Rating

From Figure 4-12, all of the UHPC mixes have a rating of "very low" chloride permeability with two mixes falling into the "negligible" category. From Figure 4-13a, it appears that the combined effect of cement type and silica powder content on the chloride ion permeability of UHPC is not clear. When averaged for all cement types, Figure 4-13b shows that the amount of silica powder

plays a role: increasing silica powder content leads to higher permeability. Specimens with 0% silica powder perform the best, averaging 277.2 coulombs passed. Those specimens outperformed ones containing 25% silica powder by 40% and those containing 15% silica powder by 17%. For comparison, regular concretes containing 35% and 40% water contents average 2073 and 4000 coulombs passed, or rather 621% and 1343% higher than the mixes containing 0% silica powder. When averaged across all silica powder contents, Figure 4-14 shows that specimens containing Portland Type I / GGBS cement exhibited the best performance on average, with all three mixes averaging 168 Coulombs passed. The mixes containing white cement averaged 340 coulombs passed, a 102% difference compared to Portland I / GGBFS. The mixes containing Portland type V averaged 495 coulombs passed, a 194% percent difference. As noted for mass loss in the freeze-thaw test results, while the variations appear large, the base values are actually small, signifying the good chloride penetration performance of all of the UHPC mixes considered.

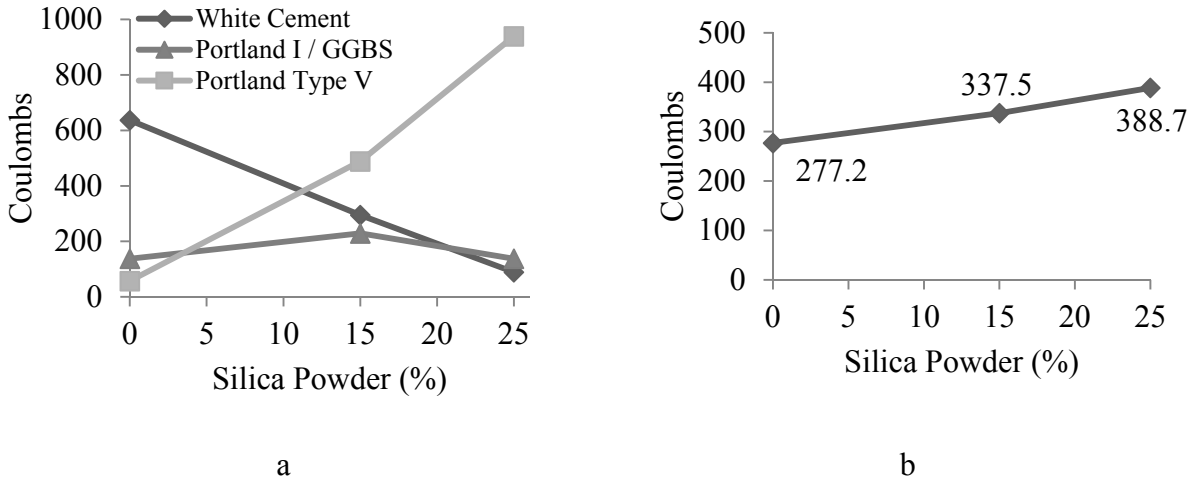

a b

Figure 4-13: a. Total Coulombs passed as a function of Silica Powder Percent; b. Average Coulombs passed as a function of Silica Powder

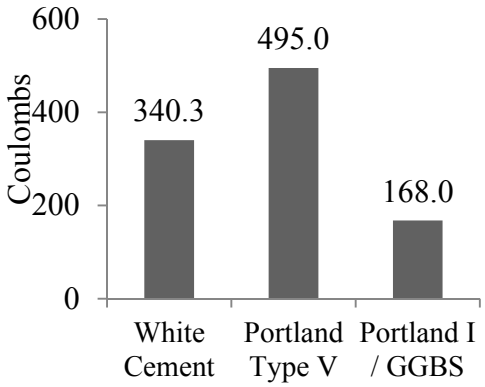

Figure 4-14: Average Coulombs passed as a function of Cement Type

4.4. DISCUSSION OF EXPERIMENTAL RESULTS

The materials tested in this research showed high durability characteristics. It is commonly accepted that the good performance of UHPC is a manifestation of the material's high packing density, which can be characterized through particle packing models. Such models consider the size and quantity of individual particulate components within a material, and show the distribution of those particles for the entire mixture. In order to achieve the densest particle packing, Andreasen and Anderson (1930) developed the Andreasen model. This paper makes use of a modified Andreasen particle packing model, as shown in equation 4-2:

$$CPFT(\%) = 100\left(\frac{d^q - d_m^q}{D^q - d_m^q}\right)$$

Equation 4-2: Modified Andreasen Model

where CPFT is equal to the cumulative percent finer than, d is the particle size for the material, d_m is the minimum particle size, D is the maximum particle size and q is the distribution coefficient. Previous studies have shown that a value of $q = 0.37$ provides higher particle packing densities for self-consolidating concretes which have similar rheology as UHPC (Brouwers, 2013). Therefore, this value was chosen for the analysis.

Figure 4-15 plots the particle size distributions for all the mixes tested in this study and compare them to the modified Andreasen model. Also plotted, for the purpose of comparison, is the distribution for regular concrete (Chia, 2002). Unlike the UHPC mixes, regular concrete deviates significantly from the ideal distribution throughout the entire range of particle sizes, suggesting that the material is sparser than UHPC. Also, regular concrete does not have any particles below 1 micron, suggesting that voids exist at this level.

Figure 4-15 shows that while variations in silica powder content affect the material's packing density differently across the particle size range; the distributions still remain close to the 'optimal' particle packing density. This provides an explanation for why there are little differences between the performances of all mixes, especially for chloride ion penetration. In essence, all the UHPCs tested in this study are so dense that they effectively resist the ingress of chloride ions. The freeze-thaw resistance in UHPCs is due to water being prevented from entering the voids. Figure 4-16 shows that all UHPCs tested had a very low water uptake percent, (<0.3% vs. approximately 1% for regular concrete (Liu, 2014)) and an unchanged RDM% indicating no internal damage.

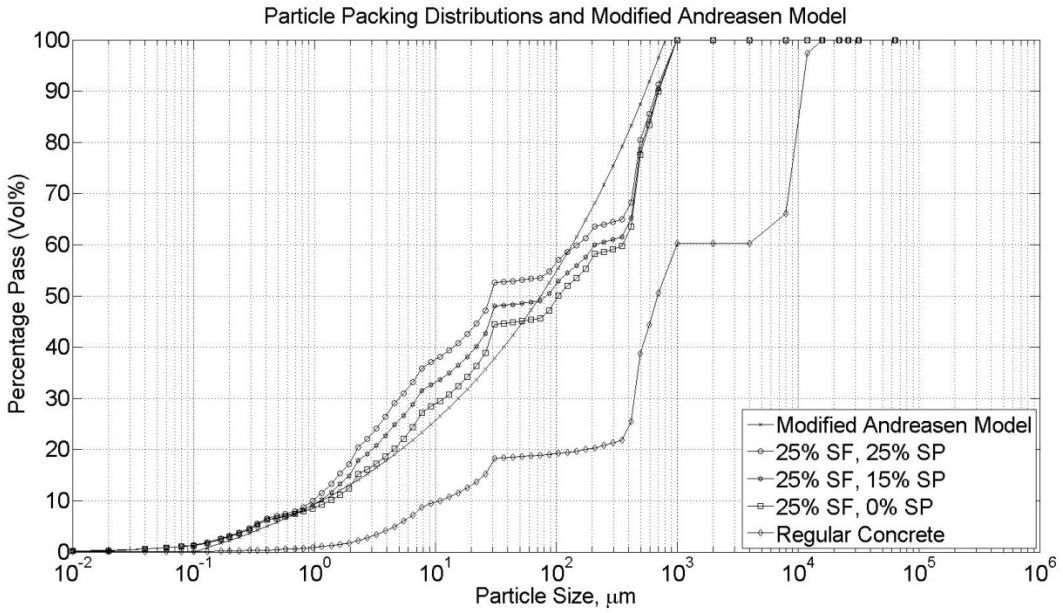

Figure 4-15: Particle Size Distributions for UHPC Mixes and Regular Concrete

One of the most important conclusions from this discussion is that silica powder has little influence on the durability of the tested UHPCs. Figure 4-15 explains why this is the case, i.e. eliminating silica powder does not significantly alter the particle size distribution. This conclusion has commercial implications because eliminating such a component from UHPC will significantly reduce its cost given the high price of silica powder, spurring widespread adoption.

Figure 4-15 also explains why changes in cement type had little effect on durability of the UHPCs tested. Each cement type had very similar particle size distributions. Thus, changes in cement type had no effect on the particle packing density of the UHPC. More work should be performed to determine the effects of cement type on other performance parameters.

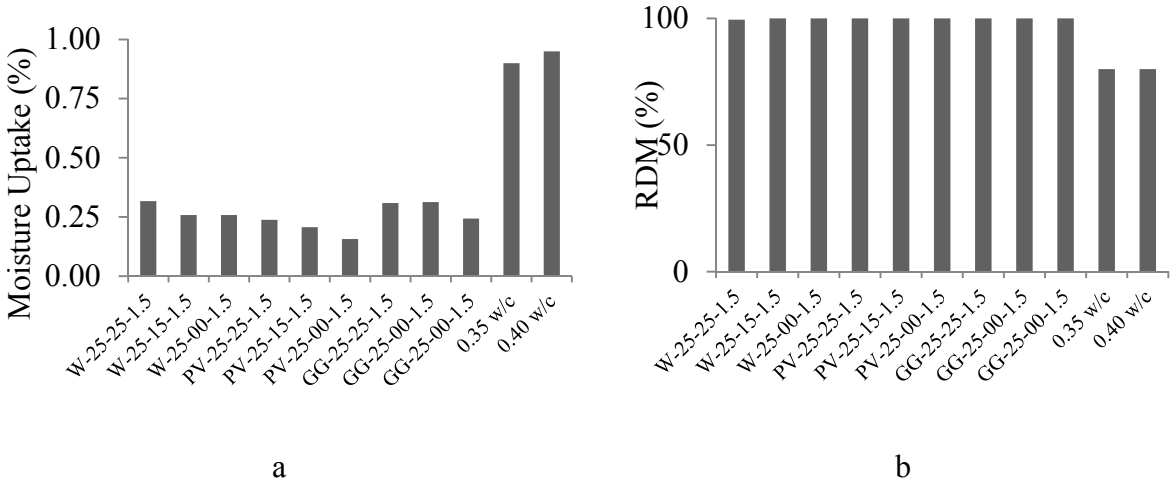

a b

Figure 4-16: Moisture Uptake and RDM% for UHPCs (27)

4.5. CONCLUSION

This experimental study investigated the durability performance of nine different blends of UHPC, including freeze-thaw resistance, chloride ion penetration resistance, and air void analysis. A modified CIF test and an air void analysis were conducted in order to evaluate freeze-thaw resistance. A rapid chloride permeability test was performed to test the concretes' resistance to the ingress of chlorides and other ions. The RDM percent change, mass loss and total air content were presented in order to gauge the concrete's freeze-thaw resistance. The coulombs passed were presented to gauge the concrete's ion permeability. The observations and findings of this study can be summarized as follows:

- All of the UHPC mixtures tested displayed exceptional resistance to freeze-thaw. All of the specimens tested experienced mass loss that was well below the mass loss limit in over 60 cycles of freeze-thaw.
- Changes in silica powder accounted for differences up to 54% mass loss in concrete's ability to withstand freeze-thaw while changes in cement type showed differences up to

43% in concrete's ability to withstand freeze-thaw. It should be noted that while the variations appear large, the absolute values on which they are based are actually small.

- The average air content for all of the specimens tested in this study ranged from 3.0% - 7.5% (1.8% - 4.0% regular concrete equivalent), below the limit for adequate resistance to freeze-thaw in regular concrete. The use of air content for assessing freeze-thaw resistance may therefore not be applicable for UHPCs. Unlike regular concrete, which relies on having sufficient void space to allow water to expand, the high freeze-thaw resistance in UHPCs is due to water being prevented from entering the material in the first place. Test results showed that all UHPCs tested had a very low water uptake percent and an unchanged RDM%, signifying no internal damage. This corresponds well to other studies of similar materials with dense matrices and shows that this phenomenon also occurs in UHPC.
- All of the UHPC mixtures show high resistance to chloride ion penetration. Concretes made with the Portland Type I / GGBS Cement blend showed the least permeability, followed by specimens made with white cement and Portland type V cement. Concretes containing silica powder at 25% showed slightly higher ion permeability than those with 15% silica powder. The least permeable concrete mixes had 0% silica powder.
- Particle size distribution studies showed that while variations in silica powder content affect the material's packing density differently across the particle size range, the resulting distributions still remain close to the optimal particle packing density. Test results confirm this observation and show that variations in silica powder content had little effect on the durability performance of the tested UHPC mixes. This signifies that this mix component could potentially be eliminated to reduce cost. Studies in Chapter 3 confirm that that

elimination of silica powder, which is a key part of proprietary mixes, does not significantly influence the short term mechanical properties of the material.

5. FACTORS AFFECTING BAR BOND DEVELOPMENT FOR UHPC

5.1. OVERVIEW

While UHPC's tensile and compression behaviors are relatively well understood, an in-depth analysis of UHPC's behavior at the component level, specifically the bonding ability between UHPC and steel bar reinforcement is lacking and the meager published data is contradictory. In the study presented in this chapter, a series of tests was performed in order to characterize the bond relationship of a non-proprietary UHPC blend with steel bar reinforcement. A series of bar pull out tests were conducted using plain and epoxy-coated grade 60 bars with nominal sizes of #4, #5 and #6 (13 mm, 16 mm, and 19 mm). Other experimental parameters include three development lengths (2", 3" and 4"), two fiber orientations (longitudinal and transverse to the steel bar), two steel fiber volume contents (1% and 2%) and bond strength at early age curing (1, 3 and 7 days). Additionally, the results of four flexure bending tests using UHPC lap spliced joints (discussed in more detail in Chapter 6) were compared to the pull out results in order to determine the bond capacity in a realistic loading scenario. Results from pull out testing show that bonding stress capacity decreases with increased embedment length suggesting a non-uniform distribution of bond stresses. Bond capacity in lap-spliced joints was less than in simple pull out tests, but within current design limits for regular reinforced concrete.

5.2. EXPERIMENTAL PARAMETERS AND PROCEDURE:

5.2.1. Bar Pull Out Testing Program and Test Set Up

The simple bar pull out test is the most widely used measure of bond capacity in concrete due to its simplicity and ease of implementation. It is also considered to be the least accurate testing

method as this test method tends to overestimate the bond capacity (6). With this set up, when the steel bar is placed into tension, the surrounding concrete is placed into compression. This in turn causes compressive struts to form between the supports and the surface of the bar, placing the bar surface and bearings under compression. Unlike real structures, the surface's compressive forces are caused by the load application, and not the relative movement between the concrete and the bar. In order to minimize this effect during the testing, a modified method of supporting the concrete was implemented (Figure 5-1a).

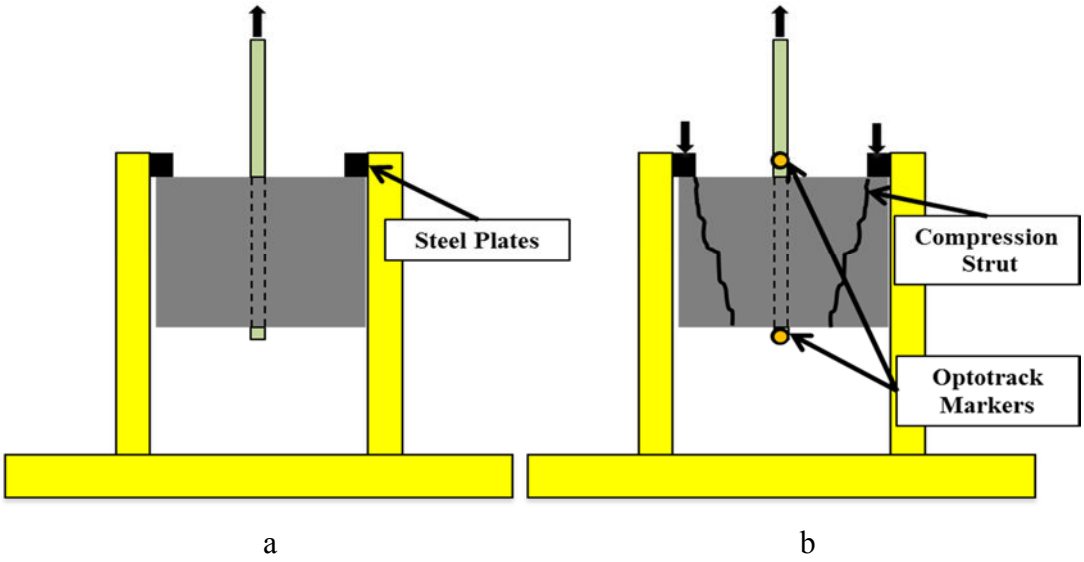

Figure 5-1: (a) Test Set Up for Bar Pull Out (b) and Instrumentation and Load Path for Specimen

Unlike the traditional bar pull out case where the entire surface of the concrete is used as a support, the new method makes use of the high bearing strength of the UHPC to minimize the surface area needed. The new configuration uses 4 small square plates, with an area of 0.5 in^2 (13 mm^2) to support the specimen. Each support was placed 2.75" (70 mm) away from the steel bar, distancing the concrete surrounding the bar from any compressive struts which may form during loading.

Specimens were subjected to a quasi-static displacement controlled load, using a 100 kip Instron hydraulic machine, at a rate of 0.001 in/sec (0.025 mm/sec). Force applied on the specimen was recorded using a 100-kip load cell. Slip in the bar was recorded using the Optotrack displacement tracking system (Figure 5-1b), which is a non-contact measurement system that employs infrared markers.

This series of tests investigated the effects of several parameters on the bonding between the UHPC and the steel bars. As shown in Table 5-1, three different bar diameters were tested at #4, #5 and #6 (13 mm, 16 mm and 19 mm), for both plain and epoxy coated bars. Each of the bars was subjected to embedment lengths of 2", 3" and 4" (50 mm, 75 mm and 100 mm). Additionally, two different bar sizes were used to investigate the differences caused by fiber alignment during casting. Specimens were casted with fibers preferentially aligned parallel with the bar and transversely to the bar (Figure 5-2). Two different bar types were used to evaluate the effect of fiber content at 1% and 2% by volume. Finally, UHPC specimens were casted and tested at 1, 3 and 7 days cured in order to determine the early age bonding ability of the material.

The naming convention for the tests performed is as follows: the first entry represents the bar size and coating (black bars or epoxy coated), followed by the embedded length in mm, the fiber volume percentage, the casting orientation (P for parallel or T for transverse) and the age of the UHPC (1, 3, 7 or 28 days). For example, 13B-100-2%-P-28D represents a #4 (13 mm) diameter plain black bar, embedded 4" (100 mm), with 2% fibers by volume, UHPC casted parallel to the steel reinforcement at 28 days.

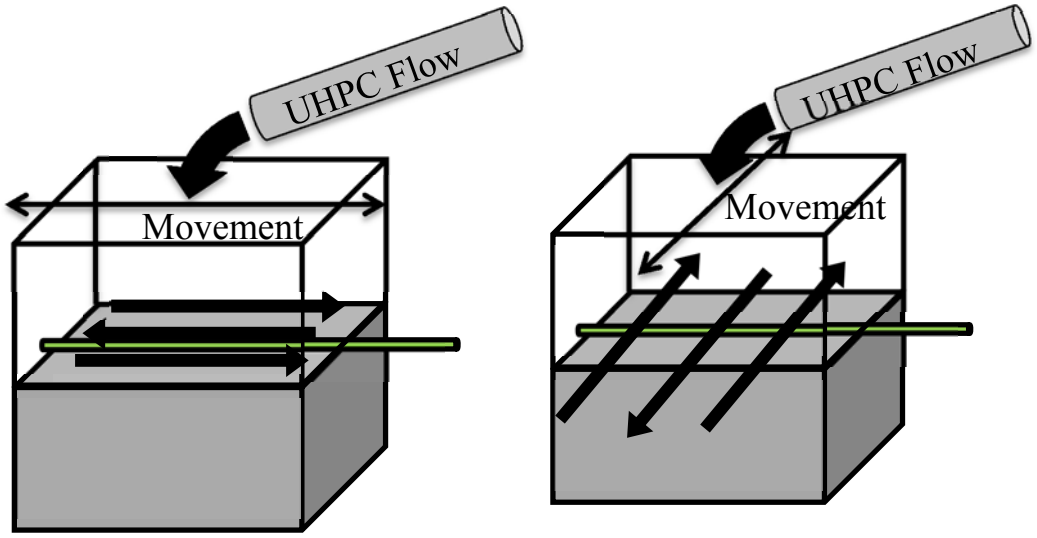

a b

Figure 5-2: (a) Fibers Aligned Parallel to Bar (b) Fibers Aligned Transversely to Bar

5.2.2. Lap Splice Joint Testing Program

Beam specimens F-100-1P-1, F-100-1P-2, F-100-2P-1 and F-100-2P-2 described in Chapter 6 represent a more realistic anchorage scenario for UHPC. As discussed later on in Chapter 6, these specimens comprise two regular precast concrete beam elements joined together at the center with a UHPC closure pour. Bottom bars are subjected to pull out in a lap splice configuration when the beams are subjected to flexural loading. The difference between pull out and lap splice testing configurations has been understood for regular concrete for some time. ACI Committee 318-05, Section 12.15.2 (and AASHTO LFRD 5.11.5.3.1) recommends multiplying the required anchorage length by 1.3 l_d when designing a non-contact lap splice vs. simple bar pull out for regular concrete.

Name	# of Tests	Bar Diameter (mm)	Coating	Embedment Length inches (mm)	Fiber Content (% vol.)	Casting Orientation	Curing Age (days)
13B-100-2%-P-28D	2	#4 (13)	None	4” (100)	2.0%	Parallel	28
13E-100-2%-P-28D	2	#4 (13)	Epoxy	4” (100)	2.0%	Parallel	28
13B-75-2%-P-28D	2	#4 (13)	None	3” (75)	2.0%	Parallel	28
13E-75-2%-P-28D	2	#4 (13)	Epoxy	3” (75)	2.0%	Parallel	28
13B-50-2%-P-28D	2	#4 (13)	None	2” (50)	2.0%	Parallel	28
13E-50-2%-P-28D	2	#4 (13)	Epoxy	2” (50)	2.0%	Parallel	28
16B-100-2%-P-28D	3	#5 (16)	None	4” (100)	2.0%	Parallel	28
16E-100-2%-P-28D	3	#5 (16)	Epoxy	4” (100)	2.0%	Parallel	28
16B-75-2%-P-28D	2	#5 (16)	None	3” (75)	2.0%	Parallel	28
16E-75-2%-P-28D	2	#5 (16)	Epoxy	3” (75)	2.0%	Parallel	28
16B-50-2%-P-28D	2	#5 (16)	None	2” (50)	2.0%	Parallel	28
16E-50-2%-P-28D	2	#5 (16)	Epoxy	2” (50)	2.0%	Parallel	28
19B-100-2%-P-28D	2	#6 (19)	None	4” (100)	2.0%	Parallel	28
19E-100-2%-P-28D	2	#6 (19)	Epoxy	4” (100)	2.0%	Parallel	28
19B-75-2%-P-28D	2	#6 (19)	None	3” (75)	2.0%	Parallel	28
19E-75-2%-P-28D	2	#6 (19)	Epoxy	3” (75)	2.0%	Parallel	28
19B-50-2%-P-28D	2	#6 (19)	None	2” (50)	2.0%	Parallel	28
19E-50-2%-P-28D	2	#6 (19)	Epoxy	2” (50)	2.0%	Parallel	28
19B-75-1%-P-28D	2	#6 (19)	None	3” (75)	1.0%	Parallel	28
19E-75-2%-T-28D	2	#6 (19)	Epoxy	3” (75)	2.0%	Trans.	28
16E-100-2%-P-1D	2	#5 (16)	Epoxy	4” (100)	2.0%	Parallel	1
16E-100-2%-P-3D	2	#5 (16)	Epoxy	4” (100)	2.0%	Parallel	3
16E-100-2%-P-7D	2	#5 (16)	Epoxy	4” (100)	2.0%	Parallel	7
16B-100-2%-T-	3	#5 (16)	None	4” (100)	2.0%	Trans.	28
16E-100-1%-P-28D	3	#5 (16)	Epoxy	4” (100)	1.0%	Parallel	28
16E-100-2%-P-28D	3	#5 (16)	Epoxy	4” (100)	2.0%	Parallel	28

Table 5-1: Experimental Parameters and Number of Tests

Some details from Chapter 6 are repeated here for the sake of readability. Full details are found in Chapter 6. Figure 5-3 shows the construction and reinforcement details for the specimen. Longitudinal bars were spaced at 6.3” (160 mm) and transverse bars were spaced at 8” (200 mm). The lower layer of reinforcement sat at a depth of 3.3” (85 mm) (measured from the top surface) while the upper layer was placed at a depth of 1.4” (36 mm). All reinforcement consisted of epoxy-coated bars with a diameter of 16 mm (#5 bars). The UHPC joint measured 4” (100 mm) wide with a lap splice length of 3.6” (90 mm). All tests were subjected to four-point bending as shown in Figure 5-4. The UHPC joint was cast in order to favor orientation of the steel fibers parallel to the reinforcement bar direction. Force in the steel bars was computed from a cracked section analysis at the joint face.

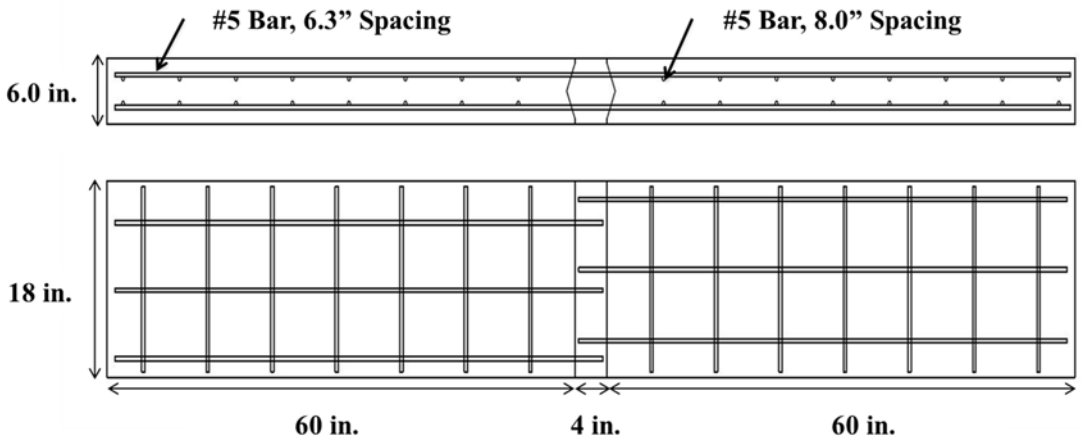

Figure 5-3: Construction and Reinforcement Details for Precast Decks with UHPC Joint

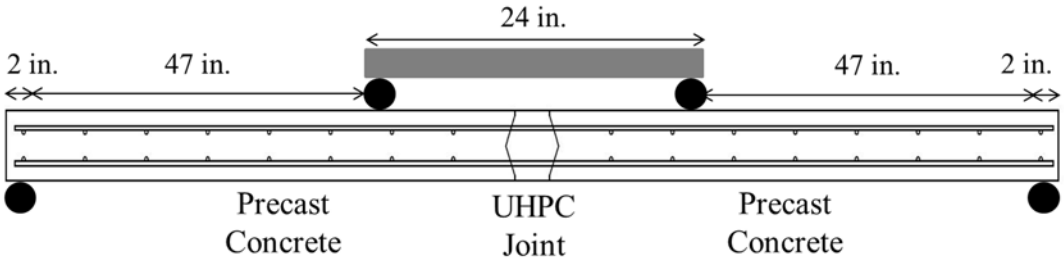

Figure 5-4: Four Point Bending Test Set Up for Flexure Test for Specimens F-100-1P-1, F-100-1P-2, F-100-2P-1 and F-100-2P-2

As discussed in Chapter 6, the beams were subjected to a displacement controlled, quasi-static load at a rate of 0.001 in/sec (0.025 mm/sec), using a 100 kip Instron hydraulic machine. Force on the specimen was recorded using a 100-kip load cell. Deformation in the UHPC joint was recorded using the Optotrack tracking system on one face of the specimen and through Digital Image Correlation on the other face.

5.2.3. Material Properties

The precast concrete beam elements were constructed using 35 MPa (5000 psi) concrete. Slump was controlled at <6" (150 mm) with a maximum aggregate diameter of 0.8" (20 mm). All steel reinforcement bars were grade 60 steel. The UHPC joint and the pull out cubes were constructed using mix GG-25-00 outlined in Chapter 3. For the simple bar pull out tests, all UHPCs consisting of 2% steel fibers by volume achieved an average 28-day compressive strength of 27.7 ksi (190.9 MPa) and 26.1 ksi (180.1 MPa) for UHPCs containing 1% steel fibers by volume. For the lap spliced joint tests, UHPCs achieved a 28 day average compressive strength of 27.9 ksi (192.36 MPa) at 2% steel fibers by volume and 26.4 (182.71 MPa) at 1% steel fibers. The regular concrete used in precast beams averaged a 28 day compressive strength of 5.25 ksi (36.23 MPa). The steel fibers are plain, smooth fibers (unlike the brass coated fibers used in chapters 3 and 4). Each fiber

is 0.75” (19 mm) long with a diameter of 0.0078” (0.2 mm) and minimum tensile strength of 285 ksi (1965 MPa).

RESULTS AND DISCUSSION

5.2.4. Bar Pull Out Results

Table **5-2** below shows the data from the bar pull out testing and lists the type of failure mode for each specimen. Testing revealed three distinct failure modes for bond (Figure 5-5); bar fracture of the steel reinforcement, slip of the bar from the UHPC, and a conical shaped failure in which the UHPC attached to the bar separates from the UHPC in the remaining cube. Data on force and bond stress are listed for the peak load at these failures. Bond stress is computed as the achieved pull out force divided by the initial surface area of the embedded portion of the bar.

(a) (b) (c)

Figure 5-5: (a) Bar Fracture, (b) Bar Slip, and (c) Conical Concrete Failure

Name	Mode of Failure			Bar Force Failure (kips)			Bond at Failure (ksi)		
	Test 1	Test 2	Test 3	Test 1	Test 2	Test 3	Test 1	Test 2	Test 3
13B-100-2%-P-28D	Fracture	Fracture	-	17.5	17.6	-	2.8	2.8	-
13E-100-2%-P-28D	Fracture	Fracture	-	17.5	17.6	-	2.8	2.8	-
13B-75-2%-P-28D	Fracture	Yield, Slip	-	15.7	14.9	-	3.3	3.1	-
13E-75-2%-P-28D	Fracture	Yield, Slip	-	16.1	15.6	-	3.4	3.3	-
13B-50-2%-P-28D	Slip	Yield, Slip	-	14.9	15.3	-	4.7	4.9	-
13E-50-2%-P-28D	Slip	Slip	-	13.8	12.0	-	4.4	3.8	-
16B-100-2%-P-28D	Slip	Slip	Slip	18.3	17.5	23.8	2.3	2.2	3.0
16E-100-2%-P-28D	Slip	Slip	Slip	18.5	20.9	22.0	2.4	2.7	2.8
16B-75-2%-P-28D	Slip	Slip	-	16.0	14.2	-	2.7	2.4	-
16E-75-2%-P-28D	Slip	Slip	-	15.5	17.0	-	2.6	2.9	-
16B-50-2%-P-28D	Slip	Slip	-	17.6	17.7	-	4.5	4.5	-
16E-50-2%-P-28D	Slip	Slip	-	17.6	18.0	-	4.5	4.6	-
19B-100-2%-P-28D	Slip	Slip	-	19.8	19.6	-	2.1	2.1	-
19E-100-2%-P-28D	Slip	Slip	-	20.1	20.8	-	2.1	2.2	-
19B-75-2%-P-28D	Cone	Cone	-	19.1	16.9	-	2.7	2.4	-
19E-75-2%-P-28D	Cone	Cone	-	21.7	17.3	-	3.1	2.5	-
19B-50-2%-P-28D	Cone	Cone	-	13.7	17.6	-	2.9	3.7	-
19E-50-2%-P-28D	Cone	Cone	-	18.0	13.7	-	3.8	2.9	-
19B-75-1%-P-28D	Slip	Slip	-	10.7	11.9	-	1.5	1.7	-
19E-75-2%-T-28D	Slip	Slip	-	15.6	16.5	-	2.1	2.2	-
16E-100-2%-P-1D	Slip	Slip	-	12.7	11.1	-	1.6	1.4	-
16E-100-2%-P-3D	Slip	Slip	-	13.6	12.7	-	1.7	1.6	-
16E-100-2%-P-7D	Slip	Slip	-	16.9	18.6	-	1.9	2.3	-
16B-100-2%-T-28D	Slip	Slip	Slip	20.6	21.0	21.4	2.6	2.7	2.7
16E-100-1%-P-28D	Slip	Slip	Slip	16.0	17.0	17.7	2.0	2.1	2.2
16E-100-2%-P-28D	Slip	Slip	Slip	17.6	21.2	21.7	2.2	2.7	2.7

Table 5-2: Test Results for Simple Bar Pull Out

5.2.5. Effect of Embedment Length

Figure 5-6 shows the effects of embedment length force-slip relation for a #4 (13 mm) dia. bar subjected to simple bar pull out. At 4" (100 mm) embedment (Figure 5-6a), all specimens failed via bar fracture, with no difference between black and epoxy coated bars. At an embedment of 3" (75 mm) (Figure 5-6b), the specimens failed in either bar fracture, or bar yielding, followed by slip in the bar. Again, differences between plain and epoxy bars were minor. At 2" (50 mm) embedment (Figure 5-6c), only one specimen yielded, followed by bar slip. The remaining specimens all experienced pure slip. At 2" (50 mm), the differences between the black and epoxy bars were more apparent, with black bars achieving a higher pull out force, and higher bond stresses. Increased ductility seen in Figure 5-6a and Figure 5-6b compared to Figure 5-6c is a result of the steel yielding prior to failure.

Figure 5-6d plots the bond stresses measured vs. embedment. As seen, when embedment was increased, the bond stresses decreased, almost linearly. This suggests that an uneven distribution of bond stresses occurs along the length of the bar. In general, three mechanisms provide resistance against the pull out of reinforcing bars; chemical adhesion, friction and the mechanical interaction between the concrete and steel. As load is applied to the specimens, chemical and frictional resistances are quickly overcome thus making the mechanical interaction the predominant resistance mechanism. Figure 5-7 shows an idealization of the reaction forces experienced by the reinforcing steel. The horizontal component of this force is referred to as the shear force. The vertical component of the bearing force creates a radial force that is responsible for splitting in the surrounding concrete.

In regular concretes, the pull out force is resisted uniformly along the length of the embedded portion of the bar (Azizinamini, 1993). In the case of high strength concretes, at low axial load

levels, the ribs closest to the loading point come into contact with concrete first, applying a bearing force to the concrete. As the load continues to increase, the bearing force increases, and the next closest rib also begin to resist the applied load. The increased bearing capacity of the concrete inhibits crushing of the concrete in the vicinity of the ribs, and thus the radial component of the force from the bearing force promotes splitting in the surrounding concrete. By the time the ultimate load is reached due to the splitting, all ribs may not be participating in resisting the load, requiring then that the first few ribs contribute the most, i.e. the bond resistance is non-uniform along the length.

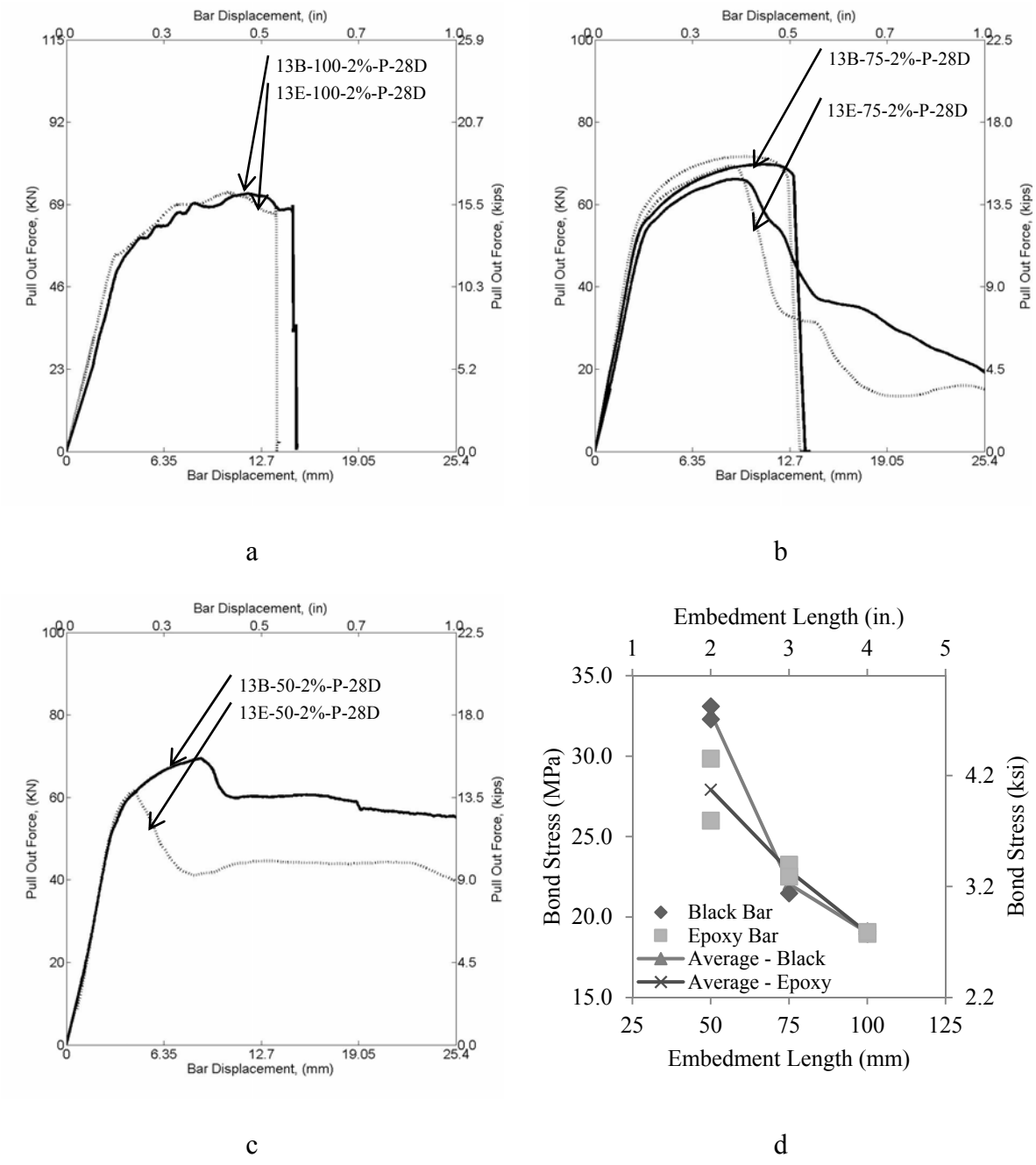

Figure 5-6: Force Slip for 13 mm bars at (a) 100 mm, (b) 75 mm, and (c) 50 mm embedment, (d) Peak Bond Stress vs. Embedment Length

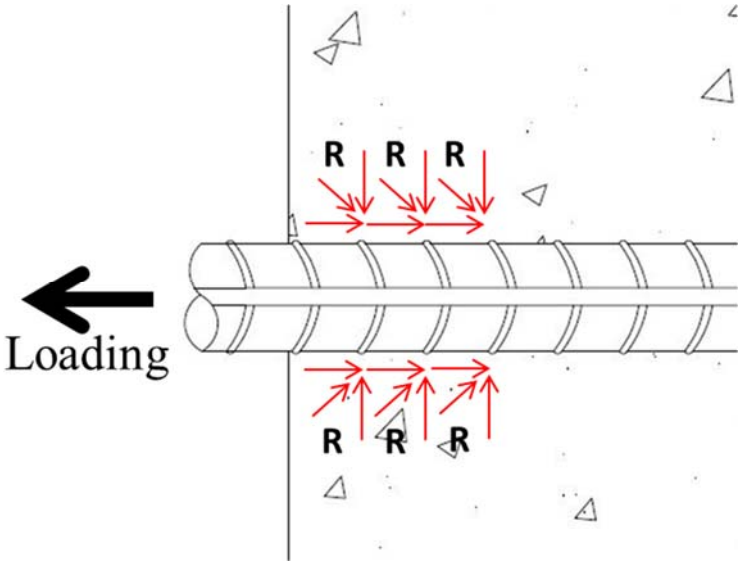

Figure 5-7: Idealized Reaction of Reinforcing Steel Embedded in Concrete, Subjected to Tension, Cross Sectional View

Figure 5-8 shows the results of embedment for #5 (16 mm) dia. bars. Unlike the #4 (13 mm) dia. bar, no #5 bars reached bar fracture. All of the specimens failed via bar slip. At 4" (100 mm), black bars were able to reach a slightly higher bond stress vs. their epoxy counter parts. This also occurred at 2" (50 mm), though at 3" (75 mm) there was no discernible difference. Again, for bar types, the total average bond stress recorded decreased with increasing embedment length. This again is attributed to the uneven force distribution along the length of the bar.

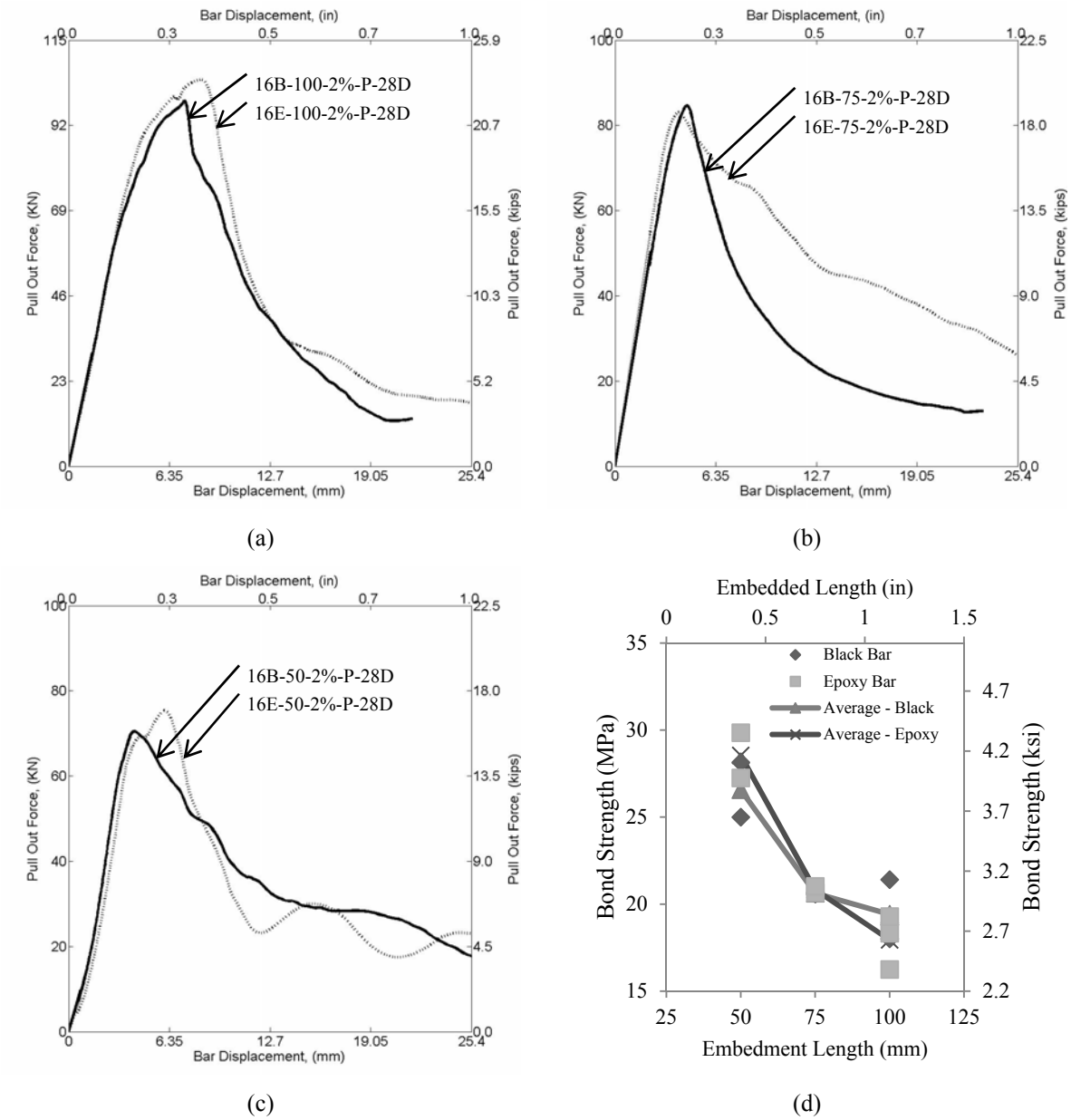

Figure 5-8: Force Slip for 16 mm bars at (a) 100 mm, (b) 75 mm, and (c) 50 mm embedment, (d) Peak Bond Stress vs. Embedment Length

Figure 5-9 shows the data for #6 (19.0 mm) dia. bars. At 4" (100 mm), all of the bars experienced slip. At 3" (75 mm) and 2" (50 mm), specimens all failed due to a conical separation in the concrete. The UHPC bonded to the bar separated from the UHPC in the cube, leading to a drop in strength. As the main failure was a tensile failure in the concrete, specimens that experienced a

cone failure showed no discernible differences between the black and epoxy coated bars. Also, as seen with the previous bar diameters, as embedment increases, the overall bond stress decreases.

The data collected on embedment from the current study differs from those reported by others. Figure 5-10a shows the bond stress data available for a #5 epoxy coated bar from previous works by Graybeal and the data collected from this study. The Graybeal bond data from the 2014 bond report (2014) shows a linear increase in the bond stress capacity with increased embedment length. However, the current study shows an opposite trend at the lower embedment lengths; increased bond stress with decreased embedment. As previously stated, the reported trend suggests that the bond development along the length of the steel bar in UHPC is non-uniform and has been observed in fiber reinforced concretes in the past (Azizinamini, 1993). In fiber reinforced concretes, the increased compressive strength delays crushing in the area surrounding the steel ribs, promoting instead splitting cracks in the surrounding concrete. As noted earlier, the ribs deeper in the embedded region may not resist the applied axial loading prior to cracking in the UHPC, and therefore the first few ribs carry the highest loads. The report by Graybeal makes mention of this phenomena, but suggests its effect may not be present in UHPC, whereas data collected from this study seems to confirm this event. Additionally, a separate Graybeal report from 2010 lists a much higher bond stress, close to 14.5 ksi (100 MPa) at a 4” (100 mm) embedment length. While some of these variations can be attributed to the test method selected (the 2014 study uses lap splices, while the 2010 study makes use of UHPC cylinders and the current study used UHPC cubes. Also both Graybeal reports use Ductal.), there are still significant differences and more work should be done here to further understand the bonding of UHPCs, especially at lower embedment lengths.

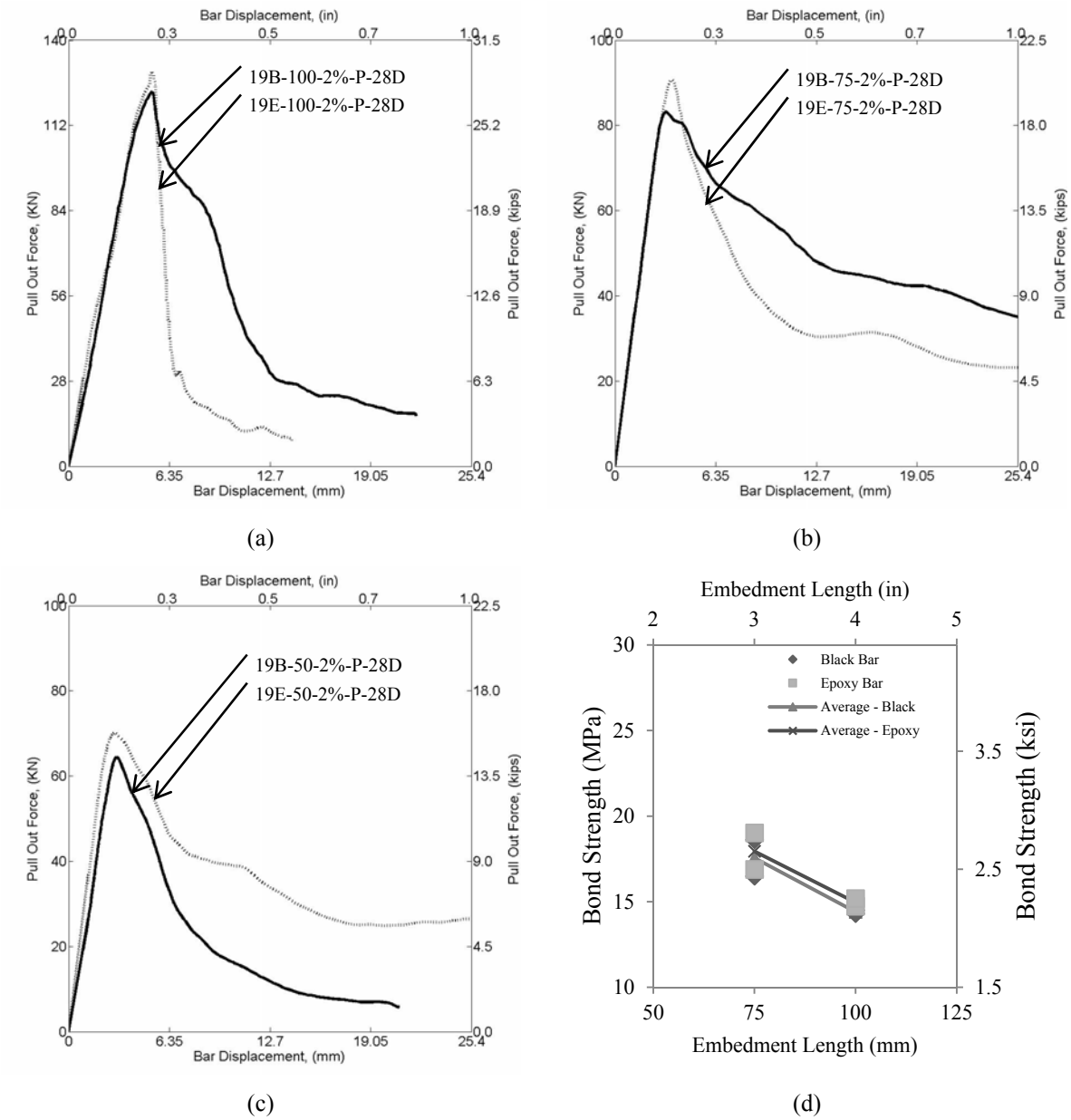

Figure 5-9: Force Slip for 19 mm bars at (a) 100 mm, (b) 75 mm, and (c) 50 mm embedment, (d) Peak Bond Stress vs. Embedment Length

Additionally, Figure 5-10 shows the reported bond values for the bar sizes tested in this study along with all other published data found by the authors. From the scatter, it is difficult to discern a clear trend, which again highlights the high variability in the reported literature. For those unspecified, bar coating used for testing was unclear.

5.2.6. Effect UHPC Cast Orientation on Bond

The effect of casting orientation and fiber alignment on bond was also investigated. Figure 5-11a shows the resulting relation for specimens with UHPC cast parallel and transversely to the steel reinforcement for a #5 (16 mm) bar. As seen, there is little difference in the achieved strengths. For the #6 (19 mm) bars, fibers aligned parallel with the bar provide a somewhat higher force resistance than those transverse to the steel bar, which leads to a 17 % difference in the peak bond stresses reached (Figure 5-11b). A closer examination of Table 5-3 shows that these differences are within the statistical range of variations in the data, and are more likely due to other factors (number of ribs embedded, etc.).

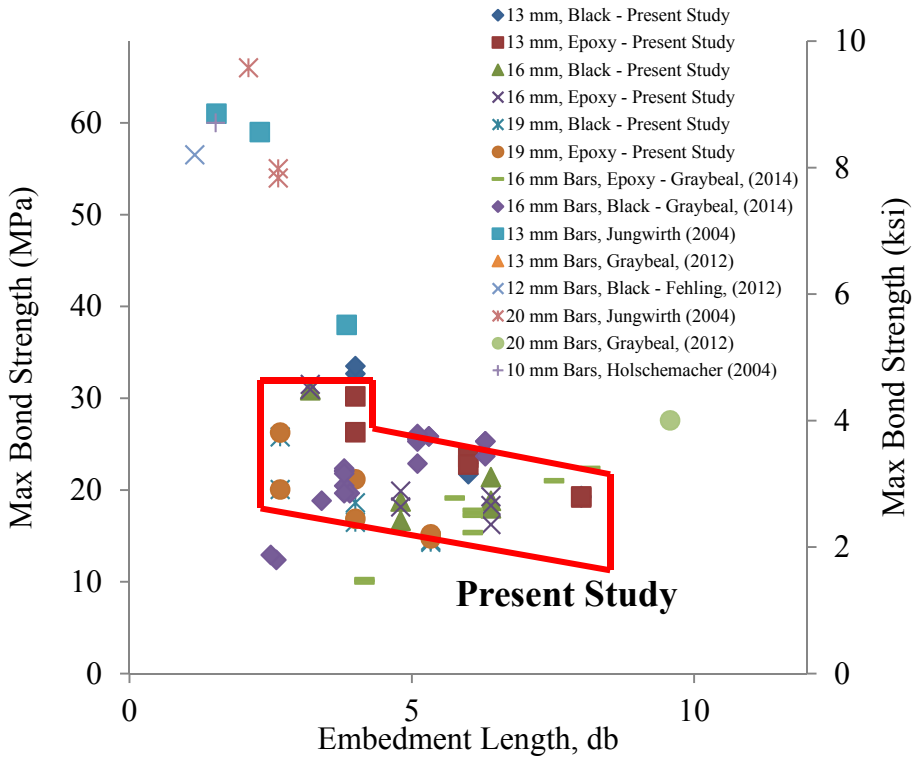

Figure 5-10: Scatter of the current data available for 13 mm, 16 mm, and 19 mm bars

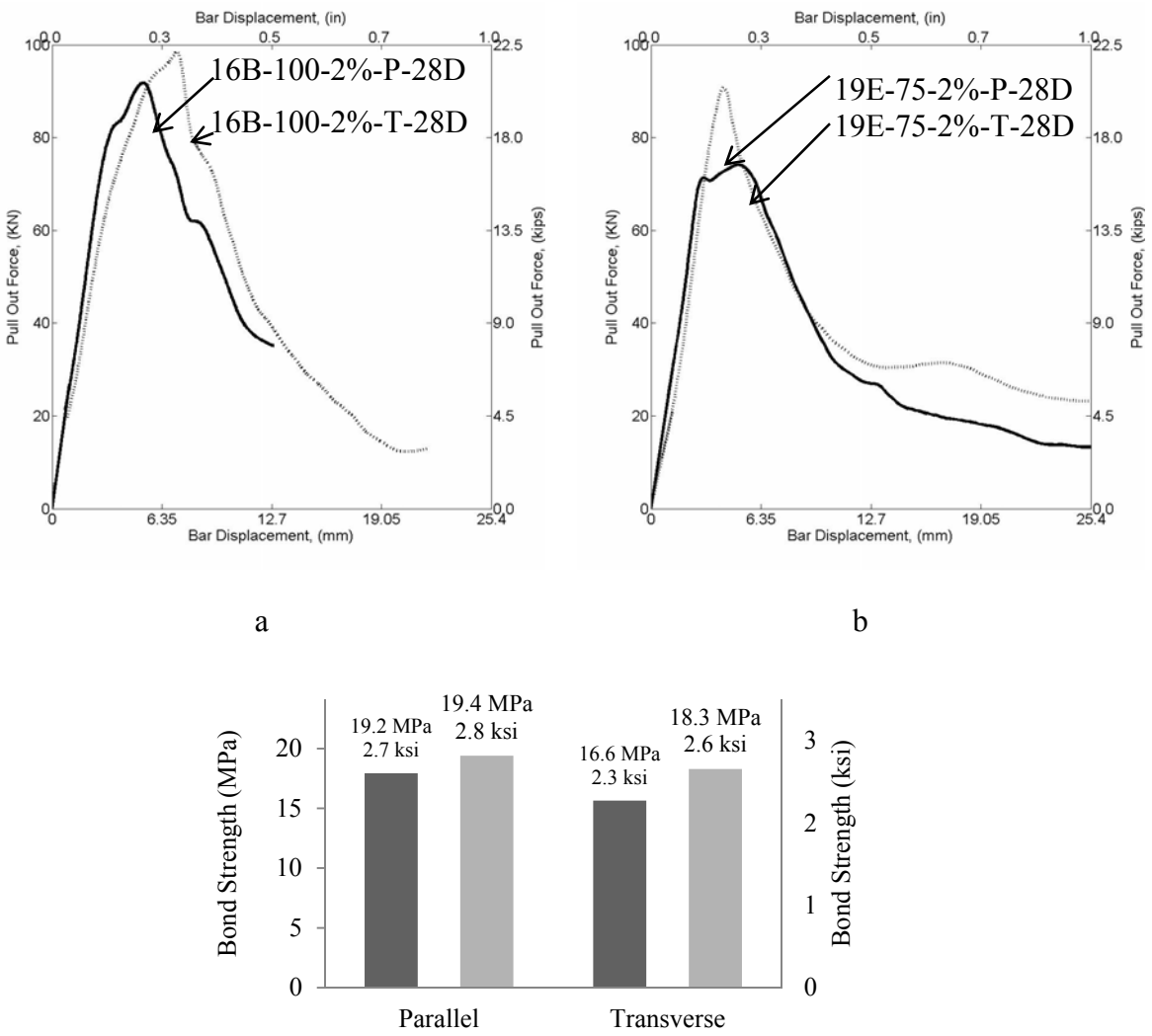

Figure 5-11: (a) Force Slip for 16mm bars with Parallel and Transverse Fibers, (b) Force Slip for 19 mm bars with Parallel and Transverse Fibers, and (c) Bond Stress Comparison (Dark Gray- 19 mm bars, Light Gray – 16 mm bars)

5.2.7. Effects of Fiber Volume Content

Two series of bar pull out tests were tested containing 1% fibers by volume and compared to those tested containing 2% fibers by volume. Figure 5-12a shows the two sets of force-slip relations for 16 mm bar specimens at 1% and 2% fibers by volume. The specimens containing only 1% fibers

developed 21% less force than those with 2% fibers. Bond stresses saw a similar reduction in strength. For the #6 (19 mm) bar specimens (Figure 5-12b), specimens containing only 1% fibers developed 36% less force than those with 2% fibers, again with similar reductions in bond stress. The larger drop in strength for the #6 (19 mm) bar is most likely due to differences in the number of ribs embedded from specimen to specimen. More testing should be performed to determine if the reduction in strength is lower with longer embedment at different fiber contents. Figure 5-12c shows the bond stresses compared for the two fiber contents. Averaging all 5 tests, average bond strength dropped 28% from specimens with 2% fibers by volume to 1% fibers by volume. Less fiber percentage by volume translates to fewer fibers bridging any cracks that may form during testing. This in turn reduces the confinement in the concrete, increases crack openings, and lowers slip resistance.

5.2.8. Early Age Testing of UHPC on Bond

An investigation into the bonding strength between UHPC and steel reinforcement was also performed at 1, 3 and 7 days cure time. From Figure 5-13a and Figure 5-13b, testing at 1 day generally yielded the lowest load strength and bond stress increasing at 3, 7 and 28 days respectively. Comparing Figures Figure 5-13c and Figure 5-13d, the compressive strength of the UHPC and the maximum bond stress achieved both increase asymptotically over the course of 28 days. Regular concrete follows a similar increase in early age strength vs. time which results from the pozzolonic reaction of the cement. As the UHPC uses the same cement found in regular concrete, a similar increase in strength over time is expected as the reaction requires time to complete. Similarly, as the pozzolonic reaction continues, the bonding between the cementitious material and the steel fibers strengthens. Enhanced fiber-concrete composite behavior increases

the total confinement available in the UHPC, which increases the bond strength. Also, the composite achieves approximately 75% of its pull-out strength after 7 days.

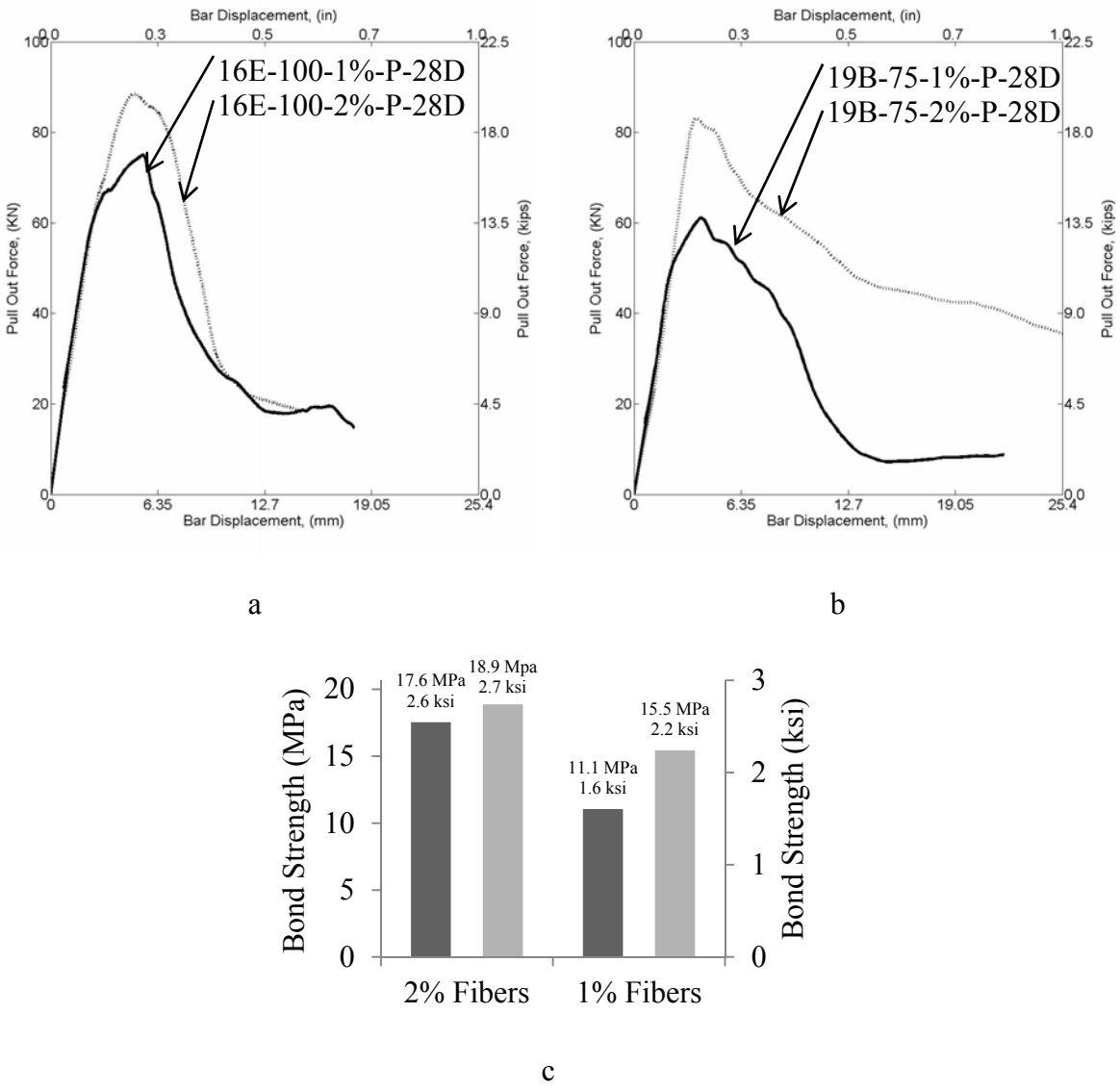

Figure 5-12: (a) Force Slip for 16 mm bars with 1% and 2% Fibers, (b) Force Slip for 19 mm bars with 1% and 2% Fibers, and (c) Bond Stress Comparison (Dark Gray – 19 mm bars, Light Gray – 16 mm bars)

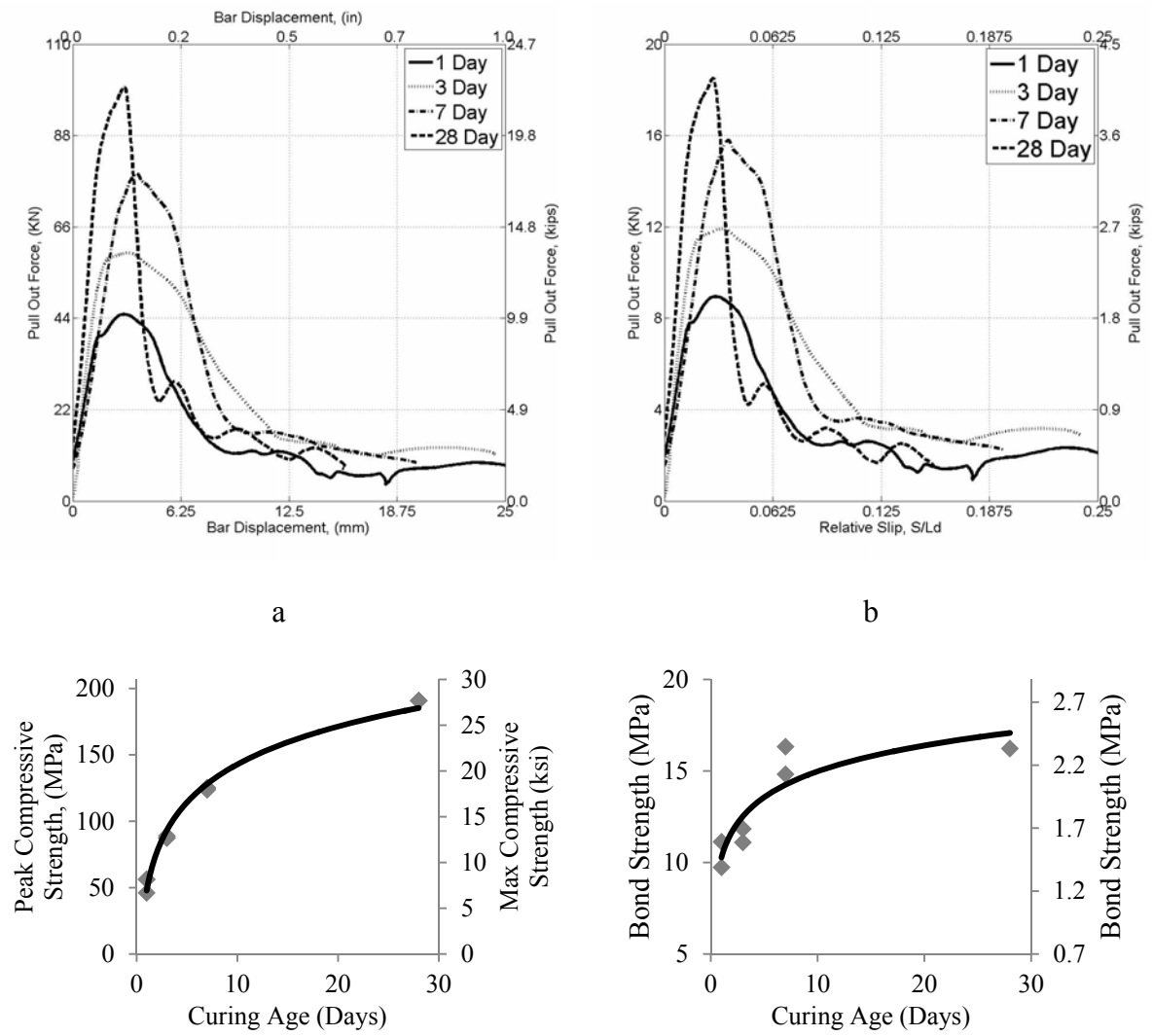

Figure 5-13: (a) Force-Slip Curve, (b) Bond Stress – Relative Slip, (c) Compressive Strength and (d) Bond Stress Data for Early Age Tests

5.2.9. Bar Pull Out vs. Lap Splice Beam Results

As discussed previously, the lap spliced specimens were constructed with the intention of comparing the bond data to that gathered from the simple bar pull out testing. All tests in this series contained #5 (16 mm) dia. bars. Pulls out tests in this configuration were embedded 100 mm, and the UHPC joints had an embedment of 4" (100 mm) and splice lengths of 3.6" (90 mm). Both UHPCs were tested at 1% and 2% fibers by volume. More details regarding the specimen details,

loading and detailed results can be found in Chapter 6. For brevity, only the results are displayed here (Table 5-3). Figure 5-14 lists the average bond stress achieved between the two series of specimens. At 2% fibers by volume, simple bar bull out specimens averaged bond stresses of 2.6 ksi (18.0 MPa), or about 12% more than the 2.3 ksi (15.7 MPa) achieved by the lap-spliced bars. For specimens containing 1% fibers by volume, specimens developed average bond strength 7% less in the lap splice vs. the pull out case. For both of these fiber volume contents, the decrease in strength sits within the current ACI (and AASHTO) limit of an increase of 1.3 l_d increase for lap spliced anchorages. Therefore, increasing simple bar test bond data by the factor prescribed by ACI (and AASHTO) is deemed acceptable for future designs of reduced UHPC anchorage lengths, albeit on the conservative side.

Test		Embedded Length	Splice Length	Force at Joint	Bond Stress
		inches (mm)	inches (mm)	kips	ksi
1	Flexure 1%	4” (100)	3.6” (90)	4.3	2.1
2	Flexure 1%	4” (100)	3.6” (90)	4.3	2.1
3	Flexure 2%	4” (100)	3.6” (90)	4.6	2.2
4	Flexure 2%	4” (100)	3.6” (90)	4.8	2.3

Table 5-3: Test Results Beam Lap Splice Tests

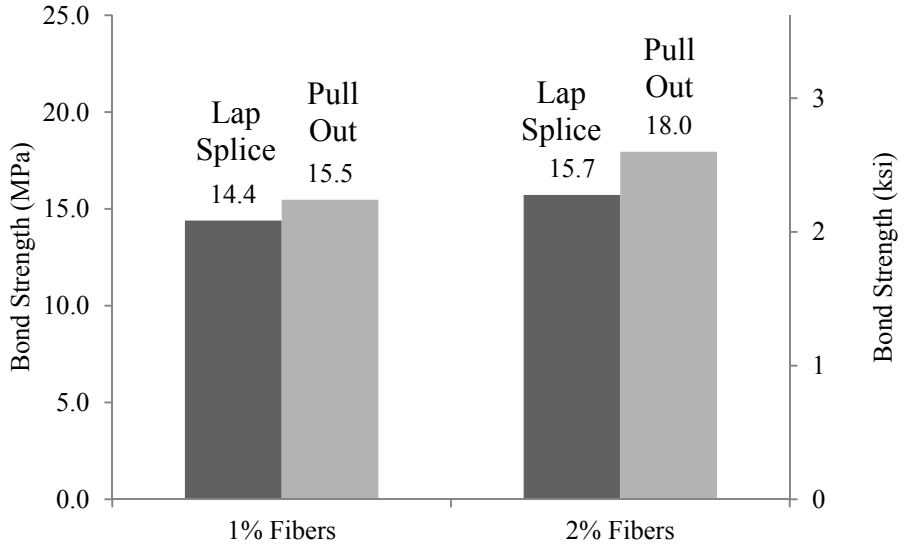

Figure 5-14: Average Bond Stresses in lap splices vs. bar pull out specimens.

5.2.10. Design Implications

Figure 5-15 shows the developed bar stress as a result of the bar coating, embedded length and bar size. The bar stress versus embedment length trend approximately follows the familiar linear relationship seen in other concretes. The data is synthesized into Equation 5-1, which can be used for estimating development lengths in UHPC. The recommendations are for the generic UHPC mix used in this study (Table 5-2), containing 2% fibers by volume and A615 grade 60 epoxy-coated and non-coated (black) bars.

$$\sigma_b = \Upsilon_{\text{config}}(23d_b + 185 + \Psi_c + \Psi_s)$$

$$\Psi_c = \begin{cases} 10 \; for \; Black \; Bar \\ 0 \; for \; Epoxy \; Bar \end{cases} \quad \Psi_s = \begin{cases} 220 \; for \; 13 \; mm \; bar \\ 110 \; for \; 16 \; mm \; bar \\ 0 \; for \; a \; 19 \; mm \; bar \end{cases} \quad \Upsilon_{\text{config}} \begin{cases} 1.0 \; for \; Simple \; Pull \; Out \\ 0.85 \; for \; Lap \; Spliced \end{cases}$$

Equation 5-1: Bar Stress as a function of Embedded Length

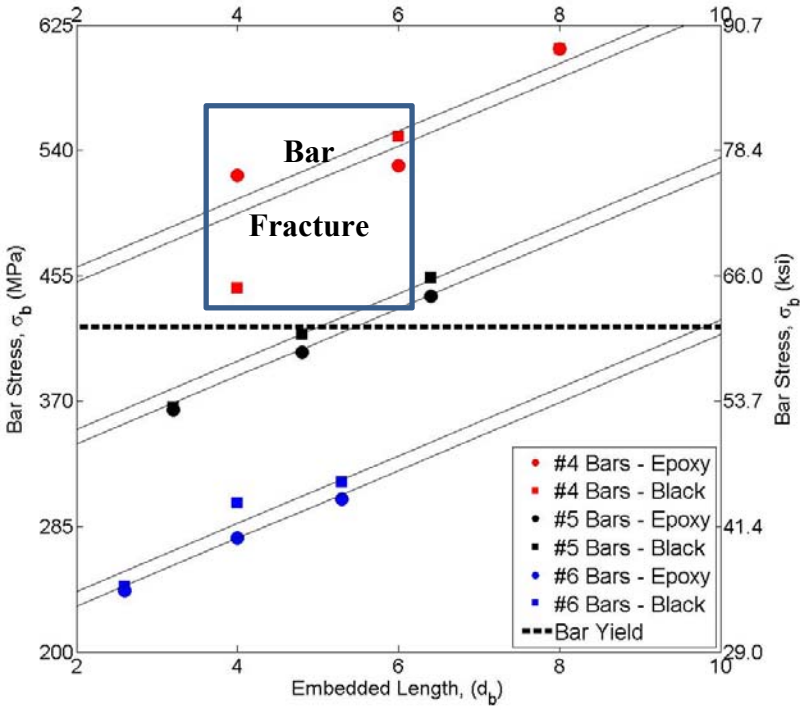

Figure 5-15: Maximum Average Bar Stress under Direct Pull Out

Where d_b is the embedded length of the bar in terms of the bar diameter, Ψ_c is the coating factor, and Ψ_s is the bar size factor. A factor of 15% accounts for the differences in bar force achieved in a pull out test vs. the lap spliced tests. This equation remains limited in scope. Future research plans to determine a more comprehensive relationship including bar cover, fiber content and other parameters.

5.3. CONCLUSION

The objective of this chapter was to investigate the bonding ability between non-proprietary UHPC and steel reinforcement bars. Simple bar pull out tests were performed at 3 different embedment

lengths, 2 bar coatings, 3 bar diameters, 2 fiber volume percentages, and 2 UHPC casting orientations. Early age bonding of UHPC was also tested at 1, 3 and 7 days. Additionally, 4 precast beams were joined together with a UHPC lap splice in order to compare the bonding between the simple pull out case and a more realistic anchorage scenario as well as the effect of fiber content.

- The bond stresses achieved in the simple bar pull out tests ranged from 1.13 ksi (7.8 MPa) to 4.8 ksi (33.1 MPa). At the lower limits of embedment lengths, increasing embedment leads to a reduction in the average bond stress achieved. This is attributed to an uneven distribution of force along the length of the bar, a fact that is established for high strength concretes. A recent series of tests on UHPC, albeit differing in set up and materials used, shows different trends than the data in this study, which suggests that additional investigations in this area are needed.
- Casting the UHPC with the alignment of the fibers transverse to the reinforcement steel showed negligible differences in bonding and strength. More testing should be done to investigate casting effects at a larger scale.
- Changes in steel fiber content by volume resulted in differences between 21% and 36% in bond strength achieved. This is due to reduced concrete strength at lower fiber contents and lower confinement provided.
- Lap spliced joints with UHPC containing 1% fibers by volume achieved just 8% less bond strength than those containing 2% fibers by volume. Since the cost of UHPC strongly depends on the fiber content, these results suggest that structural applications of UHPC with lower fiber volume contents (i.e. cheaper versions of UHPC) should be more extensively investigated in the future. Most current applications of UHPC entail the use of 2% or more of fibers by volume.

- Bond stresses in the simple bar pull out case were 12% higher than those observed in the lap spliced joints. This value currently falls within the current ACI design limits, making the current standards acceptable for future UHPC embedment design work. Since the result is based on a limited number of specimens and rather conservative, additional research is needed to confirm and refine it.

6. SIMPLIFIED UHPC JOINTS FOR BRIDGE CONSTRUCTION

6.1. OVERVIEW

This chapter investigates the use of UHPC for bridge joint connections between precast, regular concrete bridge deck elements. The proposed joints make use of UHPC's superior bond characteristics in order to provide a simple and effective method for the assembly of precast bridge elements. A total of 12 beams with joint widths of 4" (100 mm), 6" (150 mm), and 8" (200 mm) were constructed for physical testing and subsequently modeled. Of the twelve, 8 beams were tested under pure flexure. The four remaining beams were evaluated under combined shear and flexure loading conditions. Findings show that the beams with joint widths of 4" (100 mm) failed to sufficiently transfer load between the precast desks in both pure flexure and combined shear and flexure testing, resulting in splitting failure in the joint. Beams with joints at 6" (150 mm) and 8" (200 mm) were sufficient for achieving the required force transfer between the precast deck elements and were suitable for applications requiring simplified and expedited construction. Finite element simulations used to explore the effect of joint topology on system performance indicate that structural response hardly changes for the three types of joints considered.

6.2. DESIGN OF THE EXPERIMENTAL PROGRAM

As seen in Chapter 5, UHPCs exceptional ability to bond to steel bar reinforcement allows for small bar development lengths and, therefore, splice lengths. This characteristic enables smaller and simpler joints, which promote accelerated bridge construction methods. The objective of the test program in this chapter is to probe the lower limits of joint size in order to gain a better understanding of UHPC joint response.

6.2.1. Pure Flexure vs. Combined Shear and Flexure Testing

Two different testing set ups were implemented in this study. The first, a four-point bending test set up seen in Figure 6-1a places the UHPC joint in pure flexure. The second test type, an offset three-point bending set up (Figure 6-1b), subjects the UHPC joint to shear forces and moments. The shear and moments that develop along the length of the beam during testing are shown in Figure 6-1. The pure flexure test is intended to study the response of the joined beam under real world loading conditions where the influence of shear force is minimal. The combined shear and flexure test investigates response when a higher shear-moment ratio is present.

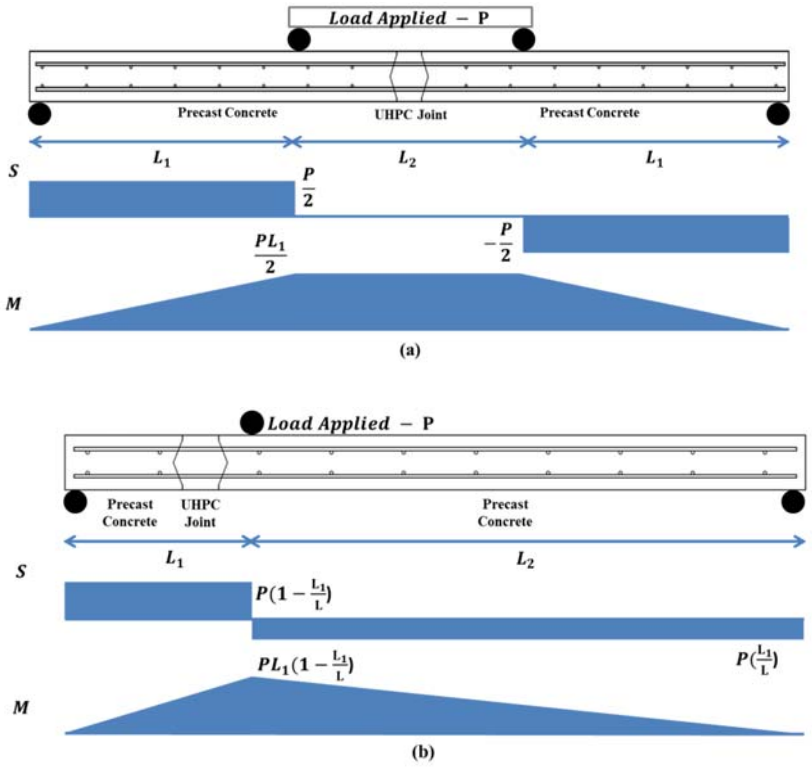

Figure 6-1: Shear and Moment forces in beams under (a) pure flexure loading and (b) combined shear and flexure testing

6.2.2. Joint Details & Selection

Currently the width of a joint for lap splice connection is determined by the lap length which is a function of the development length of the reinforcing bar, and is prescribed by ACI Committee 318 (2005). Equation 6-1 shows the current method for determining the development length for straight bar reinforcement for #6 (19 mm) bars and smaller:

$$L_d = \frac{f_y \psi_t \psi_e \lambda}{25\sqrt{f_c'}} d_b$$

Equation 6-1: Development Length for Straight Bar Reinforcement (ACI 318)

Where f_y = yield strength of the reinforcement (psi), ψ_t = reinforcement location factor, ψ_e = reinforcement coating factor, λ = lightweight concrete aggregate factor, f_c' = compressive strength of the concrete, and d_b = nominal diameter of the bar reinforcement. Equation 6-1 indicates that the required development length decreases with the square root of the compressive strength of the material. Although not explicitly developed or permitted for use with UHPC, it is interesting to note that the bond required for 25 ksi UHPC versus a regular 5 ksi concrete should be just under half of that required for regular concrete according to Equation 6-1.

Similarly, AASHTO LFRD design requires a development length for No. 11 bars or smaller to equal:

$$l_{db} = \frac{1.25 A_b f_y}{\sqrt{f_c'}}$$

Where A_b is the area of the bar in in2, f_y is the specified yield strength of the reinforcing bars (ksi), f'_c is the specified compressive strength of the concrete at 28 days (ksi) and d_b is diameter of the bar in inches.

6.2.3. Specimen Design

For ease of construction, non-contact lap splices are used in this study. Generally, contact lap splices are constructed such that the reinforcing bars are touching and tied together, minimizing displacements during the pouring of concrete. This is not a concern in precast element construction as the bars are already embedded in the precast concrete and not able to move in relation to each other. While the new low-cost alternative UHPC mix formulations used in this study have lower material costs than previous UHPC mixes, it is important to minimize the joint width as the alternative UHPC used to fill the joint still carries a higher cost as compared to conventional concrete.

Figure 6-2 shows the reinforcement and joint details for the specimens studied. For the pure flexure tests, each precast deck element measures 60" (1500 mm) in length, 18" (457 mm) wide and 6" (150 mm) deep. Joint lengths vary between 4", 6" and 8" (100, 150 and 200 mm). Longitudinal reinforcement is spaced at 6.3" (160 mm) along the width of the deck. Transverse reinforcement is spaced at 7.8" (200 mm) along the length of the deck. Reinforcement at the lower layer is placed at a depth of 3.5" (89 mm) and 1.5" (39 mm) for the upper layer.

Similarly, for the combined shear and flexure specimens, one of the precast deck element measures 60" (1500 mm) in length, 18" (457 mm) wide and 6" (150 mm) deep. The other precast element measures 13" (330 mm) long, with a width of 18" (457 mm) and depth of 6" (150 mm). Joint width is held constant at 4" (100 mm). Longitudinal reinforcement is spaced at 6.3" (160 mm) along the

width of the deck. Transverse reinforcement is spaced at 7.8” (200 mm) along the length of the deck. Reinforcement at the lower layer is placed at a depth of 3.5” (89 mm) and 1.5” (39 mm) for the upper layer.

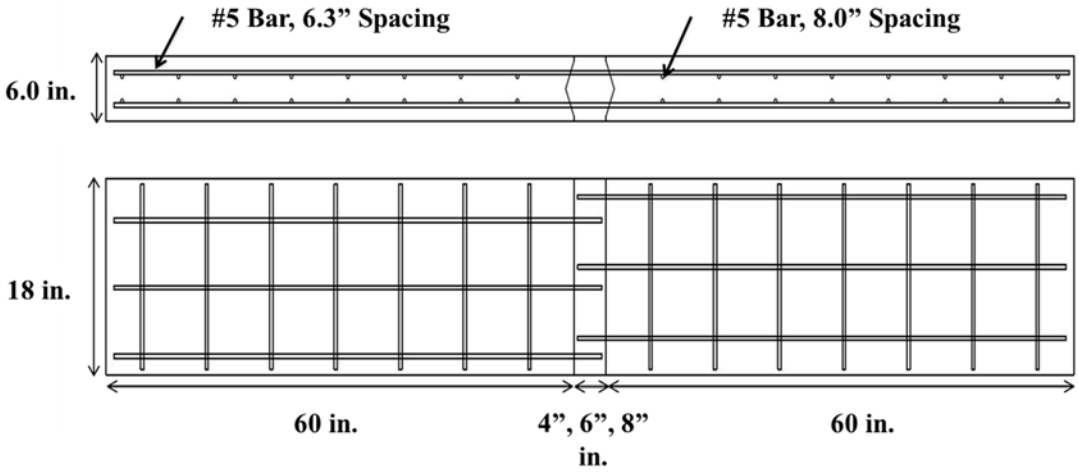

(a) Pure flexure specimens

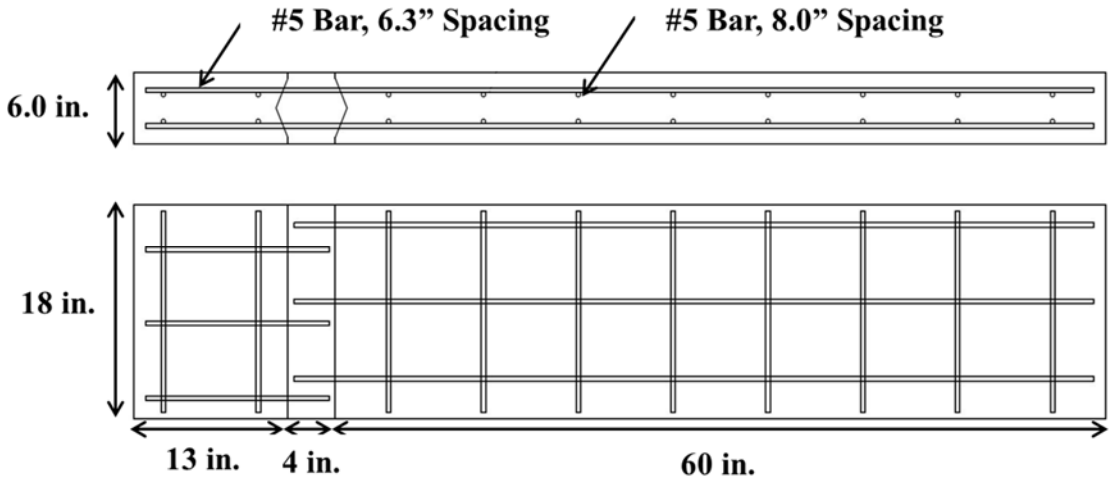

(b) Combined shear/flexure specimens

Figure 6-2: Joint Dimensions and Reinforcement Details

6.2.4. Specimens Tested and Material Parameters

Table 6-1 summarizes the main variables for the specimens tested in this study. The naming convention for the specimens is as follows: test type – joint width – fiber volume content – and test number. For example, an F-100-1P-1 mean the specimen was tested in pure flexure, with a 4" (100 mm) joint, containing 1.0% fiber volume content UHPC and was the first test in the series. All tests were performed after 28 days of concrete curing. Figure 6-2(a and b) provide a more detailed view of the lap spliced joint used for this study. The joint features a shear key design, minimizing the joint at the opening, expanding slightly in the center. This increased width at mid-depth enables an increased splice length while maintaining a small joint opening and minimizing total required volume of UHPC. Figure 6-2c shows the lap splice connection used for all of the specimens tested.

Name	Test Type	Lap Length, inches (mm) (Designed)	Lap Length, inches (Constructed)	Fiber Volume Content (%)	Inter-bar Spacing, inches	Fc' (ksi)
F-100-1P-1	Flexure	4" (100.0)	3.9	1.0%	6.3	26.1
F-100-1P-2	Flexure	4" (100.0)	3.8	1.0%	6.3	26.1
F-100-2P-1	Flexure	4" (100.0)	3.9	2.0%	6.3	27.7
F-100-2P-2	Flexure	4" (100.0)	3.9	2.0%	6.3	27.7
F-150-2P-1	Flexure	6" (150.0)	6.0	2.0%	6.3	27.7
F-150-2P-2	Flexure	6" (150.0)	5.3	2.0%	6.3	27.7
F-200-2P-1	Flexure	8" (200.0)	7.4	2.0%	6.3	27.7
F-200-2P-2	Flexure	8" (200.0)	7.5	2.0%	6.3	27.7
SF-100-1P-1	Combined	4" (100.0)	3.9	1.0%	6.3	26.1
SF-100-1P-2	Combined	4" (100.0)	3.9	1.0%	6.3	26.1
SF-100-2P-1	Combined	4" (100.0)	3.9	2.0%	6.3	27.7
SF-100-2P-2	Combined	4" (100.0)	3.8	2.0%	6.3	27.7

Table 6-1: Main Variable of Beam Specimens

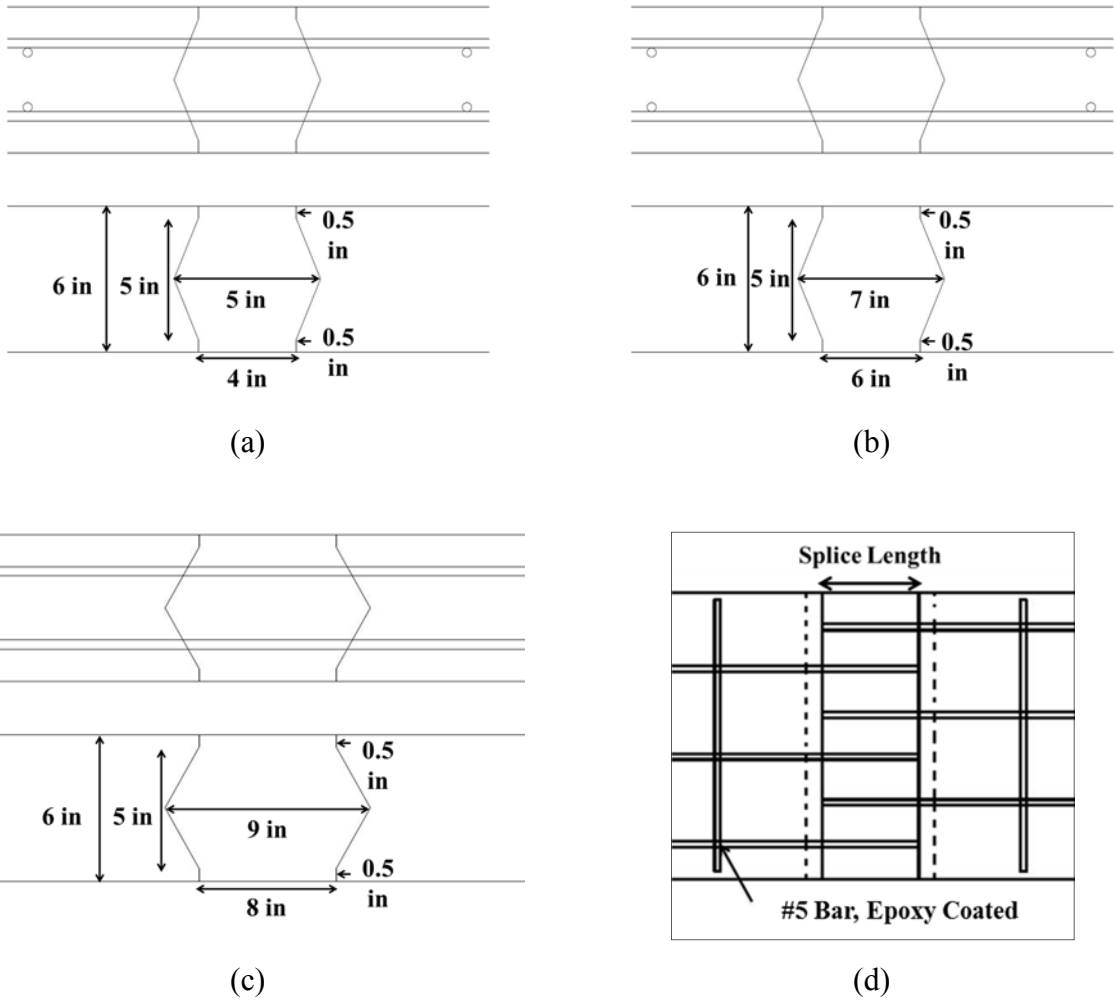

Figure 6-3 Joint Shape Details for the 4 in (a), 6 in (b) 8 in (c) joint, Lap Splice Connection Detail (d)

6.3. EXPERIMENTAL PROCEDURE

6.3.1. Test Set Up

All specimens were simply supported. Supports were placed 2" (50 mm) from either edge of the deck. Two rollers applied the load and were placed 12" (300 mm) from either edge of the joint in the pure flexure cases. A single roller was applied 4" (100 mm) from the joint interface in the combined shear and flexure case. Load was applied using a 100 kip INSTRON hydraulic loading

machine. A displacement controlled load was applied quasi-statically at 0.001 in/sec (0.0254 mm/sec).

6.3.2. Instrumentation

Load was recorded using a 100 kip load cell integrated with the hydraulic machine. Displacements were measured at the locations shown in Figure 6-4a using the Optotrack measurement system. This system uses a set of cameras to track the relative displacements of the markers shown in three dimensions. Additionally, in each of the precast segments of the beam, for the F-100 and F-200 specimens, strain gauges were placed on the lower layer of reinforcing steel, 1" (25.4 mm) from the edge of the joint interface, Figure 6-4b.

Digital imagine correlation (DIC) was used in order to map the strain developing in the UHPC joint, Figure 6-4c. In DIC, random speckle patterns are applied to the surface of the concrete, being sure to cross the UHPC-Regular concrete joint interface. A high resolution, high frame rate, camera then records the surface of the concrete, specifically the speckles, at a fixed frame rate throughout the test procedure. These images are then uploaded, and the DIC software maps the locations and movements of the speckled pattern. Measuring the relative movements and calculating displacements between the speckles allows for an accurate, 2-D, depiction of the strains occurring in the specimen, clearly highlighting crack patterns.

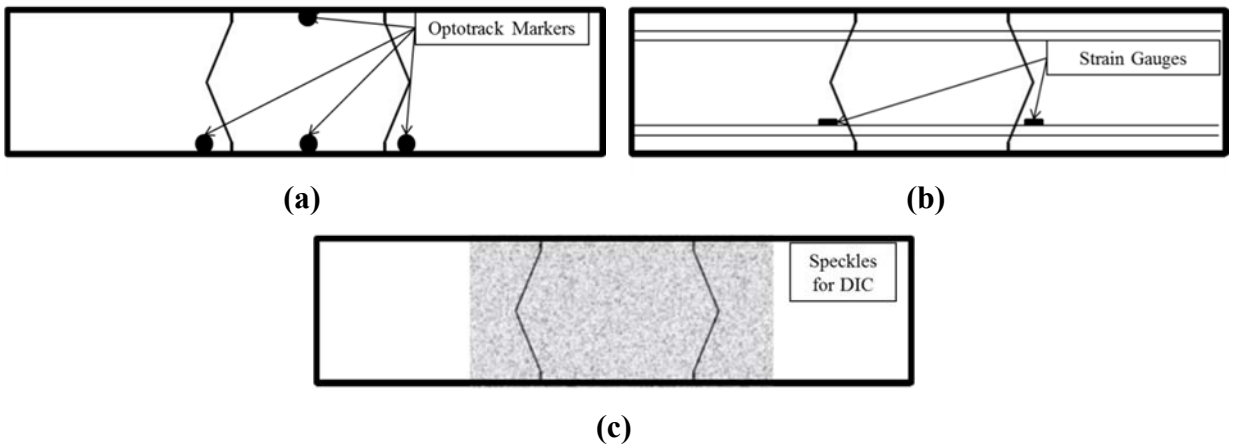

Figure 6-4: Instrumentation of the Precast Bridge Deck Beams

Data collected from the strain gauges placed on the deformed bars was used to verify the point during the test at which steel yielded. Data from the Optotrack system and DIC were used to measure deflections and strains occurring throughout the joint during testing. Data collected on the load and displacements were then plotted. The resulting curves were then processed through a moving average filter to account for minute changes due to the sensitivity of the equipment.

6.4. MATERIALS

The concrete used to construct the precast bridge deck elements consists of regular 5000 psi (35 MPa) concrete, with a 6" (150 mm) slump and maximum aggregate size of 0.78" (19 mm). The deformed bars all consisted of grade 60, epoxy coated steel and can be seen in Figure 6-5.

Figure 6-5: Deformed #5 (16 mm) Epoxy Reinforcement Bar

The UHPC mix design used to fill the joint and complete the lap splice follows the low-cost mix recommended in Chapter 3 (GG-25-00). The performance parameters for this mix can be found in Table 3-4.

6.5. CONSTRUCTION OF THE PRECAST CONCRETE SPECIMENS

Construction of the specimens for this study was performed in a simple, and easy to replicate process. Wood forms were first constructed with dimensions as designed. Once the rebar was placed, the shape of the joint's interface was created using a high-density foam and cut to the according dimensions (Figure 6-6b). Once the bars were in place and the bars were properly instrumented, the regular concrete was poured into the forms. Vibration was used to ensure proper installation of the regular concrete. After pouring, the surface of the concrete was smoothed and leveled so as to provide an adequate loading surface.

Twenty-four hours after the regular concrete had been cast; the foam was removed, exposing the inner surface of the joint. The two precast sections were brought together, and the splice properly aligned and measured. The bars were cleaned of any dirt and debris that had accumulated during the casting of the decks. The UHPC was then mixed and poured as described in Section 3.2.2. For this study, the UHPC was poured so as to favor fiber orientation in parallel to the deformed bars (Figure 6-6c). The specimens were then allowed to cure at room temperature for 28 days. Following the prescribed curing time, the forms were removed and the speckles were painted onto the joint surface for the DIC measurements (Figure 6-6d).

(a)

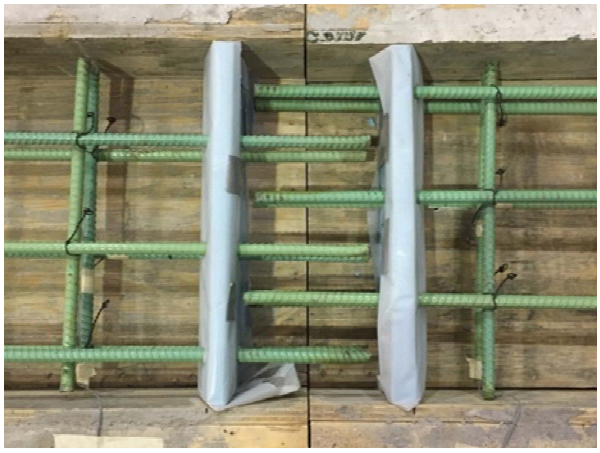

(b)

(c)

(d)

Figure 6-6: Forms and Placed Bars (a), Lap Splice (b), Poured UHPC Joint (c), and Set up with DIC (d)

6.6. RESULTS AND DISCUSSION

A summary of the results from the experimental testing for all of the specimens can be seen in Table 6-2.

Name	Embedded inches	Splice inches	Failure Mode	Force at Failure kips (Force/2)	Bond ksi
F-100-1P-1	4	3.5	Splitting	4.3	2.1
F-100-1P-2	4	3.5	Splitting	4.3	2.1
F-100-2P-1	4	3.5	Splitting	4.6	2.2
F-100-2P-2	4	3.5	Splitting	4.8	2.3
F-150-2P-1	6	5.9	Steel Yield	6.5	2.1
F-150-2P-2	6	5.8	Steel Yield	6.3	2.3
F-200-2P-1	8	7.8	Steel Yield	6.3	1.8
F-200-2P-2	8	7.8	Steel Yield	6.8	1.8
SF-100-1P-1	4	3.7	Splitting	15.2	2.1
SF-100-1P-2	4	3.9	Splitting	13.1	1.8
SF-100-2P-1	4	3.8	Splitting	16.3	2.2
SF-100-2P-2	4	3.8	Splitting	18.5	2.5

Table 6-2: Summary of Results from Experimental Testing

6.6.1. Comparison of Calculated Bar Stress versus Measured Bar Stress

Figure 6-7 shows the computed bar stresses calculated from the peak load recorded by the load cell compared to the measured strain (converted to stress) from the instrumented deformed bars. From the scatter, the calculated and measured data show no significant variation, though the calculated bar stresses generally measure slightly higher than those measured with the strain gauge. Thus the data is reliable and can be used for evaluation of the test data.

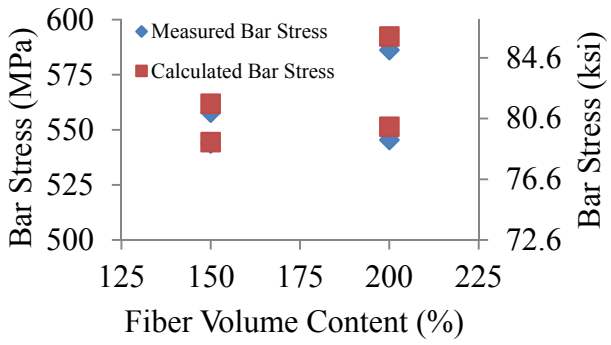

Figure 6-7: Comparison of Calculated and Measured Bar Stresses

6.6.2. F-100 Specimen Tests

Figure 6-8c and Figure 6-8d shows the force-displacement behavior of the four F-100 specimens subjected to flexural loading. For all tests, the load-displacement relation remained linear up to about 80% of the peak load. At this point, the load began to drop, corresponding to initial cracking at the center of the joint as can be seen by the horizontal cracks in Figure 6-8a and Figure 6-8b. The first crack to develop was the horizontal crack spanning the UHPC joint followed by a crack at the interface between the UHPC and regular concrete. For the rest of the loading, all deflections in the beam were localized at this interface. Figure 6-8a also shows the DIC images from the beams. As seen, all of the damage occurred in the joint, and that the corresponding crack pattern shows that a splitting failure occurred, where the reinforcement steel separated from the UHPC. No significant crushing in the regular concrete or UHPC was observed prior to the steel bar yielding. The peak force averaged 8.2 kips (36.5 KN) for specimens with 1% fibers (F-100-1P) by volume and 9.1 kips (40.5 KN) for those with 2% fibers (F-100-2P) by volume.

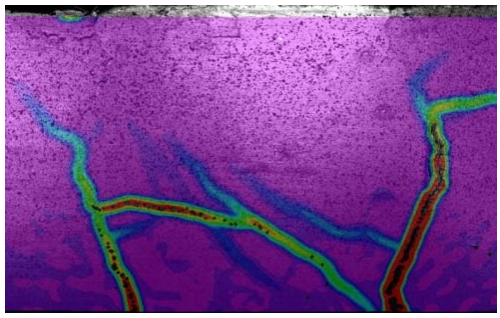

(a)

(b)

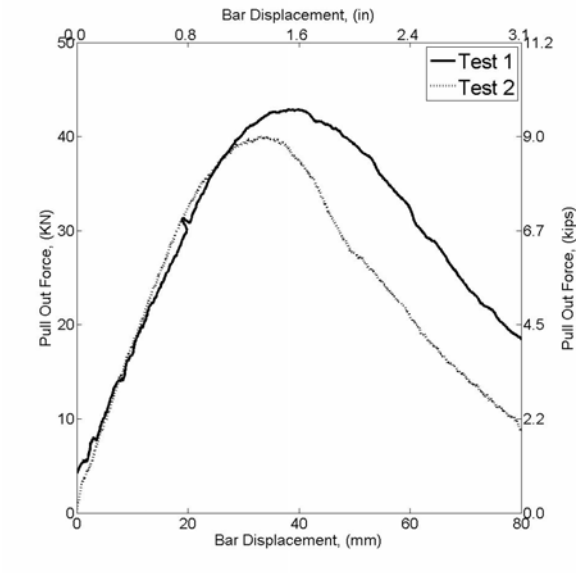

(c)

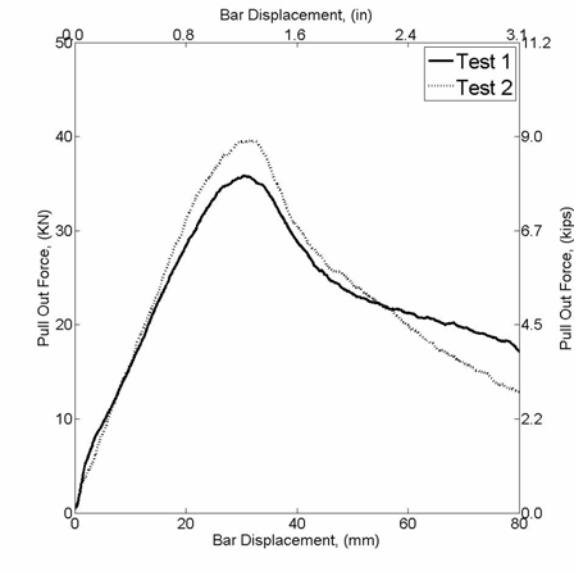

(d)

Figure 6-8: (a) DIC of 100 mm joint specimens, (b) Splitting Failure in deformed specimen, (c) Load-Deflection Curves for 100 mm specimens with 2% fibers and (d) 100 mm specimens with 1% fibers.

6.6.3. F-150 and F-200 Specimens

Both F-150-2P and F-200-2P specimens were able to transfer the load in the joint past steel bar yield in the specimens. Figure 6-9c shows the load-displacement curve for both of the F-150-2P specimens tested. The load-deflection begins with an elastic increase in the load being applied. This is followed by a region of decreased slope in the load-deflection, caused by yielding of the steel reinforcement. As steel yielded, flexural cracking was observed in the regular concrete

regions of the deck. Load continues to climb until reaching a maximum average value of 13.3 kips (59.2 KN). At this point, a sudden crushing of the regular concrete at the UHPC joint interface occurs, observed in the load-deflection curve as the drop off in the load occurring at 2.55" (65 mm) of midspan deflection. At this point the beam was no longer able to carry additional load, and began to gradually drop towards zero. No damage was observed in the UHPC joint.

Figure 6-9d shows the load-displacement curve for both of the F-200-2P specimens tested. Similarly to the F-150-2P specimens, the load-deflection begins with an elastic increase in the load being applied. Again, this is followed by a region of decreased slope in the load-deflection, caused by yielding of the steel reinforcement. Flexural cracking in the regular concrete regions of the deck were also observed. Load continued to climb until reaching a maximum average value of 12.6 kips (56.0 KN). Again, at the point of maximum load, a sudden crushing of the regular concrete at the UHPC joint interface occurs, observed in the load-deflection curve as the drop off in the load occurring at 65 mm of mid-span deflection for F-200-2P-1 and 3.2" (80 mm) for F-200-2P-2. At this point the beams were no longer able to carry additional load, and began to gradually drop towards zero. As in the F-150-2P tests, no damage was observed in the UHPC joint.

Figure 6-9a shows the results from the DIC typical for both F-150-2P and F-200-2P specimens. The figure clearly shows that all of the deformation in the beam is occurring at the UHPC joint – regular concrete interface, and not across the joint itself as observed in the F-100 tests, confirming that the UHPC and steel reinforcement remained bonded throughout testing. Additionally, Figure 6-9b shows that the same lack of damage and cracking occurs on the other side of the beam, with small crack openings visible the UHPC-regular concrete interfaces.

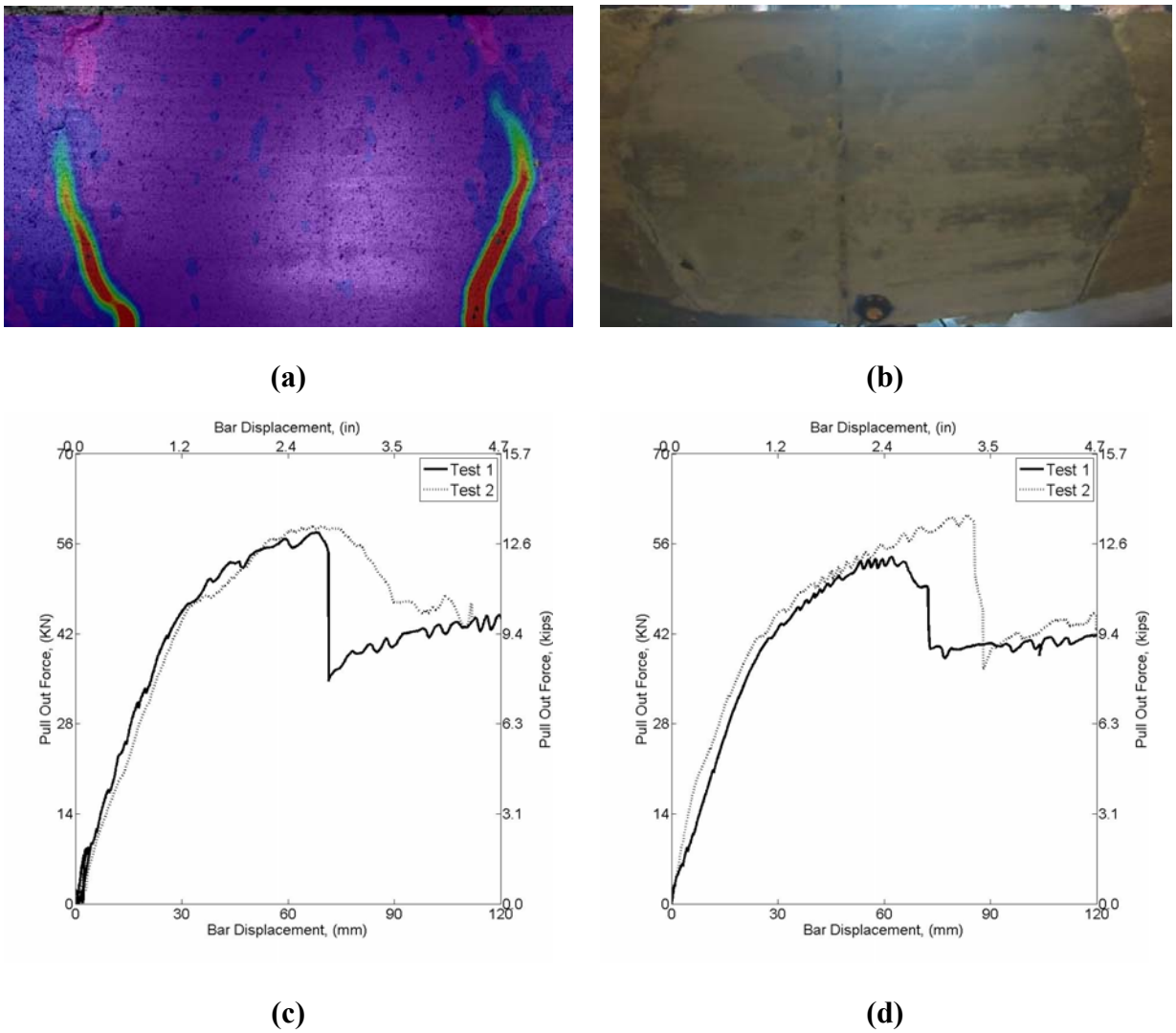

Figure 6-9: (a) DIC of 150 mm joint specimens, (b) Splitting Failure in deformed specimen, (c) Load-Deflection Curves for 150 mm specimens and (d) 200 mm specimens.

6.6.4. Effect of Fiber Content in Pure Flexure

As discussed in the previous sections, F-100-1P and F-100-2P specimens were both unable to successfully join the two precast regular concrete deck elements, resulting in a bar pull out failure to occur within the joint. The difference of 1% fibers by volume accounted for an average decrease in maximum force (and bond stress) of 8%. Cracked section calculations at the joint shows that at the point of maximum load, F-100-1P specimens experienced average bar force of 36.5 kips (162.3 KN) and F-100-2P specimens experienced an average bar stress of 40.5 kips (180 KN). Figure 6-10

plots the maximum force reached for the two tests with respect to the fiber volume content of the UHPCs. Extrapolating from the existing data and assuming no problems with mix workability due to increased fiber content, a UHPC with a minimum fiber content of 3.5% would be required if using a 100 mm wide joint in order to successfully connect two pre-cast regular concrete elements. This represents an increase of 75% fibers versus F-100-2P specimens, and a 25% increase in fibers versus the F-150-2P. As previously discussed in chapter 3, fibers are the most costly components of UHPC, and thus the use of a wider joint width becomes more economical than the smaller joint with an increase in fibers.

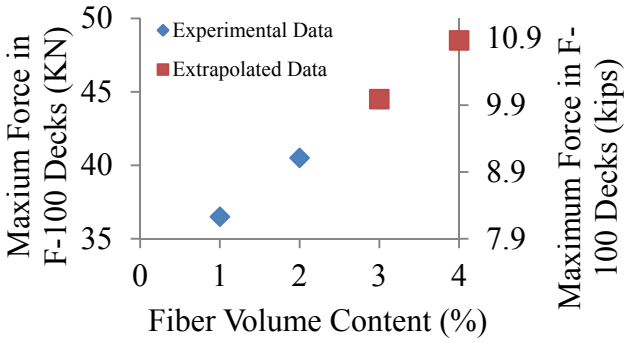

Figure 6-10: Maximum Force in F-100 Decks at a Function of Fiber Volume Content

6.6.5. Effect of Joint Size

Unlike F-100-1P and 2P specimens, both the F-150-2P and F-200-2P specimens were able to complete the joint connection. Figure 6-11 shows the moment (KN-m) at the joint as a function of the joint width for all tests with UHPC containing 2% fibers by volume. At 4" (100 mm), the maximum average moment achieved, 9 kip-ft. (12.2 KN-m), is the lowest. At 6" (150 mm) the average maximum moment achieved is 12.4 kip-ft. (16.9 KN-m) and 13.2 kip-ft. (17.8 KN-m) at 8" (200 mm). The increased width of 50 mm (a 34% increase in width and subsequently, quantity

of UHPC needed) between the F-150 and F-200 specimens only achieved an increase in moment capacity of 5.5%. In order to minimize required quantity of UHPC, the F-150-2P joints would provide the best UHPC use – beam strength ratio, despite the marginal gain in moment capacity.

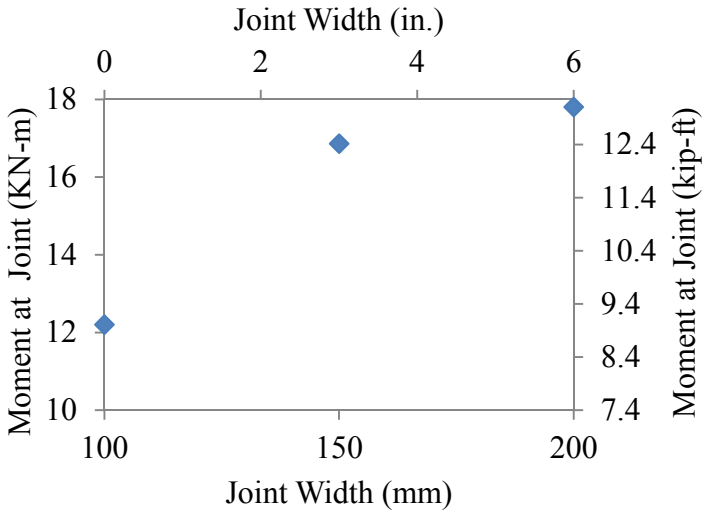

Figure 6-11: Moment at Joint as a function of Joint Width

6.6.6. Combined Shear and Flexure Testing

For the SF-100-1P specimens the load-displacement curve remained linear up to about 95% of the peak load. At this point, the load began to drop, corresponding to initial cracking at the center of the joint as can be seen by the horizontal cracks in Figure 6-12a and Figure 6-12b. The first crack to develop was the horizontal crack spanning the UHPC joint followed by a crack at the interface between the UHPC and regular concrete. For the rest of the loading, all deflections in the beam were at this interface. Figure 6-12a also shows the DIC images from the beams. Similarly to the F-100-1P and F-100-2P specimens, all of the damage occurred in the joint, and that the corresponding crack pattern shows that a splitting failure occurred, where the reinforcement steel separated from the UHPC. No significant crushing in the regular concrete or UHPC was observed

prior to the steel bar yielding. The peak force averaged 13.7 kips (61 KN) for specimens with 1% fibers (SF-100-1P) by volume and 16.9 (75.5 KN) for those with 2% fibers (SF-100-2P) by volume. Damage showed in Figure 6-12a and Figure 6-12b were representative for SF-100-1P-1, 2 and SF-100-2P-2. For SF-100-2P-1, the concrete between the UHPC joint and the closest support experienced a splitting crack, reducing the overall force achieved in the beam. This event can be seen as the sudden drop off in force on the load displacement curve.

6.6.7. Effect of Fiber Content in Combined Shear and Flexure

On average, SF-100-1P specimens containing 1% fibers by volume achieved 19% less force prior to failure than their SF-100-2P counterparts. This result is unsurprising as bonding in UHPC is directly related to the steel fiber contents, as discussed in Chapter 5. SF specimens containing 1% steel fibers by volume averaged 8% less bar force at failure that their pure flexure counterpart with 1% fibers by volume. At 2% fibers by volume, the difference in bar forces achieved between F-100-2P and SF-100-2P specimens was less pronounced, suggesting that the UHPC's capacity in shear increases non-linearly with increases with fiber content. More testing on UHPC specimens in shear should be conducted in order to further clarify these results.

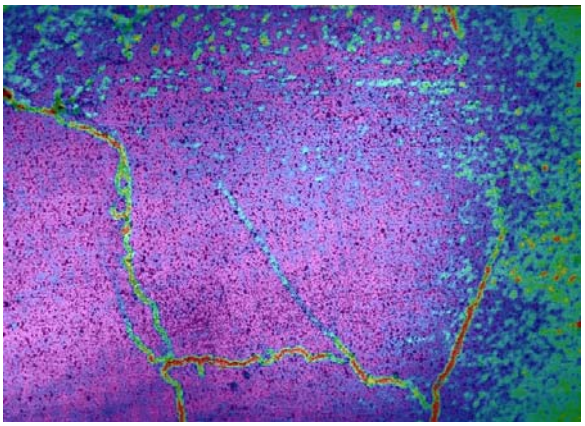

(a) **(b)**

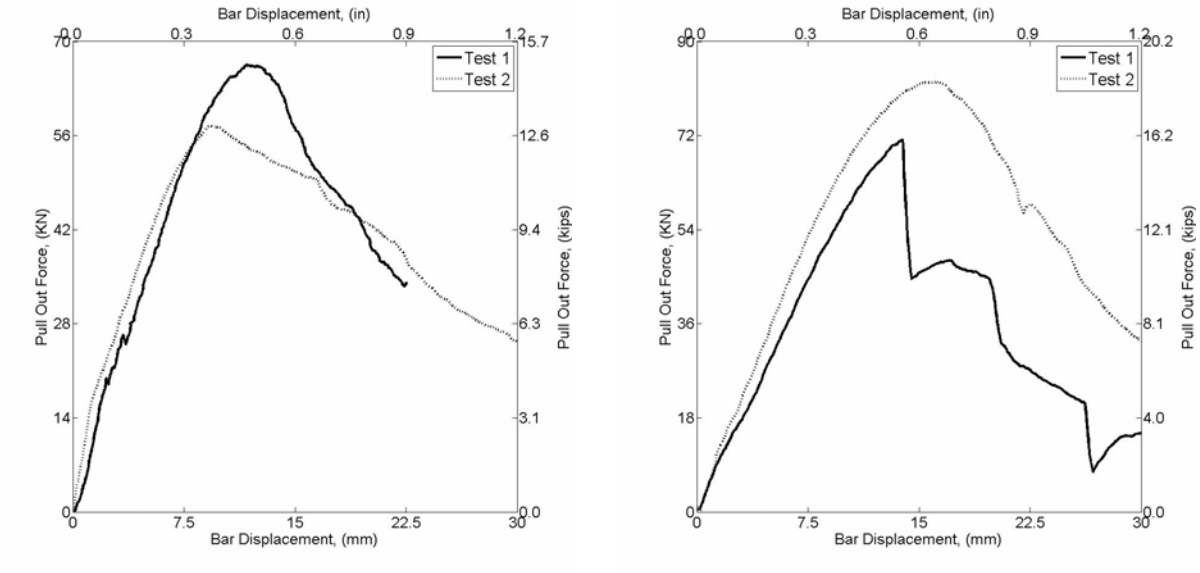

(c) **(d)**

Figure 6-12: (a) DIC of 100 mm joint, SF specimens, (b) Splitting Failure in deformed specimen, (c) Load-Deflection Curves for 100 mm specimens, 1% fiber by vol. and (d) 100 mm specimens, 2% fiber by vol.

6.7. FINITE ELEMENT MODEL AND PARAMETRIC STUDY

6.7.1. Model Setup

A two dimensional finite element model was developed for the LS-DYNA platform. The model makes use of 2-D plane stress elements. The model was discretized and meshed using Hypermesh, and can be seen in Figure 6-13. Each model consists of three components; 2 precast regular concrete elements and 1 UHPC joint. Specimen dimensions and reinforcement details follow those prescribed previously for the F-150-2P and F-200-2P specimens.

Reinforcing steel was modeled using one dimensional, linear beam elements. The steel bars and surrounding concrete were assumed to be perfectly bonded. As only reinforcing steel from the F-

150-1P and F-200-2P specimens remained fully bonded, only those two specimens were used in this portion of the study.

Steel material behavior was modeled using a piecewise linear plasticity model (LS-DYNA card #24). Steel material properties were determined through experimental testing, with the following parameters: yield stress, σ_y = 67 ksi (450 MPa) with a young's modulus, E = 29000 ksi (200 GPa). After yield, the tangent modulus E_{tan} was set to 175 ksi (1.2 GPa). Figure 6-12 shows the finite element model (a) and mesh (b) developed for use in this study for the F-150-2P specimens (at 6").

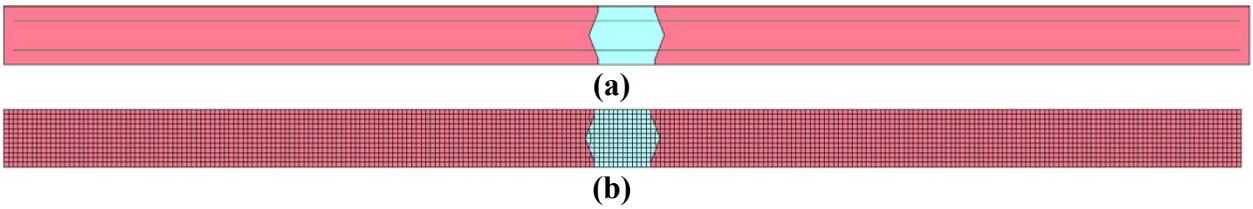

Figure 6-13: (a) Finite Element Model and (b) Mesh for F-150-2P Specimens

6.7.2. UHPC and Concrete Material Models

The concrete material model used in this study was previously developed model for high performance fiber reinforced composites (Hung, 2010), and calibrated for use with UHPC based on the experimental results previously reported. The model, based upon a hybrid rotating/fixed crack approach, allows perpendicular cracking of the concrete and is capable of modeling the tensile and compressive response for UHPC. The tensile response is characterized by three regions, a linear elastic portion followed by some strain hardening and then a softening of the concrete. Figure 6-14a shows the typical tensile response of uniaxial testing on UHPC specimens as well the material model response used in this study. Figure 6-14b shows the compressive response of

UHPC under loading experimentally as well as the model's material response. For the regular concrete material, the same hybrid rotating/fixed crack model was employed, calibrating it with typical concrete responses. Table 6-3 outlines the material properties used.

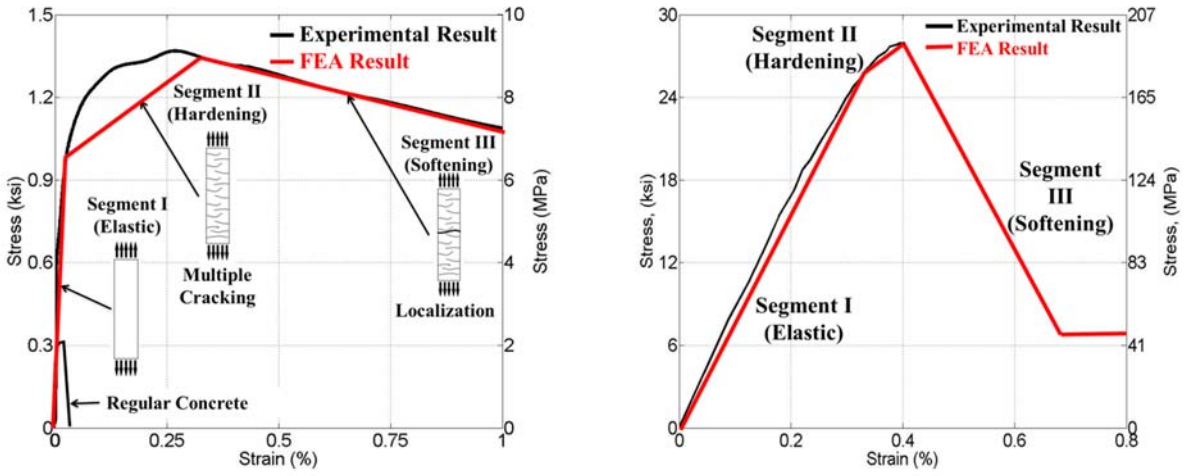

(a) (b)

Figure 6-14: Typical UHPC Tensile Response for Joint Fill Material (a) tension and (b) compression

Name	Tensile Pre-Cracking Stress (Strain)	Tensile Post-Cracking Stress (Strain)	Elastic Modulus	F'c (ksi)
UHPC	0.75 ksi (0.0001)	1.2 ksi (0.0002)	751 ksi	26.8
Regular Concrete	0.35 ksi (0.0001)	0.01 ksi (0.0002)	157 ksi	5.0

Table 6-3: Material Parameters for FEM

6.7.3. Parametric Study

The finite element model was validated using the experimental data and from there, a parametric study was performed to determine the effect of the joint's surface topology on the overall performance of the beams. Three different joint designs were modeled and analyzed and can be seen in Figure 6-15. For each joint type, modeling was performed for a 6" (150 mm) joint as well

as an 8” (200 mm) joint. Figure 6-15a shows the original joint design tested experimentally and used for the model validation (F-150-2P). Figure 6-15b shows a non-tapered (NT) joint design, and Figure 6-15c shows the flat surface (FS) joint design modeled for the parametric study. The NT and FS joint designs were selected, as they both are more easily constructed designs. A summary of the simulations performed can be found in Table 6-4.

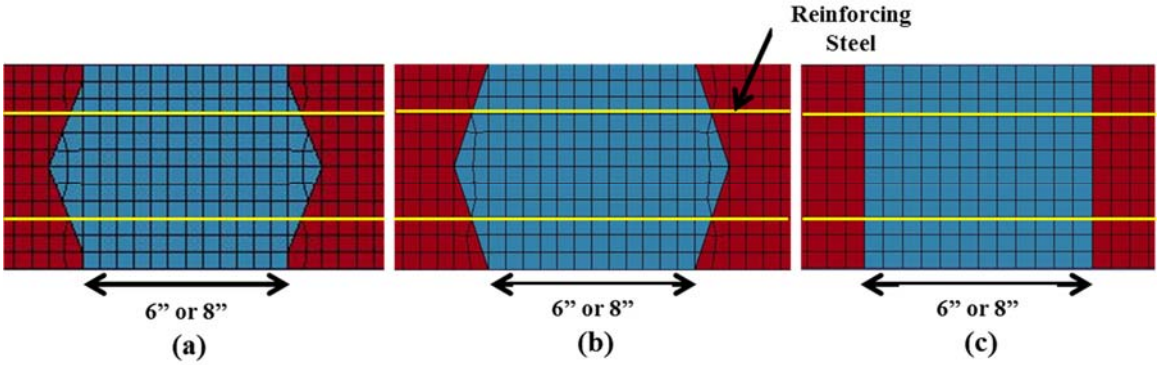

Figure 6-15: (a) Original Joint Design for FEA, (b) non-tapered joint design, and (c) flat joint design.

Name	Joint Type	Joint Size inches (mm)
F-150	Flexure (as F-150-2P)	6” (150)
NT-150	Non-Tapered	6” (150)
FS-150	Flat Surface	6” (150)
F-200	Flexure (as F-200-2P)	8” (200)
NT-200	Non-Tapered	8” (200)
FS-200	Flat Surface	8” (200)

Table 6-4: Summary of Simulated Beams

6.7.4. Model Validation

Results from the experimental testing of beams F-150-2P and F-200-2P were used for model validation. From Figure 6-16a, the numerical results (red line) show good correlation with the results from the experimental testing (black line), including capturing the steel yield, and later on the concrete crushing which occurs for the F-150-2P specimens. Additionally, the deformed shape matches well with the observed experimental deformations (Figure 6-17). While some discrepancies exist, the values from the simulation match reasonably well with the experimental values, and the minor discrepancies between the simulation and experimental data are attributed to experimental scatter. The same conclusion can be reached for the results of the F-200-2P model validation seen in Figure 6-16b.

6.7.5. Results of Parametric Study

For the 150 mm joints, the results from the FEA showed little variation between the F-150, NT-150 and FS-150 joints. All three load-displacement curves began elastically, up until 80% of their max load, at which point the steel reinforcement began to yield. Yielding continued, with the load increasing until approximately 65 mm midpoint deflection. At this point, the concrete at the top of the UHPC-regular concrete interface was crushed, resulting in a drop off in the force capacity of the beam. There was no noticeable difference between the F, NT and FS joints.

Similarly, the F-200, NT-200 and FS-150 joints show little variation. Again, all three load-displacement curves began elastically, up until 80% of their max load, at which point the steel reinforcement began to yield. Yielding continued, with the load increasing until approximately 70 mm midpoint deflection. At this point, the concrete at the top of the UHPC-regular concrete interface was crushed, resulting in a drop off in the force capacity of the beam.

As these simulations were performed under pure flexure for all three joint types, their respective topologies were not fully engaged leading to the primarily flexure failure mechanism. In a more realistic scenario, the shear strength of the UHPC at the joint interface would become important, as more joints are not solely subjected to flexure. Results from the combined shear and flexure testing could not be used for model validation as the primary failure modes in those tests was a bar pull out failure in the joint and thus, a parametric study could not be done for the combined shear and flexure case. UHPC specimens under shear should be further studied to gain more insight into the behavior.

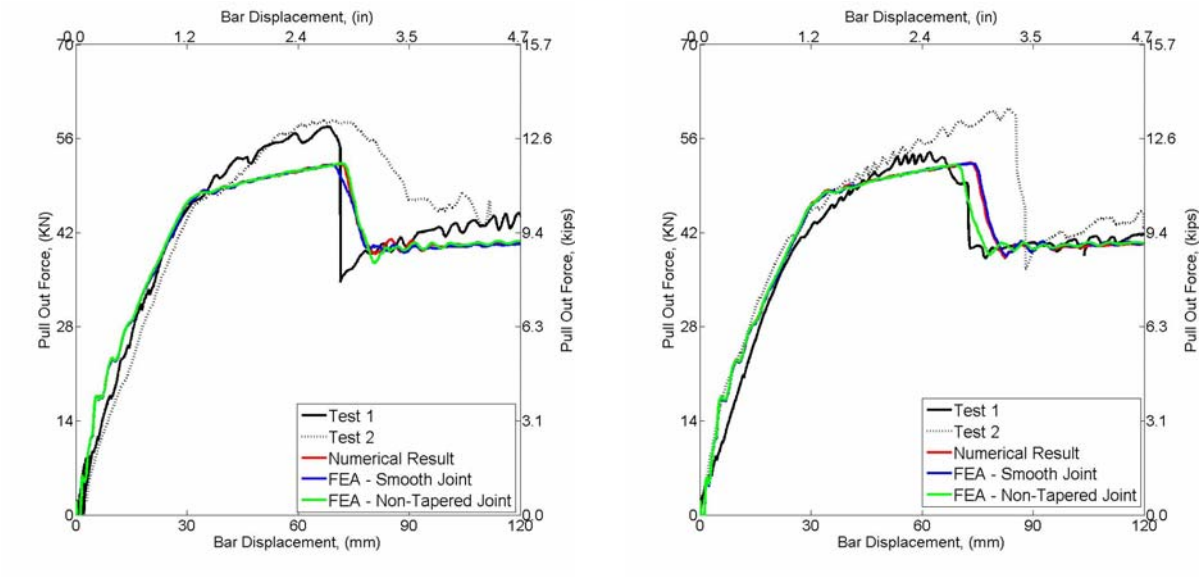

(a) **(b)**

Figure 6-16: Experimental FEA Load-Deflection for (a) 150 mm joints and (b) 200 mm joints

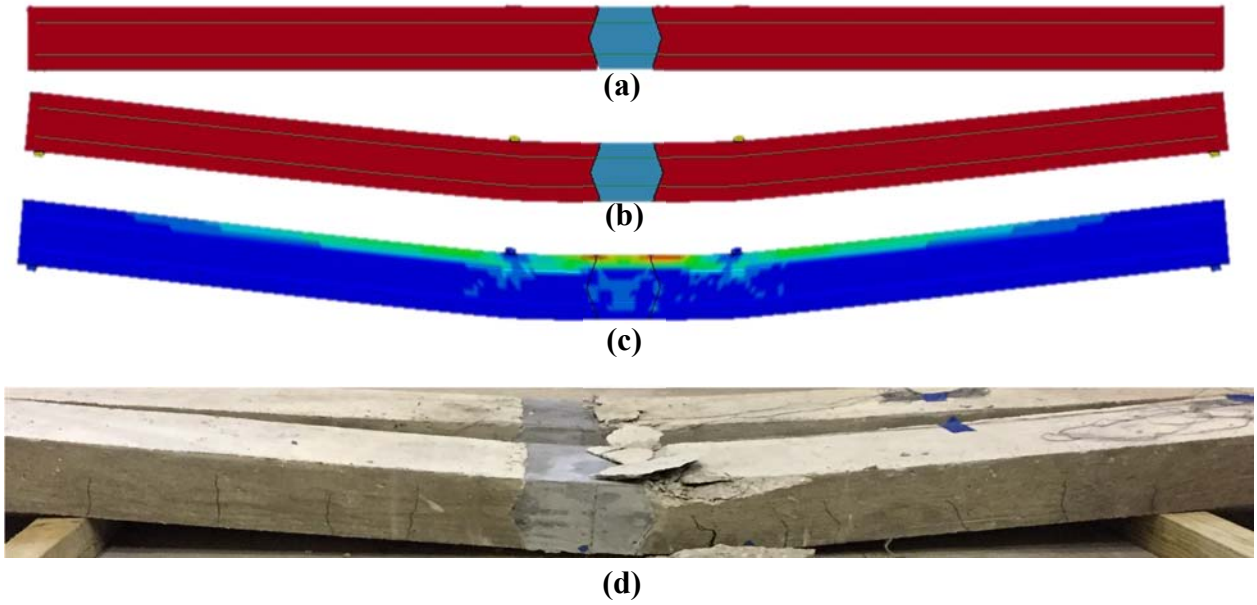

Figure 6-17: (a) Un-deformed shape, (b) deformed shape and (c) von Mises Strain for 150 mm, (d) Plot of the cracks developed and (e) and Damaged Beam after Testing, Actual joint

6.8. CONCLUSION

The objective of the study in this chapter was to evaluate the use of ultra-high performance concrete for simplified joint connections between precast bridge deck elements. The study evaluated three different joint widths, two different fiber volume content UHPCs and two separate loading schemes to simulate real-world loading conditions. The conclusions are as follow:

- All F-100 and SF-100 (4" joint) specimens failed with a splitting failure occurring at the UHPC joints. Bond between the UHPC and deformed bars was insufficient, causing the beams to reach failure prematurely.
- F-150 and F-200 (6" and 8" joints) specimens all failed through steel yield in the deformed bars, followed much later on by crushing in the regular concrete. These specimens were able to carry load through the joints all the way through the desired failure mode.

- F-100 (4” joint) specimens containing 1% fibers by volume achieved an average of 8% lower capacity (and hence bond stress in the joints) than those containing 2% fibers. Extrapolating the test results suggests that a 4” (100 mm) joint may be possible when utilizing a greater steel fiber ratio (~3%). However, increased fiber content leads to greater cost and, possibly, problems with mix workability. Mixes with such high fiber contents were not tested in this work.
- SF-100 (4” joint) beams performed worse than F-100 beams at 1% fibers by volume, though the difference at 2% fibers by volume was non-apparent. This suggests the increase in shear strength in UHPC increases non-linearly with an increase in steel fiber content compared to flexure strength and should be investigated further.
- Changes in the topology of the joint showed no difference in structural performance in the parametric study, under pure flexural loading.

Intentionally left blank

7. SUMMARY, MAJOR CONCLUSIONS AND FUTURE RESEARCH

7.1. SUMMARY AND MAJOR CONCLUSIONS

The primary objectives of this project were: 1) to develop a cost-optimized version of non-proprietary UHPC and characterize its mechanical and durability properties, and 2) investigate the possibility of using UHPC for field-cast joints that commonly occur in precast construction. To achieve these objectives, the first phase of the work looked into the material components of non-proprietary UHPC, and through an analysis of their costs, quantities, and availabilities, a new low-cost alternative UHPC mix formulation was designed. The material cost of this alternative mix is half of the original UHPC mix. Using the new alternative low cost mix, and a select few seen as reduced cost alternatives, a detailed investigation of their mechanical and durability properties was conducted. Mechanical property characterization focused on quantifying tensile properties and compressive strength, while durability studies addressed the material's air voids, resistance to freeze-thaw and chloride penetration. All tested mixes had exceptional mechanical and durability properties.

The proposed mix deviates from traditional UHPC mixtures in that it uses a 50:50 mix of Portland Type I and Ground Granulated Blast Furnace Slag (GGBS) as a binder, lacks any Silica Powder (inert filler) and requires no post-placing treatment. The use of GGBS improves the material's 'greenness' making it a more sustainable cementitious product. Specifications for making the new UHPC were proposed.

UHPC derives its unique properties from its high packing density, which is achieved by carefully controlling the size and distribution of the constituent particles, and incorporating steel fibers. For example, unlike regular concrete which relies on having sufficient void space to allow water to

expand, the high freeze-thaw resistance in UHPCs is due to water being prevented from entering the material in the first place.

The test results suggest that fiber volume contents of 1.0% or 1.5% could significantly reduce the chance for crack localization under dead load or working conditions, respectively, in structural applications. Coupled with the material's inherent resistance to chloride ion penetration, controlling crack localization further limits the ingress of chloride ions and protects steel reinforcement from corrosion.

Following material characterization, the next phase of the research investigated the bonding performance between steel reinforcement and UHPC. The study spanned several experimental parameters (embedment, bar size & type, UHPC fiber content/orientation, etc.), and ultimately led to a design guideline for achieving specific bar stresses when reinforcement is embedded in UHPC. This was then followed by a series of beam tests using two precast regular concrete sections joined together with a UHPC joint. The results of this testing showed that a 150 mm (6") UHPC was sufficient for precast bridge construction.

7.2. PROMISE AND COMMERCIAL POTENTIAL OF UHPC

The non-proprietary UHPC developed in this work has strong potential for use in structures that will be significantly more durable than currently possible with conventional materials. Therefore, every structure built at the moment using current technology is an opportunity lost to start building a longer lasting infrastructure that is considerably cheaper to maintain in the long run.

The current cost of a cubic yard of the nonproprietary UHPC developed in this work is \$267/yd^3 for the cementitious material alone. The addition of fibers at 1.5% by volume would enable the use of UHPC for structural applications, while minimizing the fiber cost. Each cubic yard of UHPC

requires 193 lbs. of steel fibers. Ordering from a supplier within the United States currently costs $1.98 per pound. Adding this $382/yd^3 fibers cost to the base $267/yd^3 brings the total cost to $659/yd^3, roughly 5x the present cost of regular concrete.

Several suppliers outside of the United States produce steel fibers at a reduced unit cost, as low as $0.30 per pound (e.g. http://tinyurl.com/h474res, accessed on 12/30/2015). Using these suppliers, and assuming that the fiber quality is similar to the US products, will reduce the current cost of UHPC (including fibers) to $325 per cubic yard, which is only about twice the cost of regular concrete.

7.3. AN OPPORTUNITY FOR THE STATE OF MICHIGAN

One of the reasons for the high US fiber costs is the lack of demand. As UHPC usage increases and demand for steel fibers surges, it is expected that the cost will drop. The State of Michigan, with its focus on vehicle manufacturing, is well suited to be major fiber industry hub given that steel fibers are made from chopped high strength wires that are used in steel-belted tire products.

7.4. A BRIGHT FUTURE

For an initial increase in material cost compared to regular concrete, whether 2x or even 5x, the benefits of UHPC can be substantial compared to traditional concrete products. With UHPC's enhanced strength in tension and compression, thinner and more elegant structures can be built. Not only that, the use of GGBS in the proposed mix improves the material's 'greenness' making it a more sustainable cementitious product. With durability that boasts no deterioration after 60+ cycles of freeze-thaw and virtually no chloride penetration, UHPC structures will have extremely

low maintenance requirements, and therefore costs, for lifespans that are substantially longer than currently possible.

7.5. FUTURE RESEARCH NEEDS

To achieve the promise of UHPC as the material for the next generation of infrastructure, research is needed on multiple fronts. Fibers properties need to be optimized and the effect of fiber coatings on UHPC response explored. Commercial production of UHPC remains a challenge. At present, UHPC must be mixed in a paddle mixer and cannot be made and delivered in a ready-mix concrete truck. Research is needed to explore innovative mixing methods that require only small incremental changes to existing mixing technology so that widespread adoption of the material can be facilitated. Research into alternative high range water reducers is also needed so as to ensure that the UHPC described herein is not dependent on a single source. Also, research on UHPC structures and structural components is rare in the literature and research efforts are needed to ensure that established design methods apply to UHPC systems and develop new ones, as needed.

8. REFERENCES

AASHTO T 132-87. Standard Method of Test for Tensile Strength of Hydraulic Cement Mortars. American Association of State and Highway Transportation Officials. 8 pages. 2009.

AASHTO T 277-86, Rapid Determination of the Chloride Permeability of Concrete, American Association of States Highway and Transportation Officials, Standard Specifications - Part II Tests, Washington, D. C., 1990.

ACI Committee 318-05 (2005). Building Code Requirements for Structural Concrete (ACI 318-05) and Commentary (ACI 318R-05), American Concrete Institute Committee 318, Farmington Hills, MI.

ACI Committee 408 (2003). Bond and Development of Straight Reinforcing Bars in Tension. ACI 408R-03, American Concrete Institute Committee 408, Farmington Hills, MI.

Acker, P. and Behloul, M., "Ductal® Technology: A Large Spectrum of Properties, A Wide Range of Applications," Proceedings of the International Symposium on Ultra High Performance Concrete, Ed., Schmidt, M., Fehling, E., and Geisenhanslüke, C., Kassel University Press, Kassel, Germany, 2004, pp. 11–23.

Ahlborn, T.M. et al., "Durability and Strength Characterization of Ultra-High Performance Concrete Under Variable Curing Regimes," Proceedings of the Second International Symposium on Ultra High Performance Concrete, Ed., Fehling, E., Schmidt, M., and Stürwald, S., Kassel University Press, Kassel, Germany, 2008, pp. 197–204.

Ahlbourn, Theresa. "ULTRA-HIGH PERFORMANCE CONCRETE FOR MICHIGAN BRIDGES." Final Report, MDOT, Michigan Tech (2008): 1-152. Web.

Alexander, M.g, and B.j Magee. "Durability Performance of Concrete Containing Condensed Silica Fume." Cement and Concrete Research 29.6 (1999): 917-22. Web.

Alkaysi, M., El-Tawil, S., Liu, Z. and Hansen, W. (2016), "Effects of Silica Powder and Cement Type on Long Term Durability of Ultra High Performance Concrete (UHPC)," Accepted for Publication in the ACI Materials Journal.

Andreasen, A.H.M. and Andersen, J., 'Ueber die Beziehung zwischen Kornabstufung und Zwischenraum in Produkten aus losen Körnern (mit einigen Experimenten)', Kolloid-Zeitschrift 50 (1930) 217-228.

Andreassen and J. Andersen: Kolloid Z. 50 (1930) p. 217–228.

ASCE 7: Minimum Design Loads for Buildings and Other Structures. N.p.: ASCE Library, n.d. Print.

ASTM Standard C109, Standard Test Method for Compressive Strength of Hydraulic Cement Mortars (Using 2-in. or (50-mm) Cube Specimens)', ASTM International, West Conshohocken, PA. (2009)

ASTM Standard C1202, "Standard Test Method for Electrical Indication of Concrete's Ability to Resist Chloride Ion Penetration", ASTM International, West Conshohocken, PA. (2009) 6 pp.

ASTM Standard C457, 'Standard test method for microscopical determination of parameters of the air-void system in hardened concrete', ASTM International, West Conshohocken, PA. (2009) 14 pp

Azizinamini, A., Stark, M., Toller, J.J., and Ghosh, S.K., 1993, "Bond Performance of Reinforcing Bars Embedded in High-Strength Concrete," ACI Structural Journal, V. 90, No. 5, Sep.-Cot., pp. 554-561.

Bonneau, O. et al., "Mechanical Properties and Durability of Two Industrial Reactive Powder Concretes," ACI Materials Journal, Vol. 94, No. 4, July–August 1997, pp. 286–290

Borges, Paulo H. R., Lucas F. Fonseca, Vitor A. Nunes, Tulio H. Panzera, and Carolina C Martuscelli. "Andreasen Particle Packing Method on the Development of Geopolymer Concrete for Civil Engineering." Journal of Materials in Civil Engineering (2013): 130413134609008. Web.

Brouwers HJH, Radix HJ, Self-compacting concrete: the role of the particle size distribution. In: The first international symposium on design, performance and use of self-consolidating concrete (SCC'2005) Changsha, Hunan, China; p. 109–18. 200

Castro, A. L., and Pandolfelli, V. C. (2009). "Review: Concepts of particle dispersion and packing for special concretes production." Cerâmica, 55(333), 18–32

Cheng, An, Ran Huang, Jiann-Kuo Wu, and Cheng-Hsin Chen. "Influence of GGBS on Durability and Corrosion Behavior of Reinforced Concrete." Materials Chemistry and Physics 93.2-3 (2005): 404-11. Web

Cheng, An, Ran Huang, Jiann-Kuo Wu, and Cheng-Hsin Chen. "Influence of GGBS on Durability and Corrosion Behavior of Reinforced Concrete." Materials Chemistry and Physics 93.2-3 (2005): 404-11. Web.

de Larrard, F. and Sedran, T., "Optimization of Ultra-High-Performance Concrete by the Use of a Packing Model," Cement and Concrete Research, Vol. 24, No. 6, 1994, pp. 997–1,009.

Elaty, Metwally Abd Allah Abd. "Compressive Strength Prediction of Portland Cement Concrete with Age Using a New Model." HBRC Journal 10.2 (2014): 145-55. Web.

Fehling, E., Lorenz, P., and Leutbecher, T., "Experimental Investigations on Anchorage of Rebars in UHPC," Proceedings of Hipermat 2012 3rd International Symposium on UHPC and Nanotechnology for High Performance Construction Materials, Ed., Schmidt, M.,Fehling, E.

Gilkey, Hj. "Bond with Reinforcing Steel." Significance of Tests and Properties of Concrete and Concrete Aggregates (1956): n. pag. Web.

Glotzbach, C., Fröhlich, S., and Piotrowski, S., Kassel University Press, Kassel,Germany, 2012, pp. 533–540.

Graybeal, B., "Behavior of Field-Cast Ultra-High Performance Concrete Bridge Deck Connections Under Cyclic and Static Structural Loading," FHWA, U.S. Department of Transportation, Report No. FHWA-HRT-11-023, National Technical Information ServiceAccession No. PB2011-101995, 2010.

Graybeal, B., "Bond Behavior of Reinforcing Steel in Ultra High Performance Concrete," Federal Highway Administration, FHWA-HRT-14-089, October, 2014, p. 12

Graybeal, B., "Design and Construction of Field-Cast UHPC Connnections," Federal Highway Administration, FHWA-HRT-14-084, October, 2014, p. 36

Graybeal, B., "Material Property Characterization of Ultra-High Performance Concrete," FHWA, U.S. Department of Transportation, Report No. FHWA-HRT-06-103, McLean, VA, 2006

Graybeal, B., Perry, V., and Royce, M., "UHPC Ultra-High Performance Concrete," NHI Innovations Webinar, November 18, 2010. Available at https://connectdot.connectsolutions.com/n134083201011 (Cited April 3, 2012).

Graybeal, B.A. and Hartmann, J.L., "Strength and Durability of Ultra-High Performance Concrete," Proceedings of the 3rd International Symposium on High Performance

Concrete/PCI National Bridge Conference, October 19–22, 2003, Orlando, FL, Compact Disc, Paper 47.

Graybeal, Benjamin A. "Field-Cast UHPC Connections for Modular Bridge Deck Elements." FHWA-HRT-11-022 48.6 (2014): n. pag. FHWA. Web.

Graybeal, Benjamin A. "Splice Length of Prestressing Strands in Field-cast UHPC Connections." Mater Struct Materials and Structures 48.6 (2015): 1831-839. Web.

Graybeal. "Ultra-High Performance Concrete: A State-Of-The-Art Report for The Bridge Community." Chapters 6-7 - , June 2013 - FHWA-HRT-13-060. N.p., n.d. Web. 06 Dec. 2014.

Holschemacher, K. and Weiße, D., "Economic Mix Design Ultra High-Strength Concrete," Seventh International Symposium on the Utilization of High-Strength/High-Performance Concrete, Vol. II, Publication No. SP-228, Ed., Russell, H.G., American Concrete Institute, Farmington Hills, MI, 2005, pp. 1,133–1,144.

Holschemacher, K., Weiβe, D., and Klotz, S., "Bond of Reinforcement in Ultra High Strength Concrete," Proceedings of the International Symposium on Ultra High Performance Concrete, Ed., Schmidt, M., Fehling, E., and Geisenhanslüke, C., Kassel University Press, Kassel, Germany, 2004, pp. 375–387.

Hwang, Hoonhee, and Sung Yong Park. "A Study on the Flexural Behavior of Lap-spliced Cast-in-place Joints under Static Loading in Ultra-high Performance Concrete Bridge Deck Slabs." Canadian Journal of Civil Engineering Can. J. Civ. Eng. 41.7 (2014): 615-23. Web.

Innovative Field-Cast Uhpc Joints For Precast Bridge Decks - Highways for LIFE - FHWA."

Jungworth, J., Muttoni, A., "Structural Behavior of Tension Memebers in UHPC,"Proceedings of the International Symposium on Ultra High Performance Concrete, Kassel, Germany, 2004.

Kim, D-J., Wille, K., Naaman, A. E. and El-Tawil, S. (2011), "Strength Dependent Tensile Behavior of Strain Hardening Fiber Reinforced Concrete," Proceedings of HPFRCC6, H. W. Reinhardt and G. Parra Editors, Ann Arbor, MI.

Kim, D-J, Naaman, A. E. and El-Tawil, S. (2010a), "High Performance Fiber Reinforced Cement Composites With Innovative Slip Hardening Twisted Steel Fibers" International Journal of Concrete Structures and Materials, Korean Concrete Institute, ISSN: 1976-0485, 3(2), pp. 119 – 126; DOI 10.4334/IJCSM.2009.3.2.119.

Kim, D-J, El-Tawil, S., Sirijaroonchai, K. and Naaman, A. E. (2010b), "Numerical Simulation of the Split Hopkinson Pressure Bar Test Technique for Concrete Under Compression," International Journal of Impact Engineering, 37(2), Pages 141-149.

Kim, D-J., Naaman, A.E. and El-Tawil, S. (2010c), "Correlation between Tensile and Bending Behavior of FRC Composites with Scale Effect," Proceedings of FraMCoS-7, 7th International Conference on Fracture Mechanics of Concrete and Concrete Structures, May 23-28, 2010, Jeju Island, South Korea

Kim, D-J, Naaman, A. E. and El-Tawil, S. (2008a), "Comparative Flexural Behavior of Four Fiber Reinforced Cementitious Composites," Journal of Cement and Concrete Composites, Elsevier, Vol. 30, November 2008, pp.917-928.

Kim, D-J, El-Tawil, S. and Naaman, A. E. (2008b), "Rate-Dependent Tensile Behavior of High Performance Fiber Reinforced Cementitious Composites," Materials and Structures, RILEM, ISSN 1359-5997 (in print), 1871-6873 (online).

Kim, D-J, El-Tawil, S. and Naaman, A. E. (2008c), "Loading Rate Effect on Pullout Behavior of Deformed Fibers," ACI Materials Journal, 105(6), November-December 2008, pp.576-584

Kim, D-J, Naaman, A. E. and El-Tawil, S. (2008d), "High Tensile Strength Strain-Hardening FRC Composites with Less Than 2% Fiber Content," Proceedings of the Second International Symposium on Ultra High Performance Concrete, March 05 - 07, 2008, Kassel, Germany.

Kim, D-J, El-Tawil, S. and Naaman, A. E. (2007), "Correlation between Single Fiber Pullout and Tensile Response of FRC Composites with High Strength Steel Fibers," Proceedings of HPFRCC5, H. W. Reinhardt and A.E. Naaman Editors, July 10-13, Mainz, Germany.

Kok Seng Chia, Min-Hong Zhang, "Water permeability and chloride penetrability of high-strength lightweight aggregate concrete", Cement and Concrete Research, 32 (2002) 639-645

Liu, Zhichao. FROST DETERIORATION IN CONCRETE DUE TO DEICING SALT EXPOSURE: MECHANISM, MITIGATION AND CONCEPTUAL SURFACE SCALING MODEL. Diss. U of Michigan, 2014. N.p.: n.p., n.d. Print.

Naaman, A. E., and H. W. Reinhardt. "Proposed Classification of HPFRC Composites Based on Their Tensile Response." Materials and Structures 39.5 (2007): 547-55. Web

Naaman, A.E., and Reinhardt, H.W., "Characterization of High Performance Fiber Reinfoced Cement Composites," in "High Performance Fiber Reinforced Cement Composites – HPFRCC

2,' A.E. Naaman and F.W. Reinhardt, Editors, RILEM Pb. 31, E. and FN Spon, England, 1996; pp. 1-24

Oertel, Tina, Frank Hutter, Ricarda Tänzer, Uta Helbig, and Gerhard Sextl. "Primary Particle Size and Agglomerate Size Effects of Amorphous Silica in Ultra-high Performance Concrete." Cement and Concrete Composites 37 (2013): 61-67. Web.

Piérard, J., Dooms, B., and Cauberg, N., "Evaluation of Durability Parameters of UHPC Using Accelerated Lab Tests," Proceedings of Hipermat 2012 3rd Internationa Symposium on UHPC and Nanotechnology for High Performance Construction Materials, Ed., Schmidt, M., Fehling, E., Glotzbach, C., Fröhlich, S., and Piotrowski, S., Kassel University Press, Kassel, Germany, 2012, pp. 371–376.

Piotrowski, S. and Schmidt, M., "Life Cycle Cost Analysis of a UHPC-Bridge on Example of Two Bridge Refurbishment Designs," Proceedings of Hipermat 2012 3rd International Symposium on UHPC and Nanotechnology for High Performance Construction Materials, Ed., Schmidt, M., Fehling, E., Glotzbach, C., Fröhlich, S., and Piotrowski, S., Kassel University Press, Kassel, Germany, 2012, pp. 957–964

Pyo, Sukhoon, Kay Wille, Sherif El-Tawil, and Antoine E. Naaman. "Strain Rate Dependent Properties of Ultra High Performance Fiber Reinforced Concrete (UHP-FRC) under Tension." Cement and Concrete Composites 56 (2015a): 15-24. Web.

Pyo, S., El-Tawil, S. (2015b), "Capturing the Strain Hardening and Softening Responses of Cementitious Composites Subjected to Impact Loading," Journal of Construction and Building Materials, Elsevier, 81(15), April 2015, pp. 276–283, doi:10.1016/j.conbuildmat.2015.02.028.

Pyo, S. and El-Tawil, S. (2013a), "Crack velocity-dependent dynamic tensile behavior of concrete", International Journal of Impact Engineering, V55, pp. 63-70, http://dx.doi.org/10.1016/ j.ijimpeng.2013.01.003.

Pyo, S. and El-Tawil, S. (2013b), "Dynamic Fracture Mechanics Based DIF Models for Concrete under Tensile Loading," 2013 Conference of the ASCE Engineering Mechanics Institute, August 4 – 7, 2013, Northwestern University, Evanston, IL

Pyo, S., El-Tawil, S. and Naaman, A.E. (2013c), "Parametric Study of a New Impact Testing System for Ultrahigh Performance Concrete in Tension," 2013 Conference of the ASCE Engineering Mechanics Institute, August 4 – 7, 2013, Northwestern University, Evanston, IL

Rigaud, Stephane, Phillippe Fonollosa, and Gilles Chanvillard. Concrete Composition. Lafarge, assignee. Patent US8303708 B2. 6 Nov. 2012. Print.

RILEM TC 176-IDC, M.J. Setzer, P. Heine, S. Kasparek, S. Palecki, R. Auberg, V. Feldrappe, E. Siebel, Test methods of frost resistance of concrete: CIF-Test: Capillary suction, internal damage and freeze thaw test)-Reference method and alternative methods A and B, Mater. Struct. 37 (274) (2004) 743-753.

Rong, Z.d., W. Sun, H.j. Xiao, and W. Wang. "Effect of Silica Fume and Fly Ash on Hydration and Microstructure Evolution of Cement Based Composites at Low Water–binder Ratios." Construction and Building Materials 51 (2014): 446-50. Web.

Rong, Zhidan, Wei Sun, Haijun Xiao, and Guang Jiang. "Effects of Nano-SiO2 Particles on the Mechanical and Microstructural Properties of Ultra-high Performance Cementitious Composites." Cement and Concrete Composites 56 (2015): 25-31. Web.

Saleem, Muhammad Azhar, Amir Mirmiran, Jun Xia, and Kevin Mackie. "Development Length of High-Strength Steel Rebar in Ultrahigh Performance Concrete." J. Mater. Civ. Eng. Journal of Materials in Civil Engineering 25.8 (2013): 991-98. Web.

Slater, W.a., F.e. Richart, and G.g. Scofield. "Tests of Bond Resistance between Concrete and Steel." Technologic Papers of the Bureau of Standards (1920): n. pag. Web

Steinberg, Eric. "Structural Reliability of Prestressed UHPC Flexure Models for Bridge Girders." Journal of Bridge Engineering 15 (2010): 65-72. Web.

Sutter, Lawrence L. Evaluation of Methods for Characterizing Air Void Systems in Wisconsin Paving Concrete. Madison, WI: Wisconsin Highway Research Program, 2007. Print

Swenty, M. and Graybeal, B., "Influence of Differential Deflection on Staged Construction Deck-Level Connections," FHWA, U.S. Department of Transportation, Report No. FHWAHRT-12-057, National Technical Information Service Accession No. PB2012- 111528, 2012.

Tanesi, Jussara, and Richard Meininger. "Freeze-Thaw Resistance of Concrete with marginal Air Content." Transportation Research Record 2020.-1 (2007): 61-66. Web.

Wille, K., Kim, D., and Naaman, A.E., "Strain-Hardening UHP-FRC With Low Fiber Contents," Materials and Structures, Vol. 44, No. 3, 2011, pp. 583–598

Wille, K., Naaman, A.E., and El-Tawil, S., "Optimizing Ultra-High-Performance Fiber Reinforced Concrete," Concrete International, Vol. 33, No. 9, September 2011, pp. 35–41

Wille, K., Naaman, A.E., and Parra-Montesinos, G.J., "Ultra-High Performance Concrete With Compressive Strength Exceeding 150 MPa (22 ksi): A Simpler Way," ACI Materials Journal, Vol. 108, No. 1, January–February 2011, pp. 46–54.

Wille, Kay, and Antoinne Naaman. "Pullout Behavior of High-Strength Steel Fibers Embedded in Ultra-High-Performance Concrete." ACI Materials Journal MJ 109.4 (2012): n. pag. Web.

Wille, Kay, and Christopher Boisvert-Cotulio. "Material Efficiency in the Design of Ultra-high Performance Concrete." Construction and Building Materials 86 (2015): 33-43. Web.

Wille, Kay, and Gustavo Parra-Montesinos. "Effect of Beam Size, Casting Method, and Support Conditions on Flexural Behavior of Ultra-High-Performance Fiber-Reinforced Concrete." ACI Materials Journal MJ109.3 (2012): n. pag. Web.

Wille, Kay, Antoine E. Naaman, Sherif El-Tawil, and Gustavo J. Parra-Montesinos. "Ultra-high Performance Concrete and Fiber Reinforced Concrete: Achieving Strength and Ductility without Heat Curing." Mater Struct Materials and Structures 45.3 (2011): 309-24. Web.

Wille, Kay, Dong Joo Kim, and Antoine E. Naaman. "Strain-hardening UHP-FRC with Low Fiber Contents." Materials and Structures 44.3 (2011): 583-98. Web.

Wille, K., Xu, M., El-Tawil, S. and Naaman, A.E. (2015), "Dynamic Impact Factors of Strain Hardening UHP-FRC under Direct Tensile Loading at Low Strain Rates," Accepted for publication in the RILEM Materials and Structures Journal. DOI: 10.1617/s11527-015-0581-y.

Wille, K., El-Tawil, S. and Naaman, A.E. (2014), "Properties of Strain Hardening Ultra High Performance Fiber Reinforced Concrete (UHP-FRC) under Direct Tensile Loading," Journal of Cement and Concrete Composites, Elsevier, 48, pp. 53-66, doi:10.1016/j.cemconcomp.2013.12.015

Wille, K., Naaman, A. E. and El-Tawil, S. (2011), "Ultra High Performance Fiber Reinforced Concrete (UHP-FRC) Record Performance under Tensile Loading," Concrete International, American Concrete Institute, Sept. 2011, pp. 35-41.

Wille, K., El-Tawil, S. and Naaman, A. E. (2011), “Strain Rate Dependent Tensile Behavior of Ultra-High Performance Fiber Reinforced Concrete,” Proceedings of HPFRCC6, H. W. Reinhardt and G. Parra Editors, Ann Arbor, MI.

Wipf, T., Sritharan, Sri,., “Iowa’s UHPC Implementation” Iowa Research, Bureau of Research and Technology, April, 2011

Yazıcı, Halit. "The Effect of Silica Fume and High-volume Class C Fly Ash on Mechanical Properties, Chloride Penetration and Freeze–thaw Resistance of Self-compacting Concrete." Construction and Building Materials 22.4 (2008): 456-62. Web.

Yu, R., P. Spiesz, and H.j.h. Brouwers. "Development of an Eco-friendly Ultra-High Performance Concrete (UHPC) with Efficient Cement and Mineral Admixtures Uses." Cement and Concrete Composites 55 (2015): 383-94. Web.

Yu, R., P. Spiesz, and H.j.h. Brouwers. "Development of Ultra-High Performance Fibre Reinforced Concrete (UHPFRC): Towards an Efficient Utilization of Binders and Fibres." Construction and Building Materials 79 (2015): 273-82. Web.

Yu, R., P. Spiesz, and H.j.h. Brouwers. "Effect of Nano-silica on the Hydration and Microstructure Development of Ultra-High Performance Concrete (UHPC) with a Low Binder Amount." Construction and Building Materials 65 (2014): 140-50. Web.

Intentionally left blank

9. APPENDIX A – STRESS-STRAIN PLOTS FOR ALL UHPC MIXES

This appendix lists the stress-strain plots for all tensile tests conducted on UHPC coupons. For each set of tensile tests, at least 3 specimen tensile plots are averaged in order to produce a single tensile response curve. The plots are averaged at each point along the strain range. The result is then processed through a moving average filter to account for minute changes due to the sensitivity of the equipment. See Section 3.3.1 for further details.

9.1. WHITE CEMENT MIXES

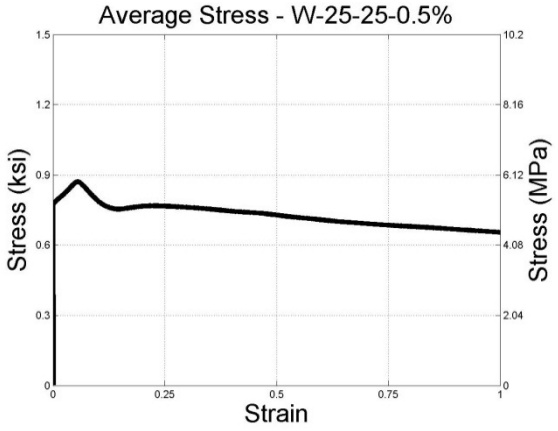

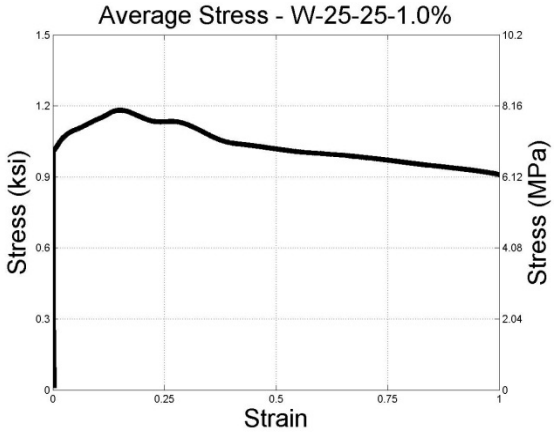

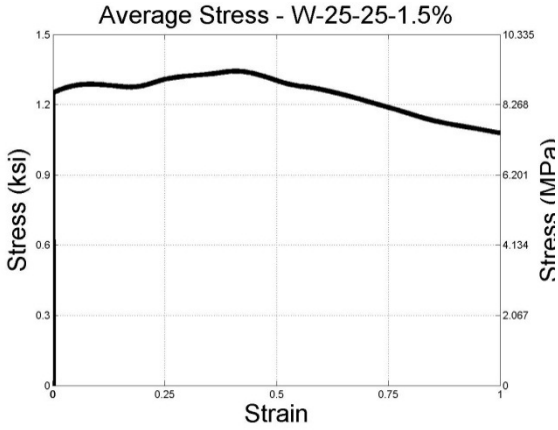

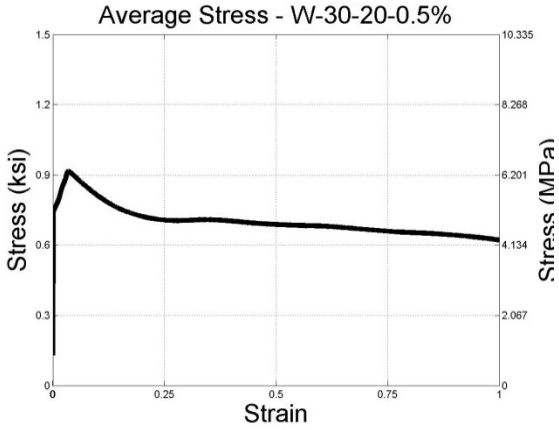

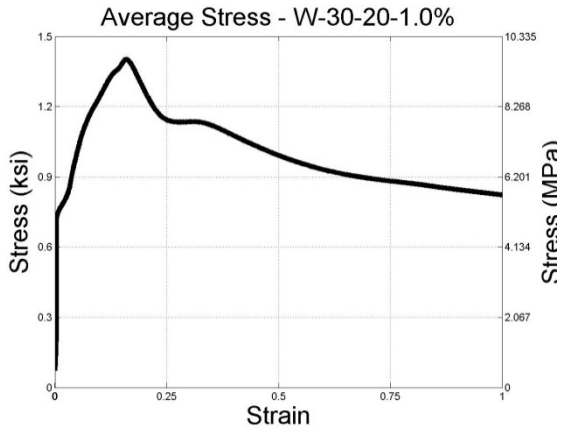
Average Stress - W-30-20-1.0%
Stress (ksi)
Stress (MPa)
Strain
0
0.3
0.6
0.9
1.2
1.5
2.067
4.134
6.201
8.268
10.335
0.25
0.5
0.75
1

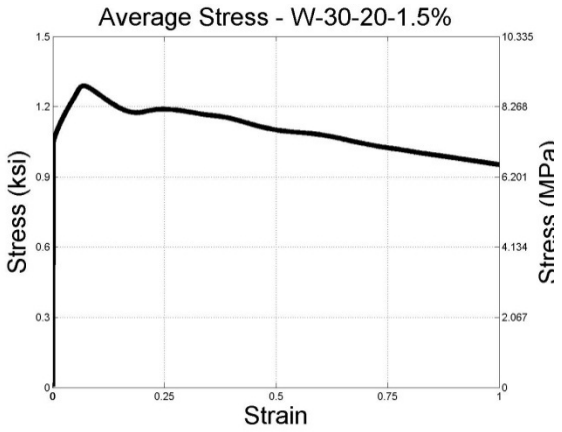
Average Stress - W-30-20-1.5%
Stress (ksi)
Stress (MPa)
Strain
0
0.3
0.6
0.9
1.2
1.5
2.067
4.134
6.201
8.268
10.335
0.25
0.5
0.75
1

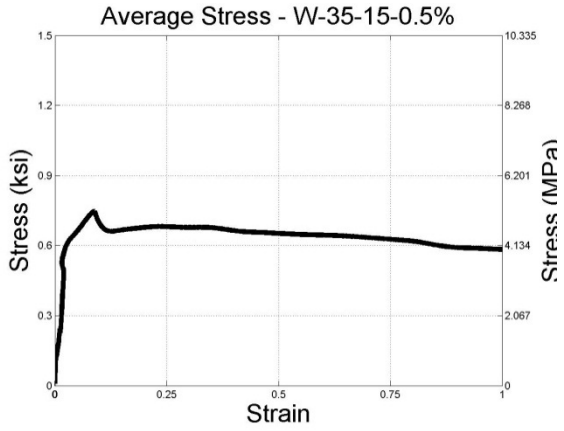
Average Stress - W-35-15-0.5%
Stress (ksi)
Stress (MPa)
Strain
0
0.3
0.6
0.9
1.2
1.5
2.067
4.134
6.201
8.268
10.335
0.25
0.5
0.75
1

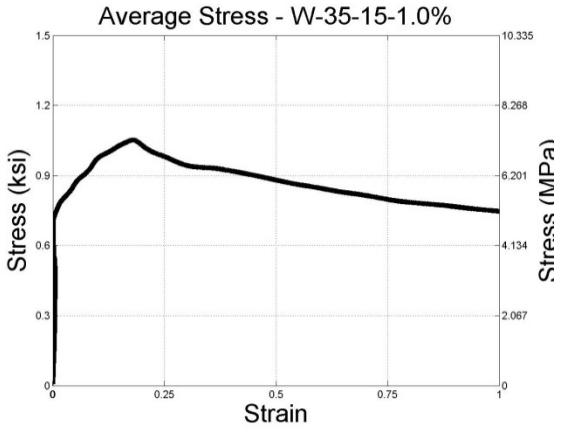
Average Stress - W-35-15-1.0%
Stress (ksi)
Stress (MPa)
Strain
0
0.3
0.6
0.9
1.2
1.5
2.067
4.134
6.201
8.268
10.335
0.25
0.5
0.75
1

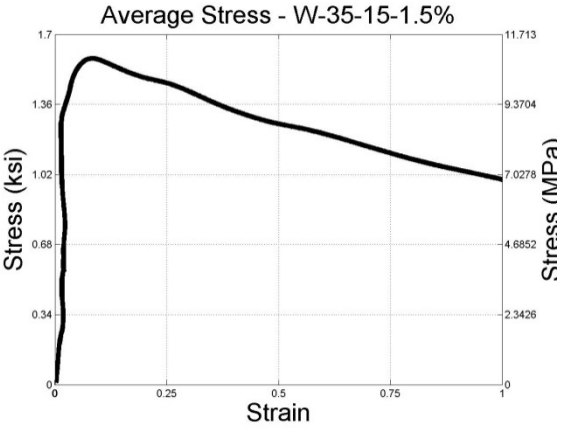
Average Stress - W-35-15-1.5%
Stress (ksi)
Stress (MPa)
Strain
0
0.34
0.68
1.02
1.36
1.7
2.3426
4.6852
7.0278
9.3704
11.713
0.25
0.5
0.75
1

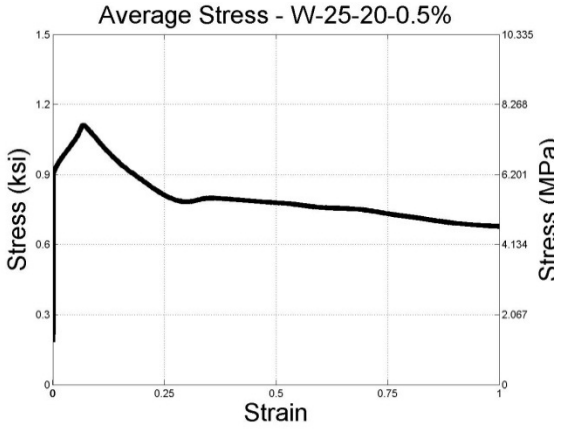
Average Stress - W-25-20-0.5%
Stress (ksi)
Stress (MPa)
Strain
0
0.3
0.6
0.9
1.2
1.5
2.067
4.134
6.201
8.268
10.335
0.25
0.5
0.75
1

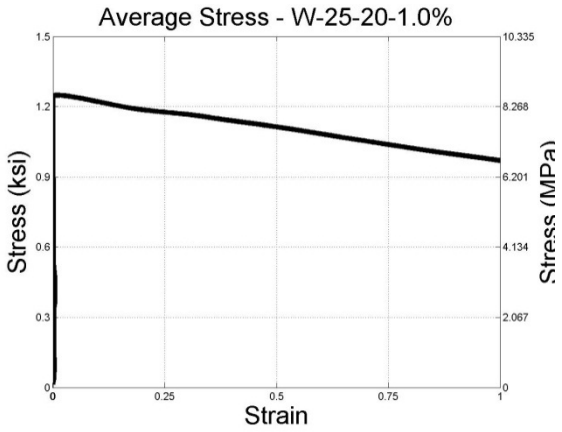
Average Stress - W-25-20-1.0%
Stress (ksi)
Stress (MPa)
Strain

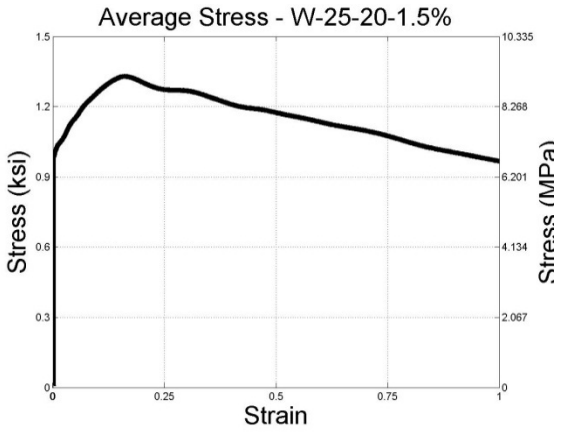
Average Stress - W-25-20-1.5%
Stress (ksi)
Stress (MPa)
Strain

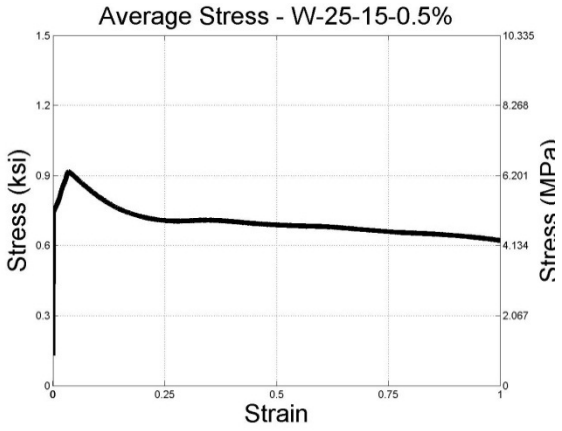
Average Stress - W-25-15-0.5%
Stress (ksi)
Stress (MPa)
Strain

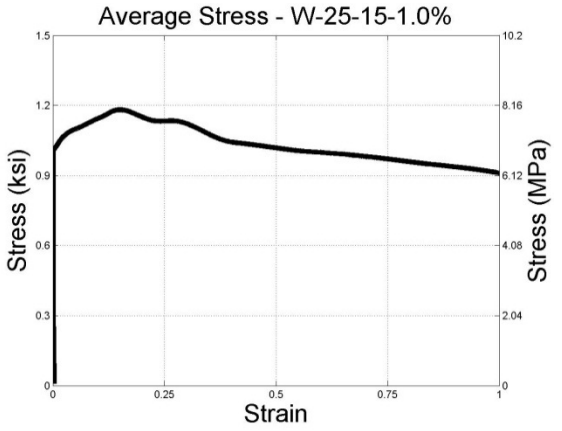
Average Stress - W-25-15-1.0%
Stress (ksi)
Stress (MPa)
Strain

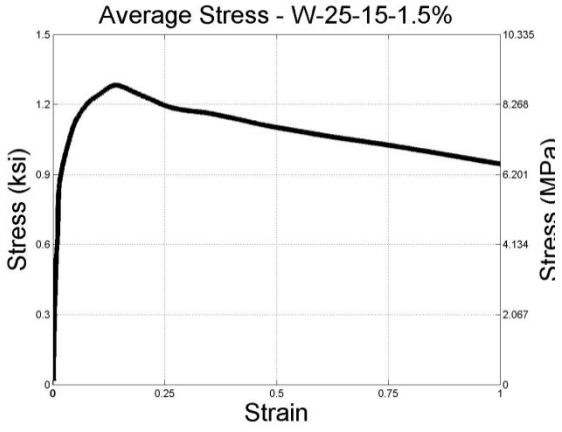
Average Stress - W-25-15-1.5%
Stress (ksi)
Stress (MPa)
Strain

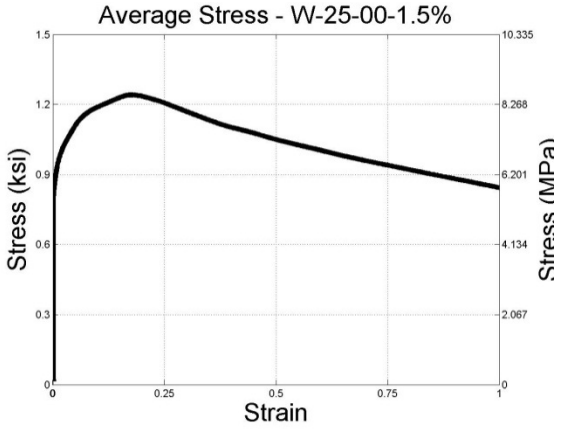
Average Stress - W-25-00-1.5%
Stress (ksi)
Stress (MPa)
Strain

9.2. PORTLAND TYPE V CEMENT MIXES

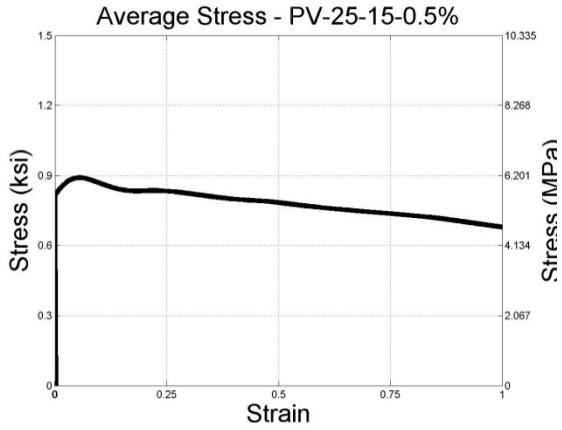

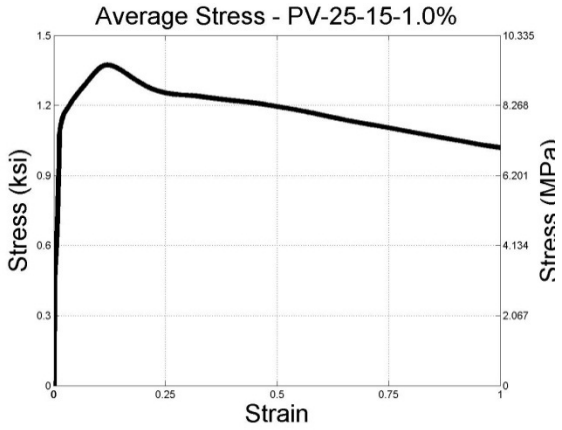

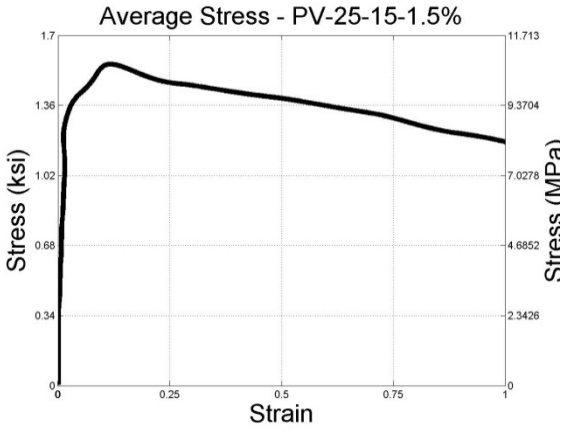

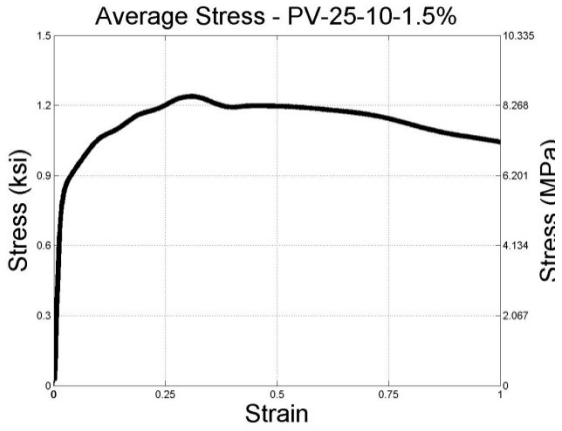

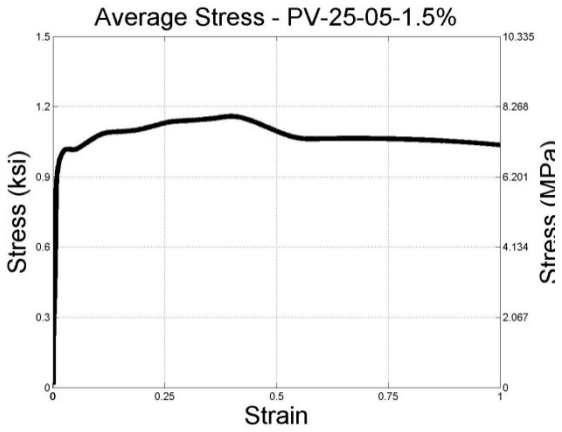
Average Stress - PV-25-05-1.5%
Stress (ksi)
Stress (MPa)
Strain
0
0.3
0.6
0.9
1.2
1.5
2.067
4.134
6.201
8.268
10.335
0.25
0.5
0.75
1

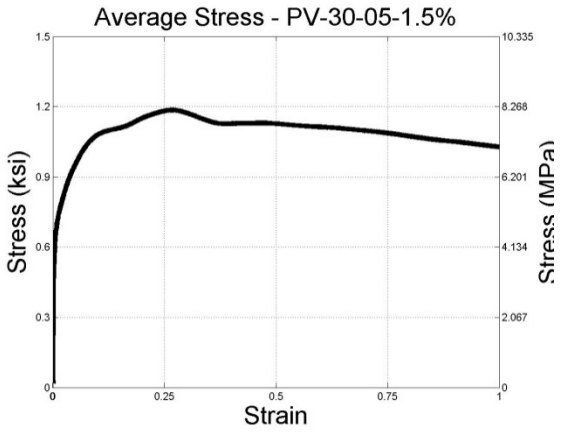
Average Stress - PV-30-05-1.5%
Stress (ksi)
Stress (MPa)
Strain
0
0.3
0.6
0.9
1.2
1.5
2.067
4.134
6.201
8.268
10.335
0.25
0.5
0.75
1

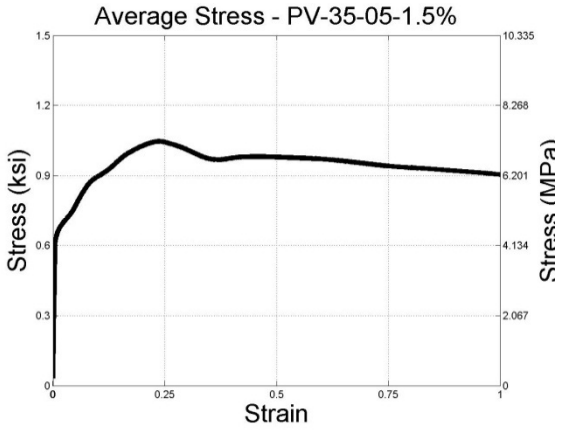
Average Stress - PV-35-05-1.5%
Stress (ksi)
Stress (MPa)
Strain
0
0.3
0.6
0.9
1.2
1.5
2.067
4.134
6.201
8.268
10.335
0.25
0.5
0.75
1

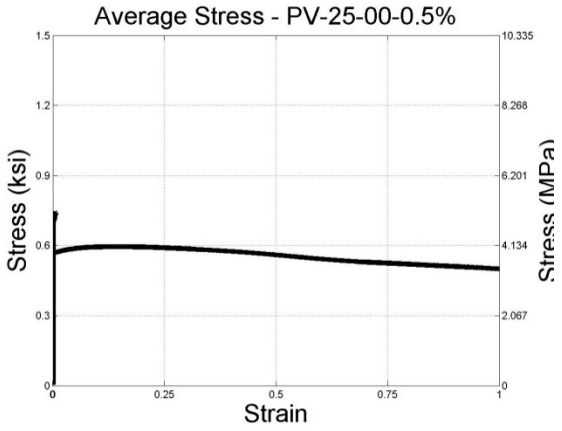
Average Stress - PV-25-00-0.5%
Stress (ksi)
Stress (MPa)
Strain
0
0.3
0.6
0.9
1.2
1.5
2.067
4.134
6.201
8.268
10.335
0.25
0.5
0.75
1

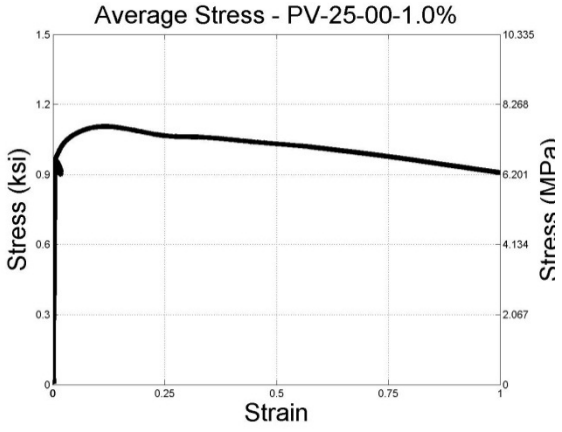
Average Stress - PV-25-00-1.0%
Stress (ksi)
Stress (MPa)
Strain
0
0.3
0.6
0.9
1.2
1.5
2.067
4.134
6.201
8.268
10.335
0.25
0.5
0.75
1

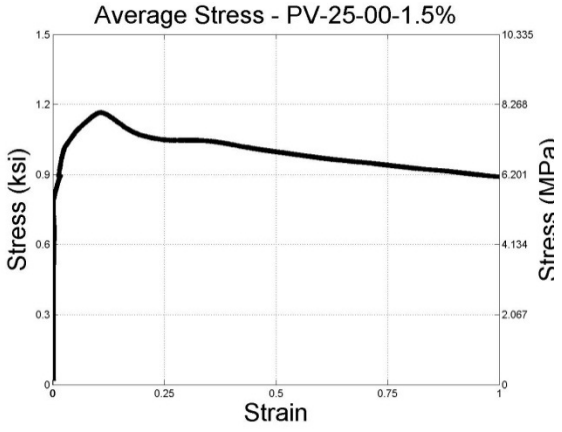
Average Stress - PV-25-00-1.5%
Stress (ksi)
Stress (MPa)
Strain
0
0.3
0.6
0.9
1.2
1.5
2.067
4.134
6.201
8.268
10.335
0.25
0.5
0.75
1

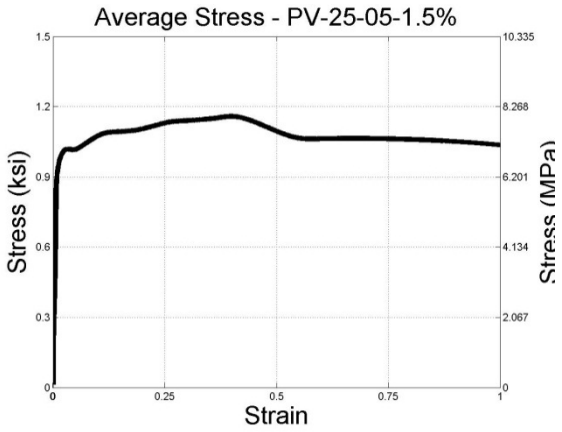
Average Stress - PV-25-05-1.5%
Stress (ksi)
Stress (MPa)
Strain
1.5
1.2
0.9
0.6
0.3
0
10.335
8.268
6.201
4.134
2.067
0
0.25
0.5
0.75
1

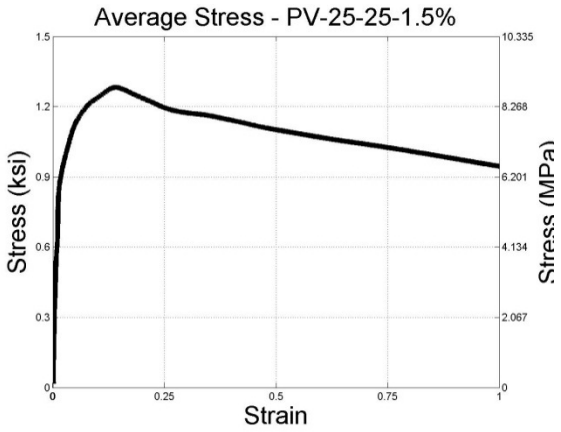
Average Stress - PV-25-25-1.5%
Stress (ksi)
Stress (MPa)
Strain
1.5
1.2
0.9
0.6
0.3
0
10.335
8.268
6.201
4.134
2.067
0
0.25
0.5
0.75
1

9.3. GGBS/PORTLAND TYPE I CEMENT MIXES

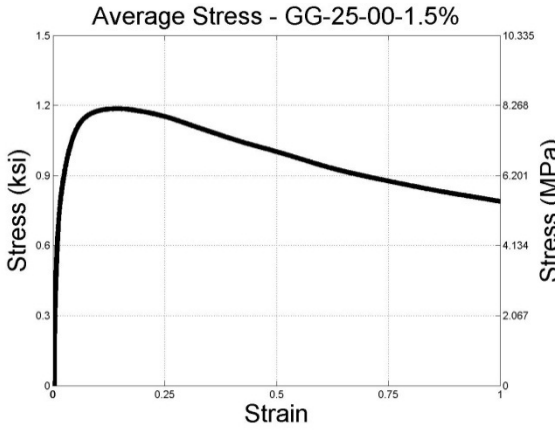

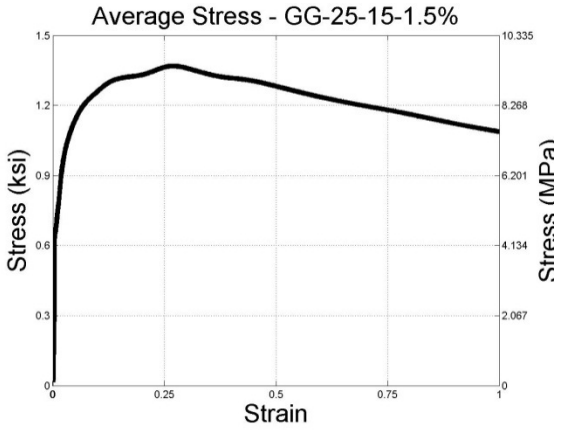

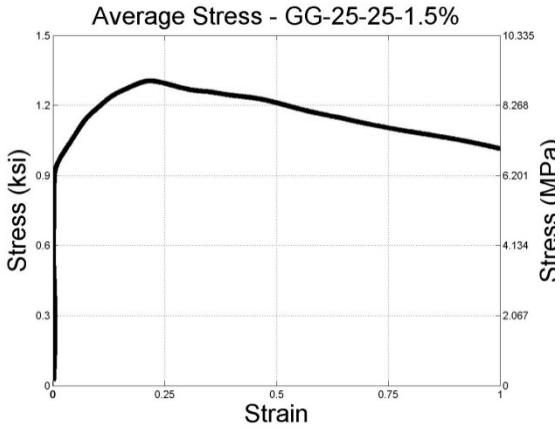

10. APPENDIX B – RESULTS OF FREEZE-THAW TESTING – RILEM

This appendix lists the raw results from the freeze-thaw testing outlined in section 4.3.1. For each specimen, the internal damage as measured by the relative dynamic modulus; moisture uptake and salt scaling are listed.

W-25-25-1.5												
	Salt scaling, g/m^2 concrete				Internal damage by RDM, %				Moisture uptake, %			
F-T cycle	UHPC 1	UHPC 1	UHPC 1		UHPC 1	UHPC 1	UHPC 1		UHPC 1	UHPC 1	UHPC 1	
0	0.0	0.0	0.0		100	100	100		0.00	0.00	0.00	
10	81.4	67.3	74.4		100	100	100		0.23	0.24	0.23	
18	112.3	89.0	100.6		100	100	100		0.25	0.27	0.26	
23	161.8	122.6	142.2		100	99	99.5		0.29	0.30	0.30	
45	177.3	137.1	157.2		100	99	99.5		0.31	0.30	0.30	
61	194.8	157.5	176.2		100	99	99.5		0.32	0.32	0.32	

W-25-15-1.5												
	Salt scaling, g/m^2 concrete				Internal damage by RDM, %				Moisture uptake, %			
F-T cycle	UHPC 2	UHPC 2	UHPC 2		UHPC 2	UHPC 2	UHPC 2		UHPC 2	UHPC 2	UHPC 2	
0	0.0	0.0	0.0		100	100	100		0.00	0.00	0.00	
14	16.4	6.6	11.5		100	100	100		0.18	0.20	0.19	
26	24.3	10.7	17.5		100	100	100		0.20	0.23	0.21	
40	32.9	24.8	28.8		100	100	100		0.20	0.25	0.22	
52	43.1	35.5	39.3		100	100	100		0.24	0.27	0.25	
68	49.3	52.1	50.7		100	100	100		0.24	0.27	0.26	

W-25-00-1.5												
	Salt scaling, g/m^2 concrete				Internal damage by RDM, %				Moisture uptake, %			
F-T cycle	UHPC 3	UHPC 3	UHPC 3		UHPC 3	UHPC 3	UHPC 3		UHPC 3	UHPC 3	UHPC 3	
0	0.0	0.0	0.0		100	100	100		0.00	0.00	0.00	
14	9.9	6.0	8.0		100	100	100		0.18	0.18	0.22	
26	22.3	9.4	15.9		100	100	100		0.20	0.20	0.23	
40	30.6	17.5	24.0		100	100	100		0.20	0.21	0.25	
52	42.1	25.5	33.8		100	100	100		0.24	0.25	0.26	
68	51.2	35.6	43.4		100	100	100		0.24	0.26	0.28	

PV-25-25-1.5											
	Salt scaling, g/m^2 concrete				Internal damage by RDM, %				Moisture uptake, %		
F-T cycle	UHPC 4	UHPC 4	UHPC 4	UHPC 4	UHPC 4	UHPC 4	UHPC 4		UHPC 4	UHPC 4	UHPC 4
0	0.0	0.0	0.0		100	100	100		0.00	0.00	0.00
14	13.6	10.7	12.2		100	100	100		0.18	0.18	0.17
26	18.7	14.0	16.4		100	100	100		0.20	0.20	0.17
40	27.3	25.6	26.5		100	100	100		0.20	0.21	0.19
52	33.8	32.2	33.0		100	100	100		0.24	0.24	0.22
68	47.4	40.5	43.9		100	100	100		0.24	0.25	0.22

PV-25-15-1.5										
	Salt scaling, g/m^2 concrete			Internal damage by RDM, %				Moisture uptake, %		
F-T cycle	UHPC 5	UHPC 5	UHPC 5	UHPC 5	UHPC 5	UHPC 5		UHPC 5	UHPC 5	UHPC 5
0	0.0	0.0	0.0	100	100	100		0.00	0.00	0.00
14	1.5	6.7	4.1	100	100	100		0.13	0.10	0.12
26	12.3	14.2	13.3	100	100	100		0.16	0.14	0.15
40	22.3	22.5	22.4	100	100	100		0.18	0.15	0.17
52	35.4	32.2	33.8	100	100	100		0.22	0.19	0.20
68	50.8	45.0	47.9	100	100	100		0.22	0.19	0.21

PV-25-00-1.5										
	Salt scaling, g/m^2 concrete			Internal damage by RDM, %				Moisture uptake, %		
F-T cycle	UHPC 6	UHPC 6	UHPC 6	UHPC 6	UHPC 6	UHPC 6		UHPC 6	UHPC 6	UHPC 6
0	0.0	0.0	0.0	100	100	100		0.00	0.00	0.00
14	26.6	20.3	23.4	100	100	100		0.10	0.10	0.10
30	50.6	42.2	46.4	100	100	100		0.13	0.13	0.13
42	75.4	64.9	70.2	100	100	100		0.14	0.15	0.15
56	85.7	70.6	78.2	100	100	100		0.16	0.15	0.16

GG-25-25-1.5										
	Salt scaling, g/m^2 concrete			Internal damage by RDM, %				Moisture uptake, %		
F-T cycle	UHPC 8	UHPC 8	UHPC 8	UHPC 8	UHPC 8	UHPC 8		UHPC 8	UHPC 8	UHPC 8
0	0.0	0.0	0.0	100	100	100		0.00	0.00	0.00
14	15.4	4.4	9.9	100	100	100		0.18	0.20	0.19
26	26.3	9.8	18.0	100	100	100		0.23	0.22	0.23
40	40.8	24.0	32.4	100	100	100		0.25	0.25	0.25
52	50.8	36.5	43.6	100	100	100		0.30	0.29	0.29
68	69.8	56.1	63.0	100	100	100		0.32	0.30	0.31

GG-25-15-1.5										
	Salt scaling, g/m^2 concrete			Internal damage by RDM, %				Moisture uptake, %		
F-T cycle	UHPC 7	UHPC 7	UHPC 7	UHPC 7	UHPC 7	UHPC 7		UHPC 7	UHPC 7	UHPC 7
0	0.0	0.0	0.0	100	100	100		0.00	0.00	0.00
14	10.8	5.4	8.1	100	100	100		0.18	0.15	0.17
26	24.3	15.4	19.8	100	100	100		0.24	0.19	0.22
40	33.2	23.6	28.4	100	100	100		0.28	0.23	0.26
52	44.0	29.0	36.5	100	100	100		0.34	0.25	0.30
68	61.1	41.7	51.4	100	100	100		0.36	0.27	0.31

GG-25-00-1.5										
	Salt scaling, g/m^2 concrete			Internal damage by RDM, %				Moisture uptake, %		
F-T cycle	UHPC 9	UHPC 9	UHPC 9	UHPC 9	UHPC 9	UHPC 9		UHPC 9	UHPC 9	UHPC 9
0	0.0	0.0	0.0	100	100	100		0.00	0.00	0.00
10	23.9	29.9	26.9	100	100	100		0.18	0.16	0.17
24	43.9	46.3	45.1	100	100	100		0.21	0.19	0.20
40	64.6	69.1	66.9	100	100	100		0.24	0.21	0.23
52	83.1	94.0	88.6	100	100	100		0.25	0.23	0.24
66	90.0	100.4	95.2	100	100	100		0.25	0.23	0.24

11. APPENDIX C – DETAILS FROM BAR PULL-OUT TESTING

This appendix lists the results from the bar pull out testing as outlined in section 5.2.1. For each parameter, at least 2 tests were performed. Below are the images for the damaged specimens taken after testing as well as the material parameters being tested.

13B-100-2%-P-28D	
Bar Diameter:	#4, Bars (13 mm)
Coating:	Epoxy
Embedded Length:	4 inches (100 mm)
Fiber Content (% vol.)	2%
Casting Orientation:	Parallel
Curing Age:	28 Days

Test 1

Test 2

13E-100-2%-P-28D	
Bar Diameter:	#4, Bars (13 mm)
Coating:	Epoxy
Embedded Length:	4 inches (100 mm)
Fiber Content (% vol.)	2%
Casting Orientation:	Parallel
Curing Age:	28 Days

Test 1

Test 2

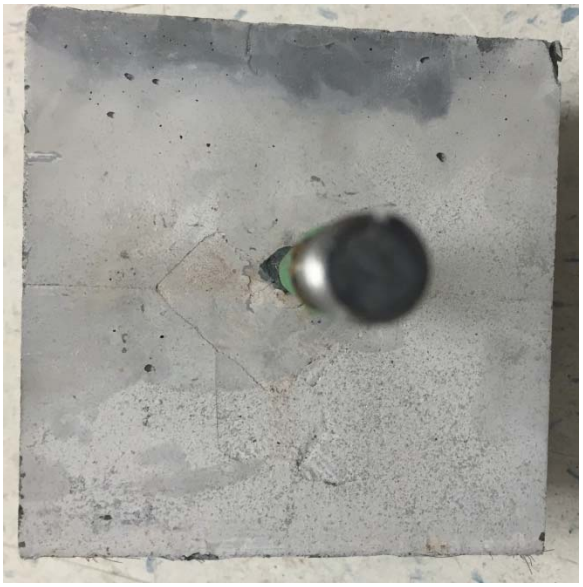

13B-75-2%-P-28D	
Bar Diameter:	#4, Bars (13 mm)
Coating:	Plain
Embedded Length:	3 inches (75 mm)
Fiber Content (% vol.)	2%
Casting Orientation:	Parallel
Curing Age:	28 Days

Test 1

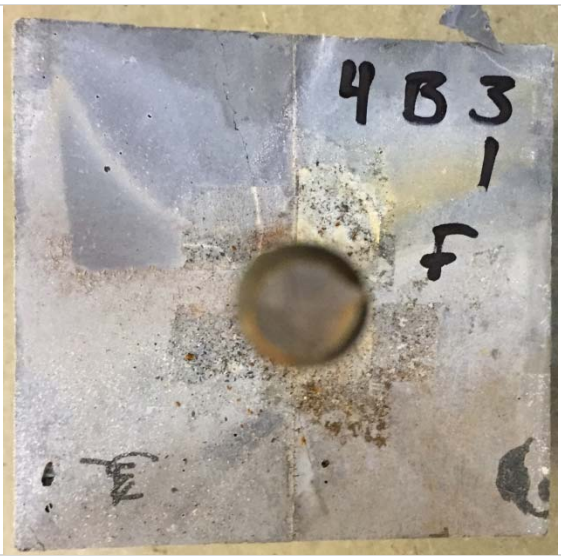

Test 2

13E-75-2%-P-28D	
Bar Diameter:	#4, Bars (13 mm)
Coating:	Epoxy
Embedded Length:	3 inches (75 mm)
Fiber Content (% vol.)	2%
Casting Orientation:	Parallel
Curing Age:	28 Days

Test 1

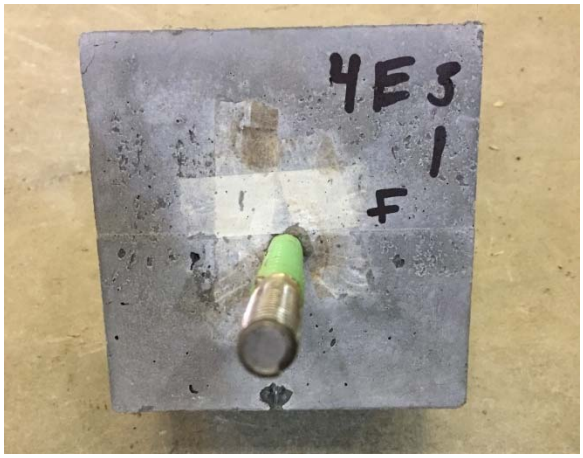

Test 2

13B-50-2%-P-28D	
Bar Diameter:	#4, Bars (13 mm)
Coating:	Plain
Embedded Length:	2 inches (50 mm)
Fiber Content (% vol.)	2%
Casting Orientation:	Parallel
Curing Age:	28 Days

Test 1

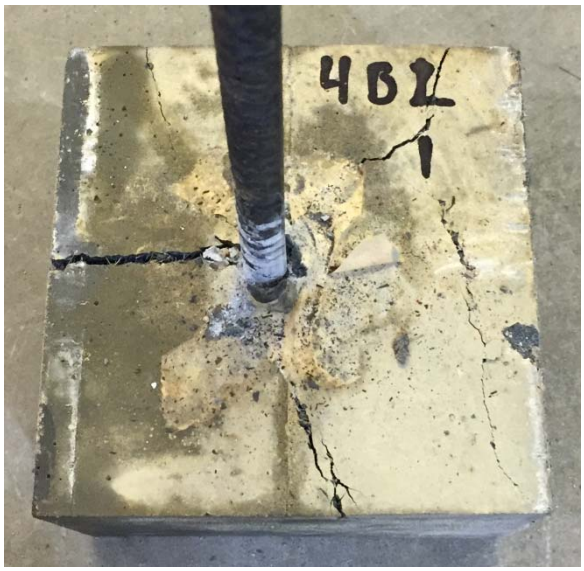

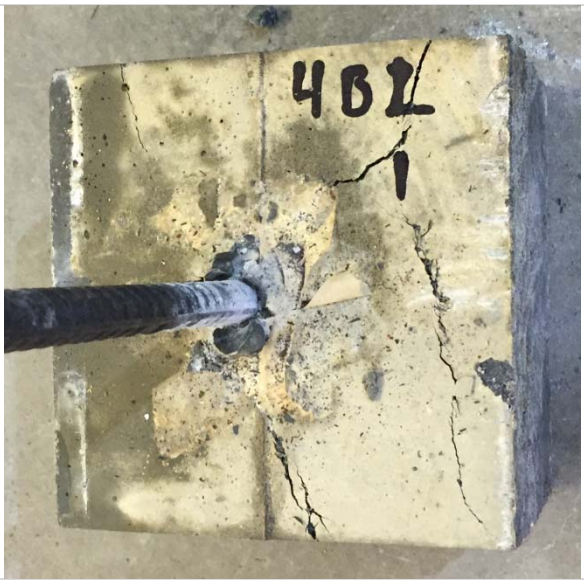

Test 2

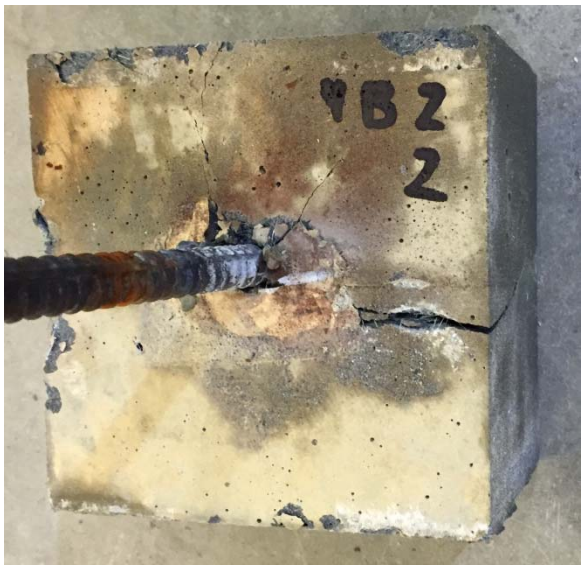

13E-50-2%-P-28D	
Bar Diameter:	#4, Bars (13 mm)
Coating:	Epoxy
Embedded Length:	2 inches (50 mm)
Fiber Content (% vol.)	2%
Casting Orientation:	Parallel
Curing Age:	28 Days

Test 1

Test 2

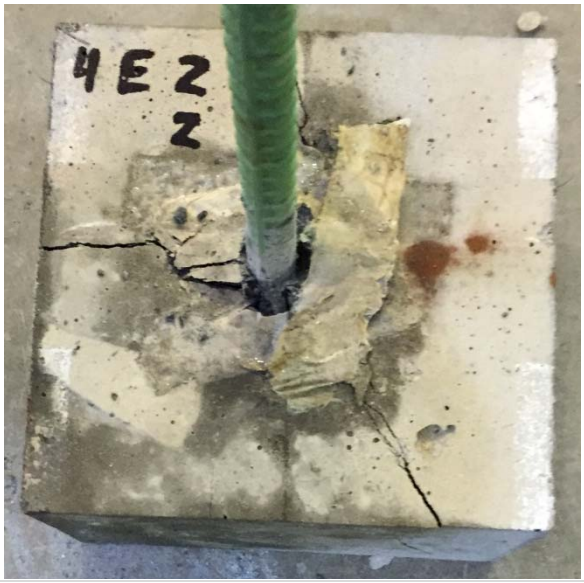

16B-100-2%-P-28D	
Bar Diameter:	#5, Bars (16 mm)
Coating:	Plain
Embedded Length:	4 inches (100 mm)
Fiber Content (% vol.)	2%
Casting Orientation:	Parallel
Curing Age:	28 Days

Test 1

Test 2

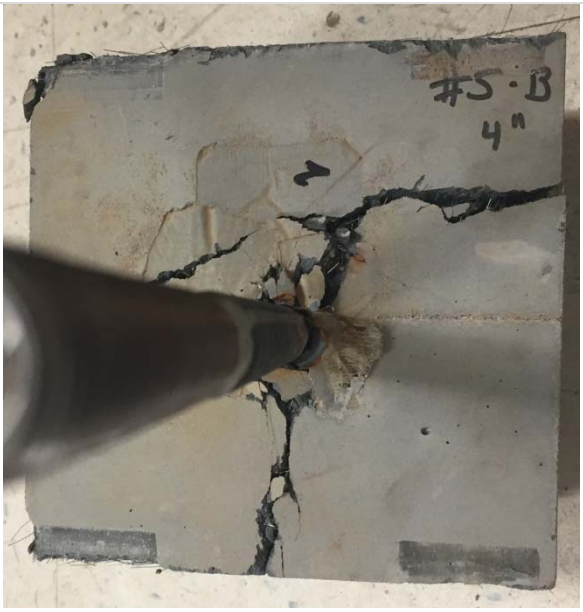

Test 3	
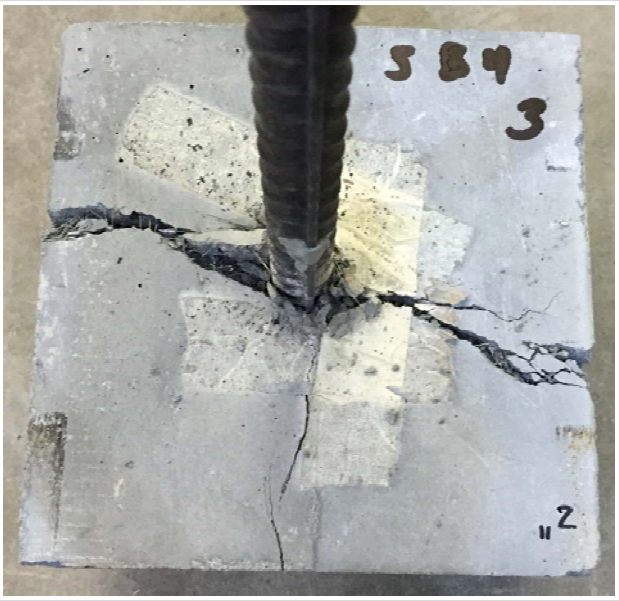	

16E-100-2%-P-28D	
Bar Diameter:	#5, Bars (16 mm)
Coating:	Epoxy
Embedded Length:	4 inches (100 mm)
Fiber Content (% vol.)	2%
Casting Orientation:	Parallel
Curing Age:	28 Days

Test 1

Test 2

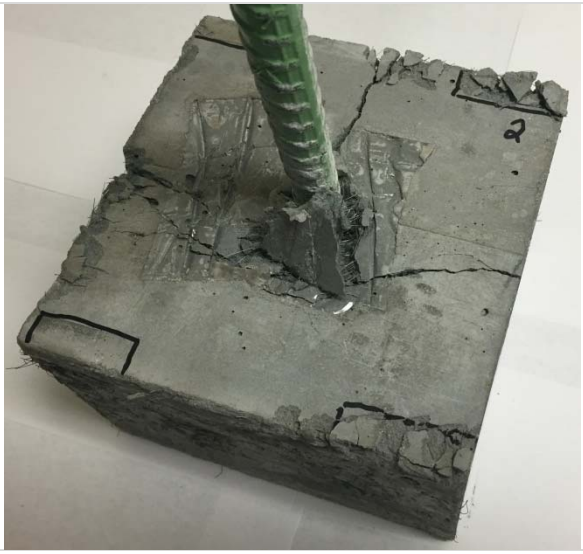

Test 3
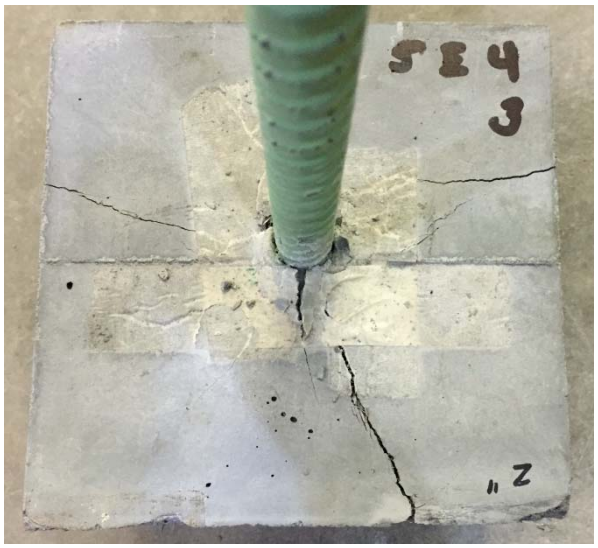 

16B-75-2%-P-28D	
Bar Diameter:	#5, Bars (16 mm)
Coating:	Plain
Embedded Length:	3 inches (75 mm)
Fiber Content (% vol.)	2%
Casting Orientation:	Parallel
Curing Age:	28 Days

Test 1

Test 2

16E-75-2%-P-28D	
Bar Diameter:	#5, Bars (16 mm)
Coating:	Epoxy
Embedded Length:	3 inches (75 mm)
Fiber Content (% vol.)	2%
Casting Orientation:	Parallel
Curing Age:	28 Days

Test 1

Test 2

16B-50-2%-P-28D	
Bar Diameter:	#5, Bars (16 mm)
Coating:	Plain
Embedded Length:	2 inches (50 mm)
Fiber Content (% vol.)	2%
Casting Orientation:	Parallel
Curing Age:	28 Days

Test 1

Test 2

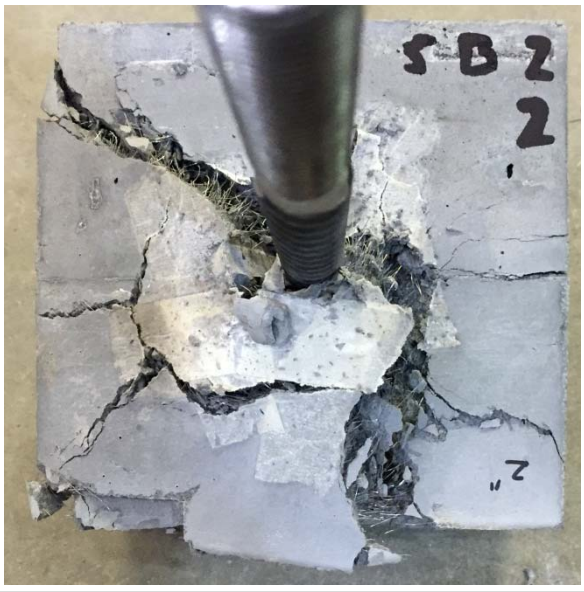

16E-50-2%-P-28D	
Bar Diameter:	#5, Bars (16 mm)
Coating:	Epoxy
Embedded Length:	2 inches (50 mm)
Fiber Content (% vol.)	2%
Casting Orientation:	Parallel
Curing Age:	28 Days

Test 1

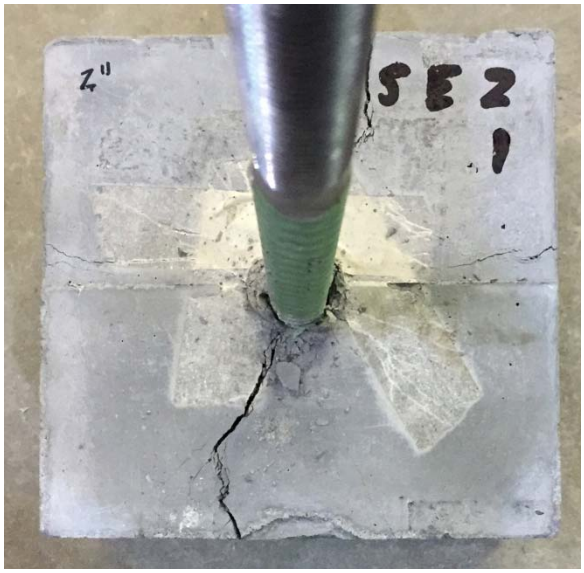

Test 2

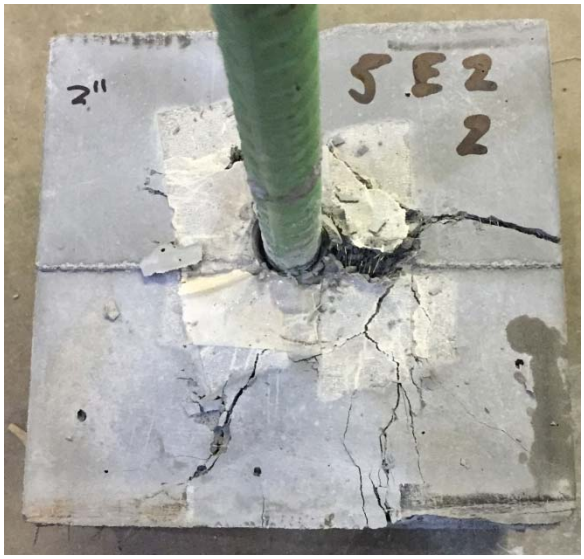

19B-100-2%-P-28D	
Bar Diameter:	#6, Bars (19 mm)
Coating:	Plain
Embedded Length:	4 inches (100 mm)
Fiber Content (% vol.)	2%
Casting Orientation:	Parallel
Curing Age:	28 Days

Test 1

Test 2

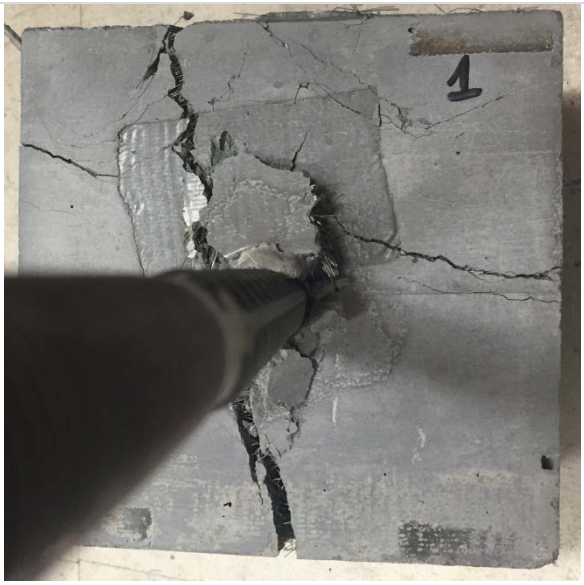

19E-100-2%-P-28D	
Bar Diameter:	#6, Bars (19 mm)
Coating:	Epoxy
Embedded Length:	4 inches (100 mm)
Fiber Content (% vol.)	2%
Casting Orientation:	Parallel
Curing Age:	28 Days

Test 1

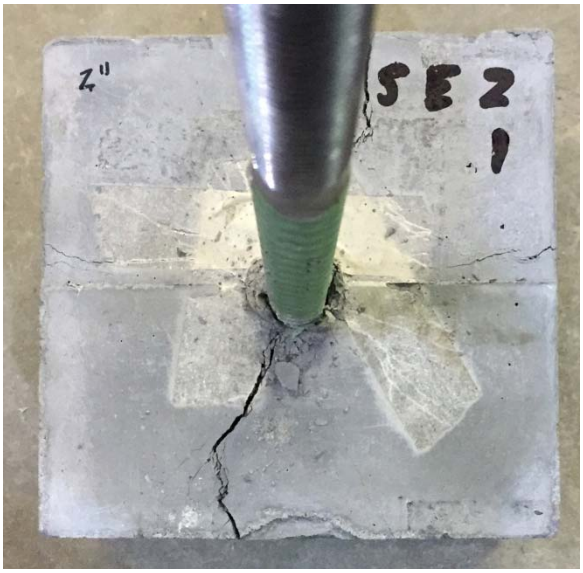

Test 2

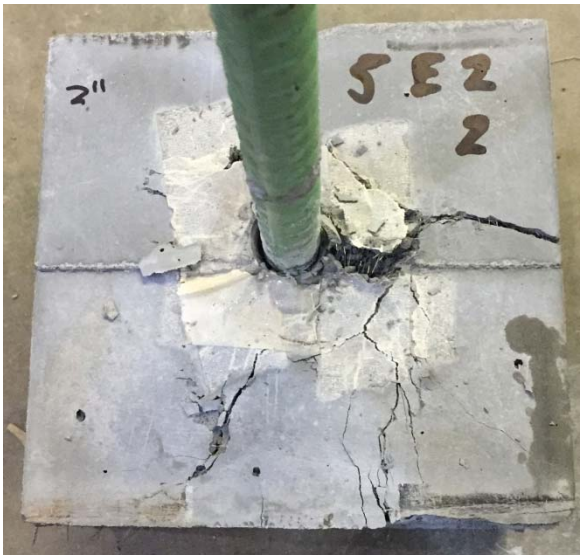

19B-75-2%-P-28D	
Bar Diameter:	#6, Bars (19 mm)
Coating:	Plain
Embedded Length:	3 inches (75 mm)
Fiber Content (% vol.)	2%
Casting Orientation:	Parallel
Curing Age:	28 Days

Test 1

Test 2

19E-75-2%-P-28D	
Bar Diameter:	#6, Bars (19 mm)
Coating:	Epoxy
Embedded Length:	3 inches (75 mm)
Fiber Content (% vol.)	2%
Casting Orientation:	Parallel
Curing Age:	28 Days

Test 1

Test 2

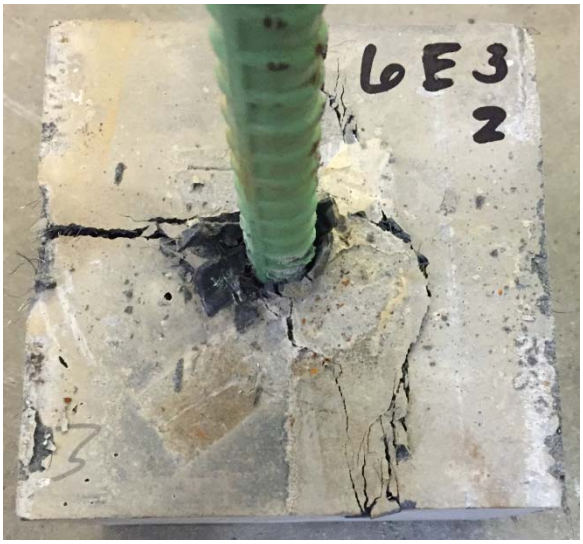

19B-50-2%-P-28D	
Bar Diameter:	#6, Bars (19 mm)
Coating:	Plain
Embedded Length:	2 inches (50 mm)
Fiber Content (% vol.)	2%
Casting Orientation:	Parallel
Curing Age:	28 Days

Test 1

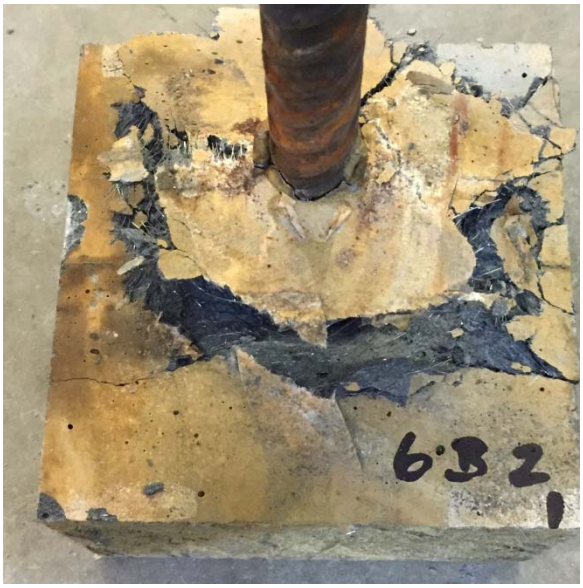

Test 2

19E-50-2%-P-28D	
Bar Diameter:	#6, Bars (19 mm)
Coating:	Epoxy
Embedded Length:	2 inches (50 mm)
Fiber Content (% vol.)	2%
Casting Orientation:	Parallel
Curing Age:	28 Days

Test 1

Test 2

19B-75-1%-P-28D	
Bar Diameter:	#6, Bars (19 mm)
Coating:	Plain
Embedded Length:	3 inches (75 mm)
Fiber Content (% vol.)	1%
Casting Orientation:	Parallel
Curing Age:	28 Days

Test 1

Test 2

19E-75-2%-T-28D	
Bar Diameter:	#6, Bars (19 mm)
Coating:	Epoxy
Embedded Length:	2 inches (50 mm)
Fiber Content (% vol.)	2%
Casting Orientation:	Transverse
Curing Age:	28 Days

Test 1

Test 2

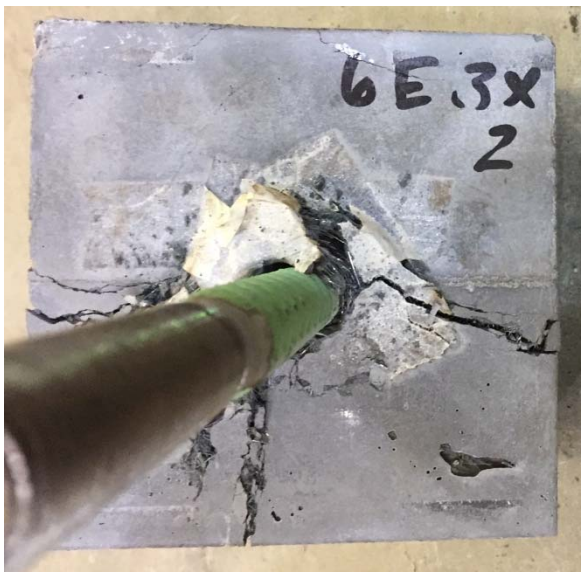

16E-100-2%-P-1D	
Bar Diameter:	#5, Bars (16 mm)
Coating:	Epoxy
Embedded Length:	4 inches (100 mm)
Fiber Content (% vol.)	2%
Casting Orientation:	Parallel
Curing Age:	1 Day

Test 1

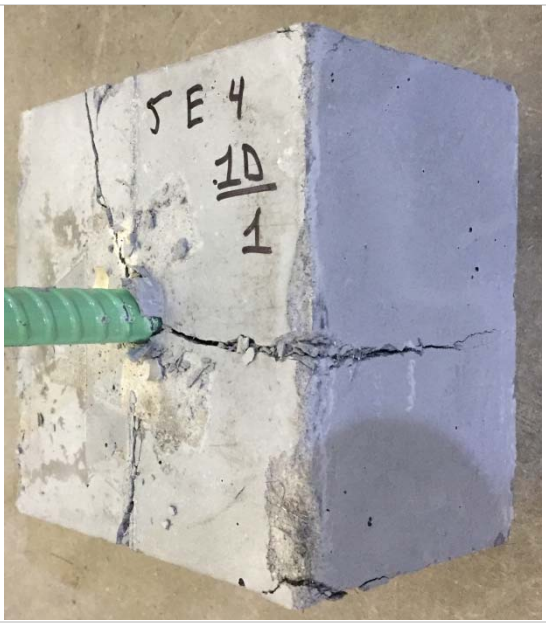

Test 2

16E-100-2%-P-3D	
Bar Diameter:	#5, Bars (16 mm)
Coating:	Epoxy
Embedded Length:	4 inches (100 mm)
Fiber Content (% vol.)	2%
Casting Orientation:	Parallel
Curing Age:	3 Days

Test 1

Test 2

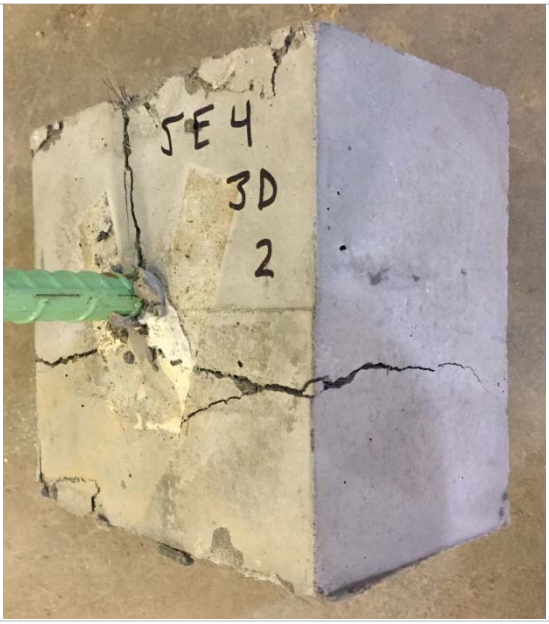

16E-100-2%-P-7D	
Bar Diameter:	#5, Bars (16 mm)
Coating:	Epoxy
Embedded Length:	4 inches (100 mm)
Fiber Content (% vol.)	2%
Casting Orientation:	Parallel
Curing Age:	7 Days

Test 1

Test 2

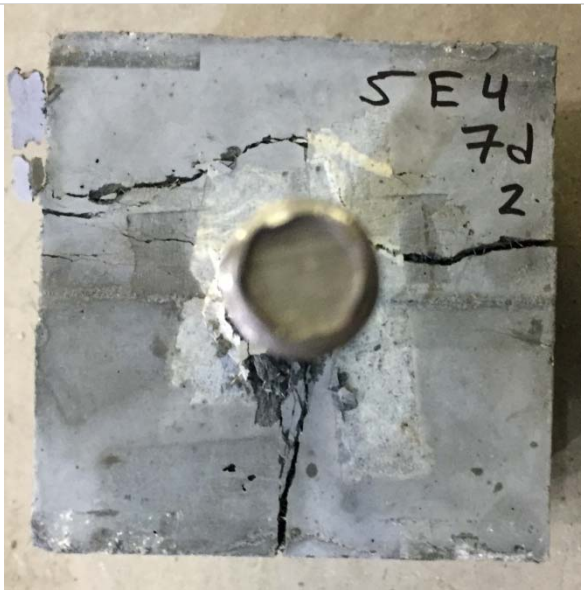

16B-100-2%-T-28D	
Bar Diameter:	#5, Bars (16 mm)
Coating:	Plain
Embedded Length:	4 inches (100 mm)
Fiber Content (% vol.)	2%
Casting Orientation:	Transverse
Curing Age:	28 Days
Test 1	
	
Test 2	
	

Test 3	
	

16E-100-1%-P-28D	
Bar Diameter:	#5, Bars (16 mm)
Coating:	Epoxy
Embedded Length:	4 inches (100 mm)
Fiber Content (% vol.)	1%
Casting Orientation:	Parallel
Curing Age:	28 Days

Test 1

Test 2

Test 3	
	

16E-100-2%-P-28D*	
Bar Diameter:	#5, Bars (16 mm)
Coating:	Epoxy
Embedded Length:	4 inches (100 mm)
Fiber Content (% vol.)	2%
Casting Orientation:	Parallel
Curing Age:	28 Days
Test 1	
	
Test 2	
	

Test 3	
	
*Cast & Tested Same Day as 16E-100-1%-P-28D	

12. APPENDIX D – DETAILS OF BEAM TESTING

This appendix lists detailed photos from the beam testing series as outlined in Chapter 6. The images are listed as assigned by test name and number. Each set contains an images recorded from the actual test, prior to the loading (shown first) as well as at the peak load (shown second). Additionally, an image as seen through the digital image correlation camera is shown (shown third). For the relevant tests, the strain (%) in the bars vs. load (KN) plots is provided (shown last).

F-100-1P-1	
Joint Width:	4 inches (100 mm)
Fiber Content (% vol.)	1%
Loading Scheme:	Pure Flexure

Prior to Test

At Peak Load

Strain Field (DIC)

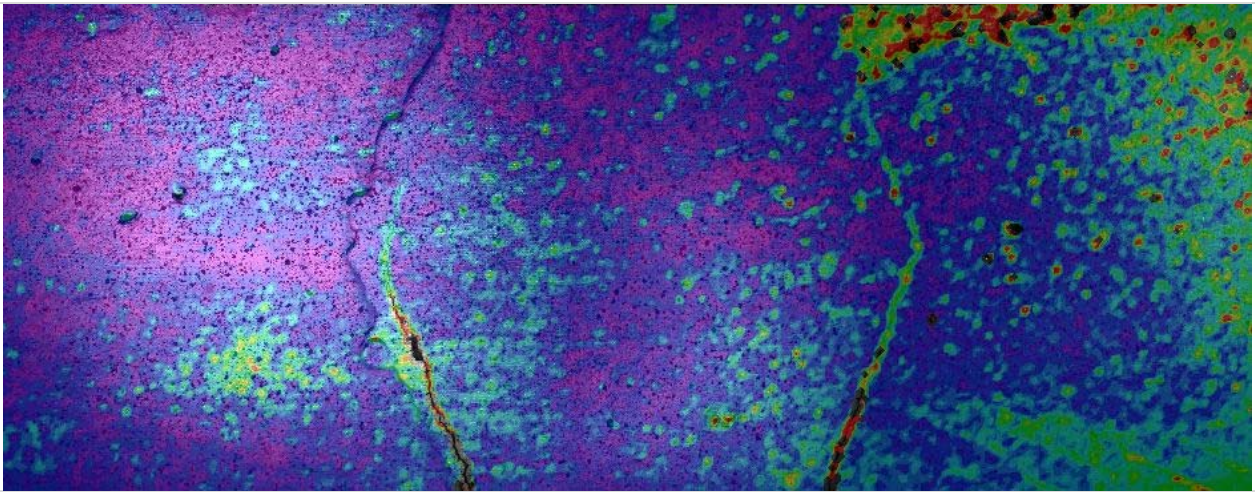

F-100-1P-2	
Joint Width:	4 inches (100 mm)
Fiber Content (% vol.)	1%
Loading Scheme:	Pure Flexure

Prior to Test

At Peak Load

Strain Field (DIC)

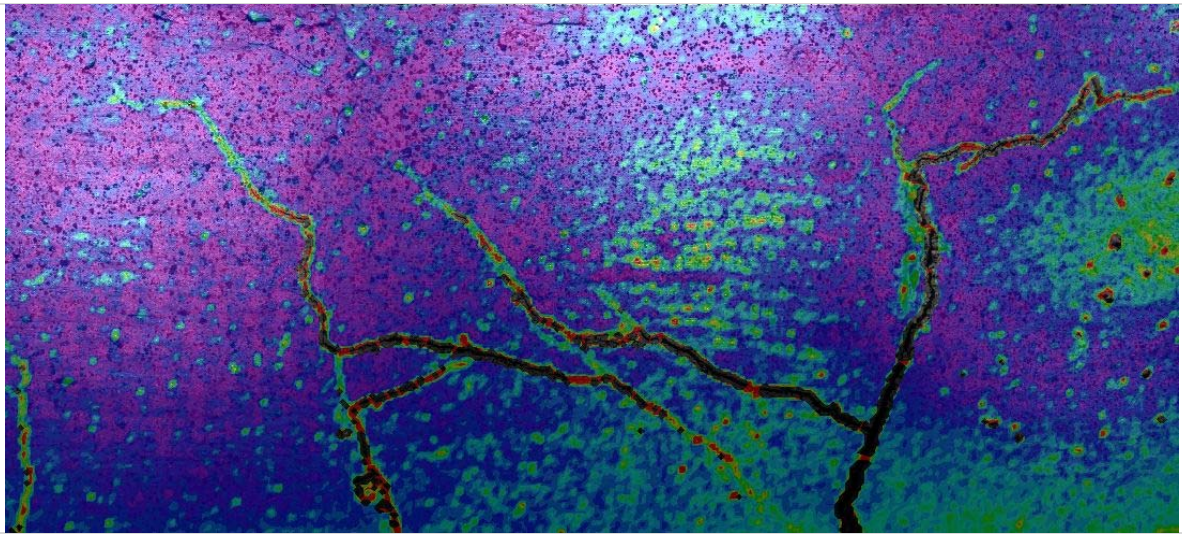

F-100-2P-1	
Joint Width:	4 inches (100 mm)
Fiber Content (% vol.)	2%
Loading Scheme:	Pure Flexure
Prior to Load	
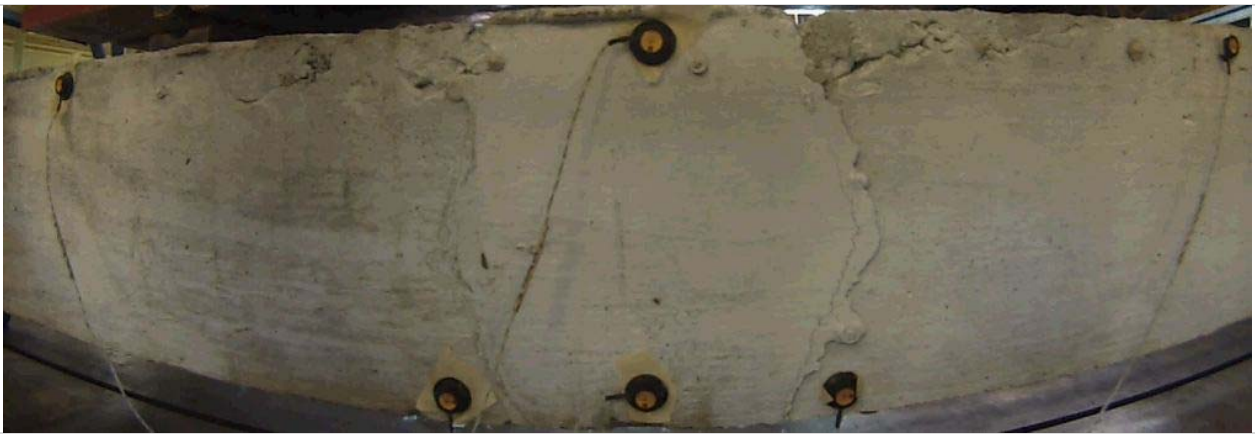	
At Peak Load	
	
Strain Field (DIC)	
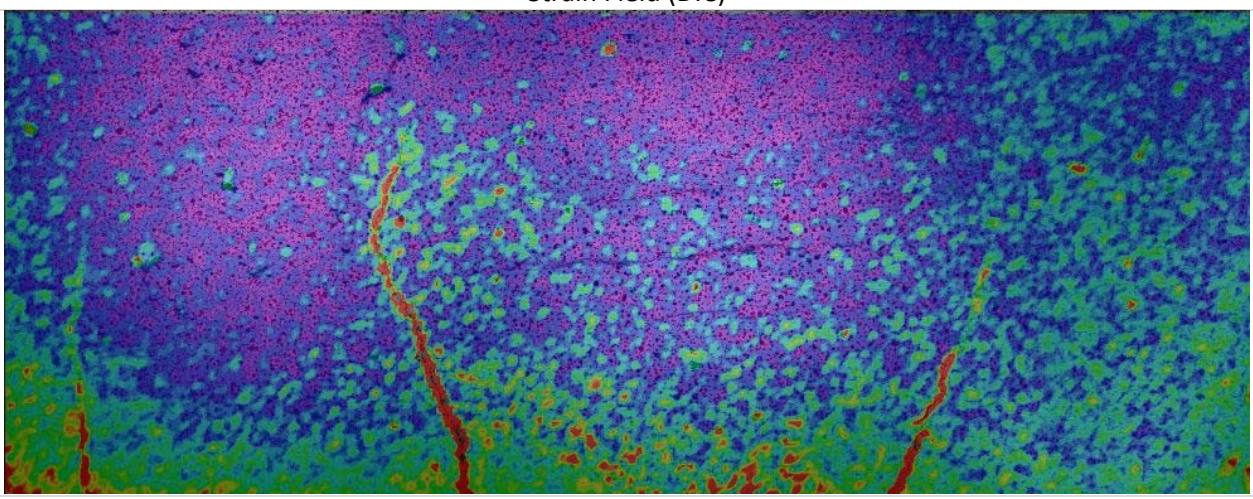	

F-100-2P-2

Joint Width:	4 inches (100 mm)
Fiber Content (% vol.)	2%
Loading Scheme:	Pure Flexure

Prior to Load

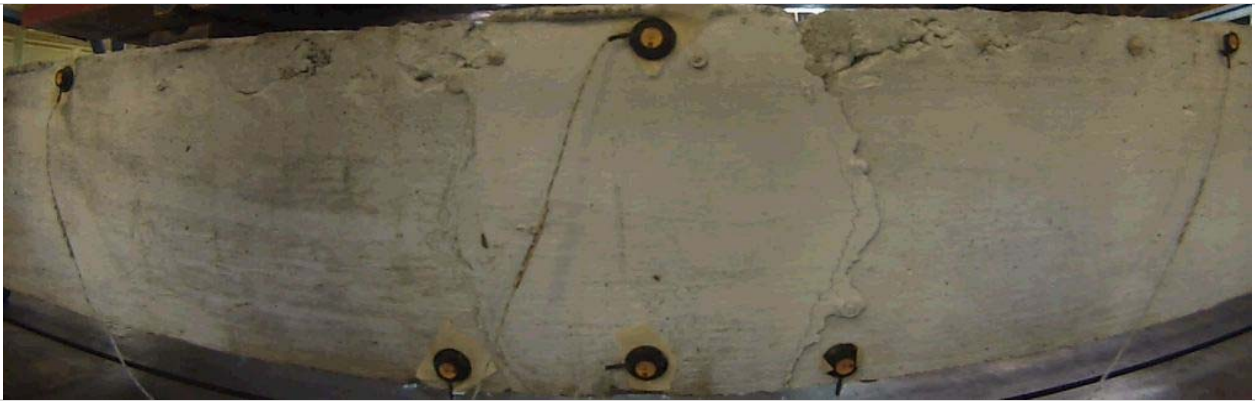

At Peak Load

Strain Field (DIC)

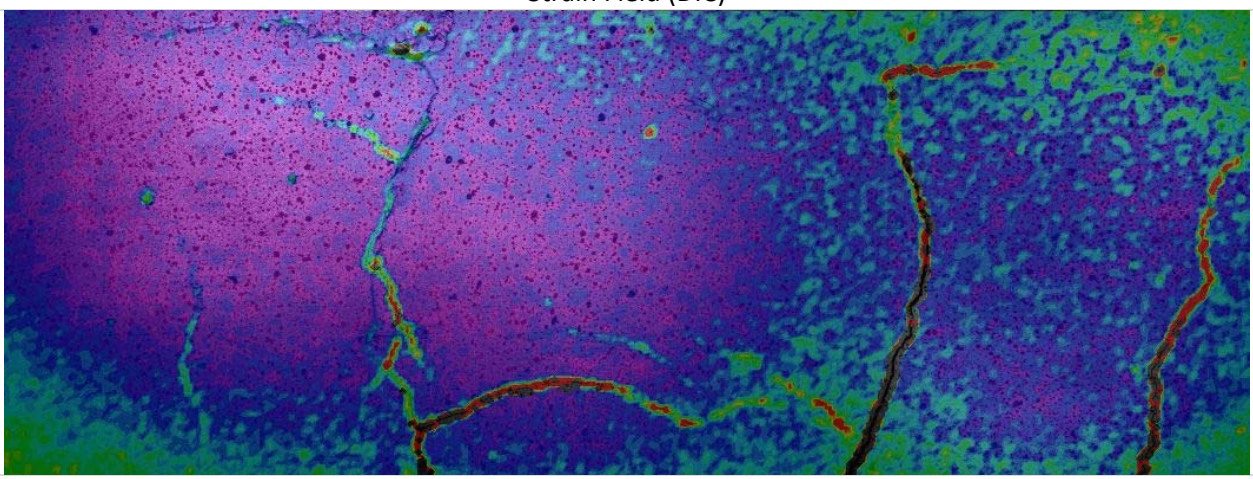

F-150-2P-1	
Joint Width:	6 inches (150 mm)
Fiber Content (% vol.)	2%
Loading Scheme:	Pure Flexure

Prior to Load

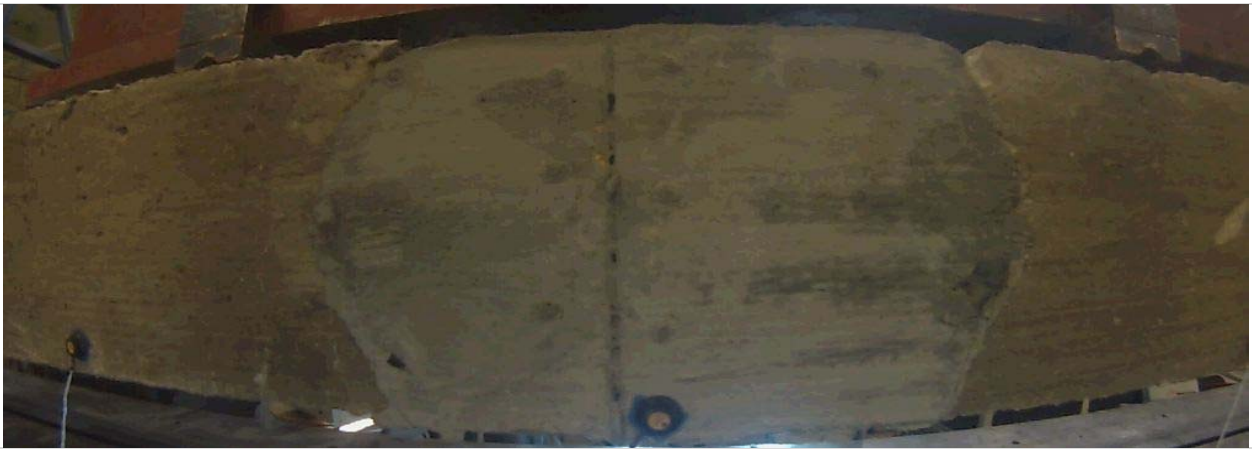

At Peak Load

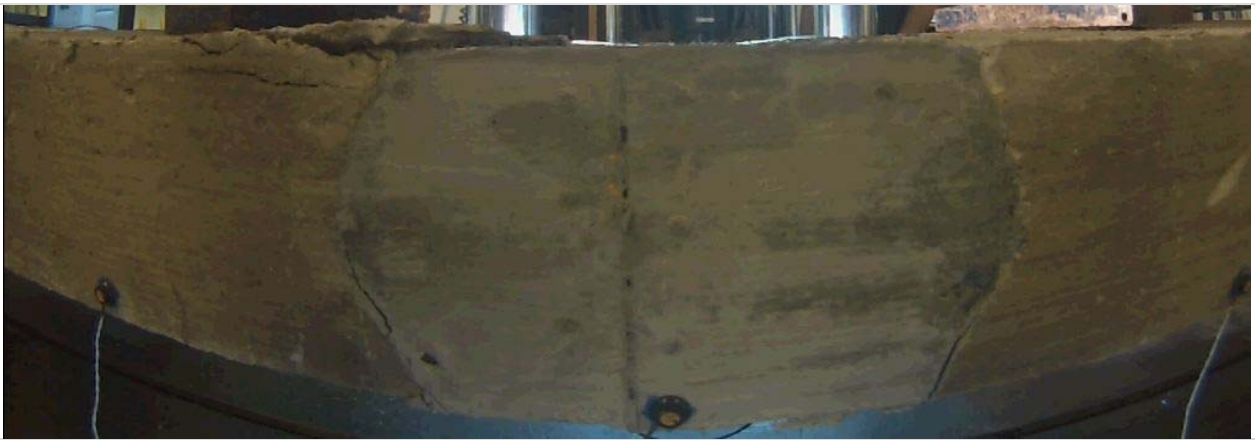

Strain Field (DIC)

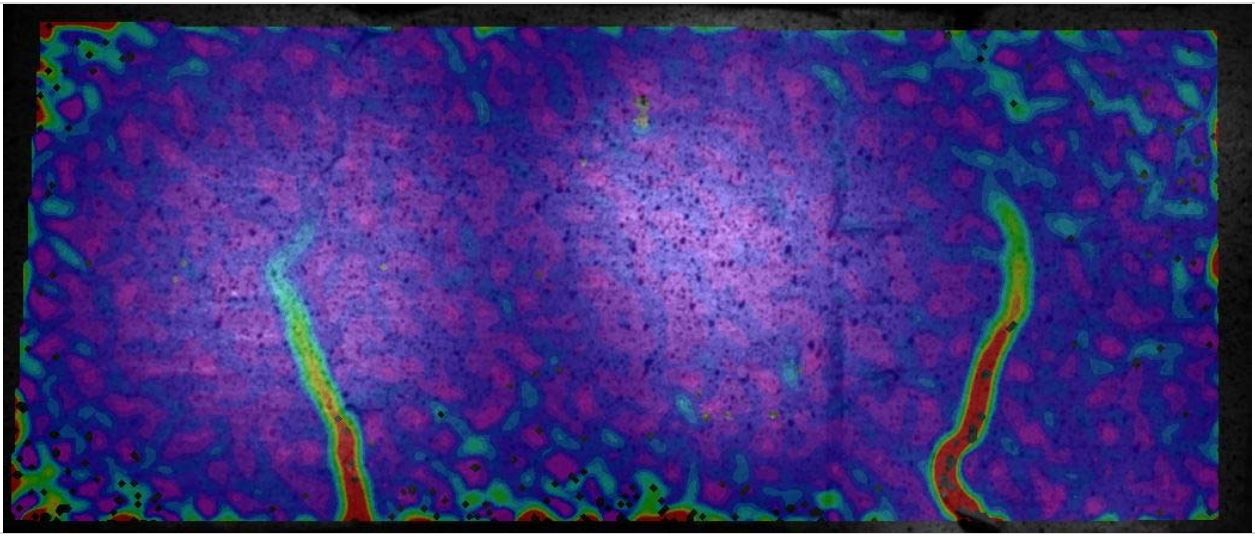

Strain (%) in Bars vs Load (KN)

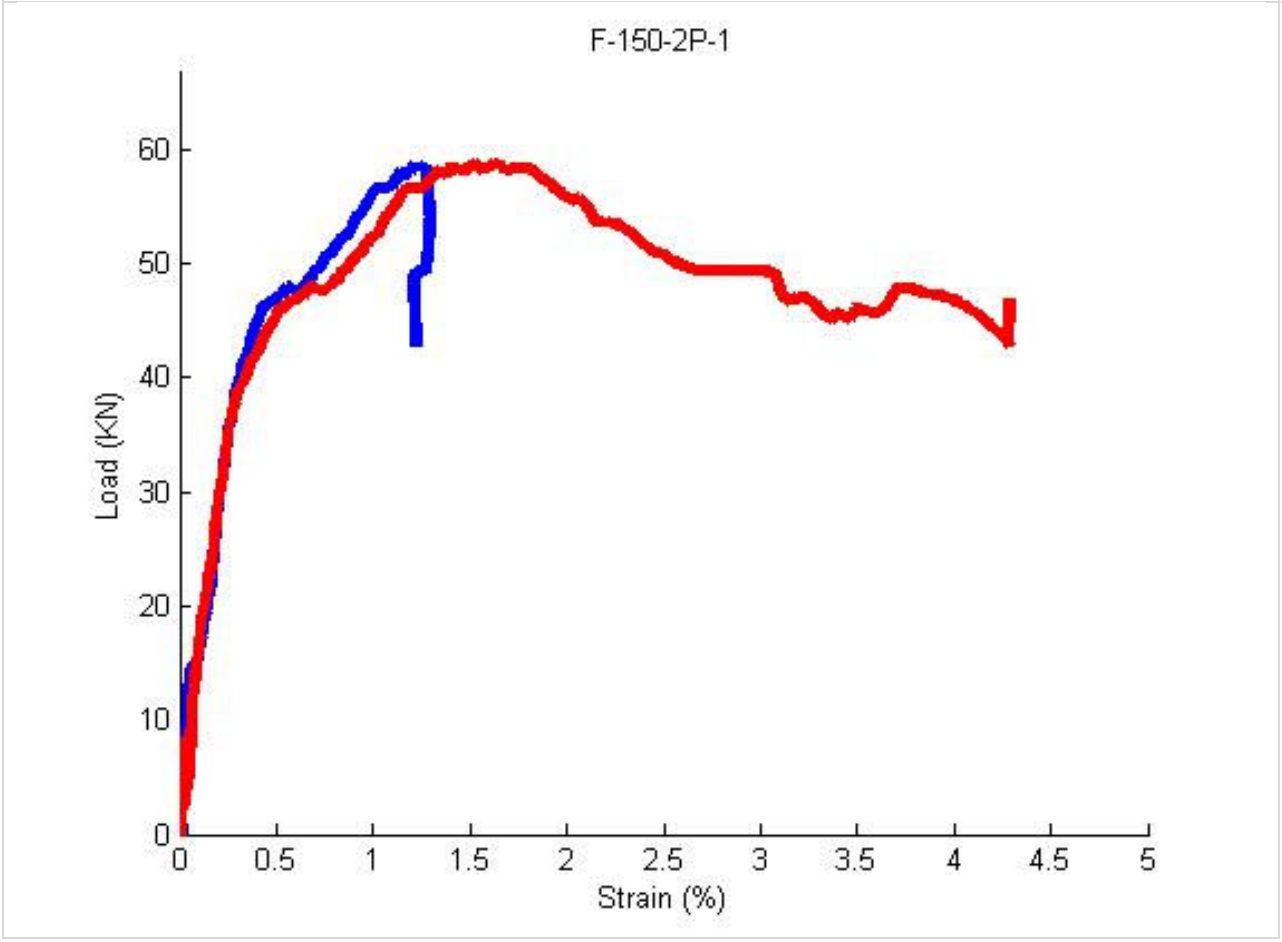

F-150-2P-2	
Joint Width:	6 inches (150 mm)
Fiber Content (% vol.)	2%
Loading Scheme:	Pure Flexure

Prior to Load

At Peak Load

Strain Field (DIC)

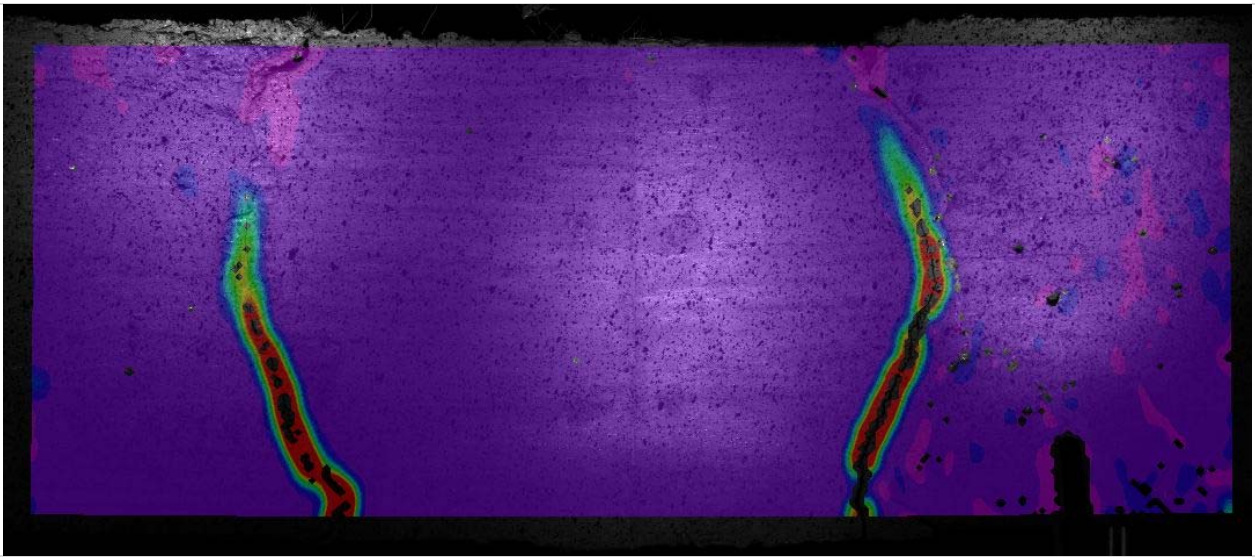

Strain (%) in Bars vs. Load (KN)

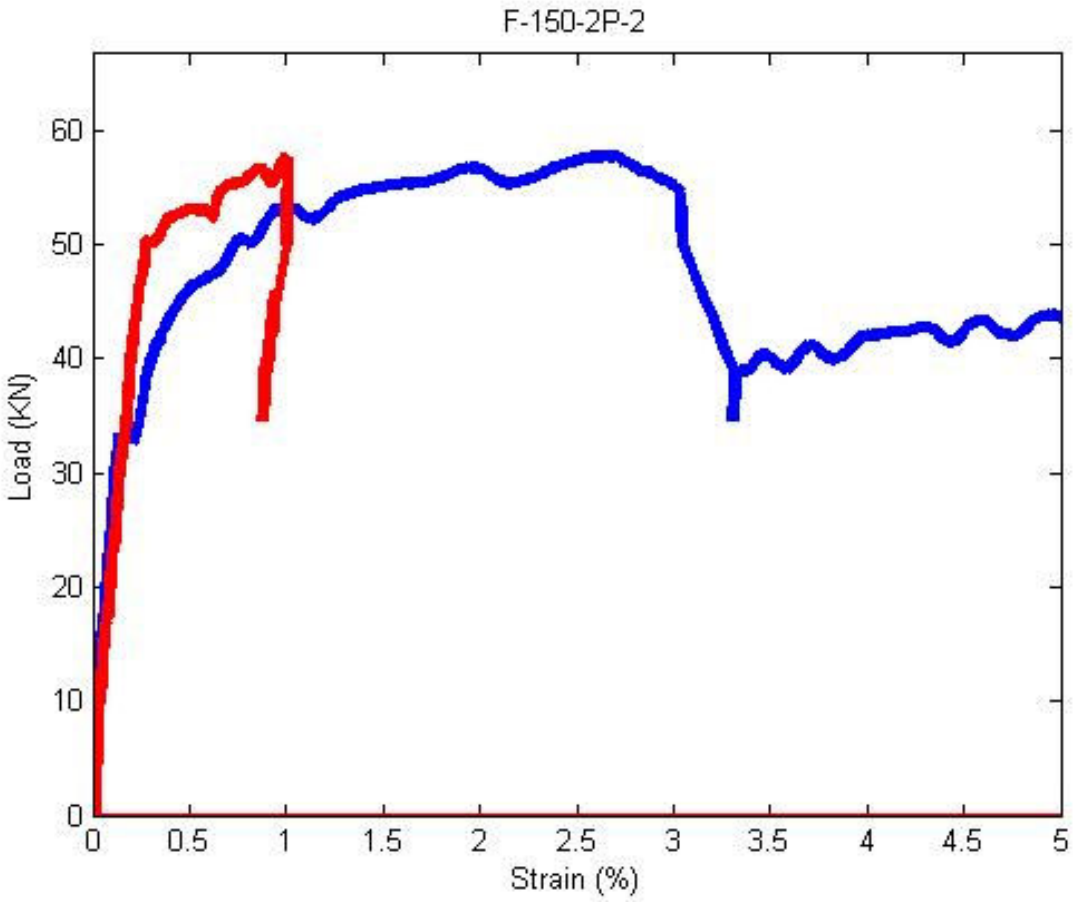

F-200-2P-1	
Joint Width:	8 inches (200 mm)
Fiber Content (% vol.)	2%
Loading Scheme:	Pure Flexure

Prior to Load

At Peak Load

Strain Field (DIC)

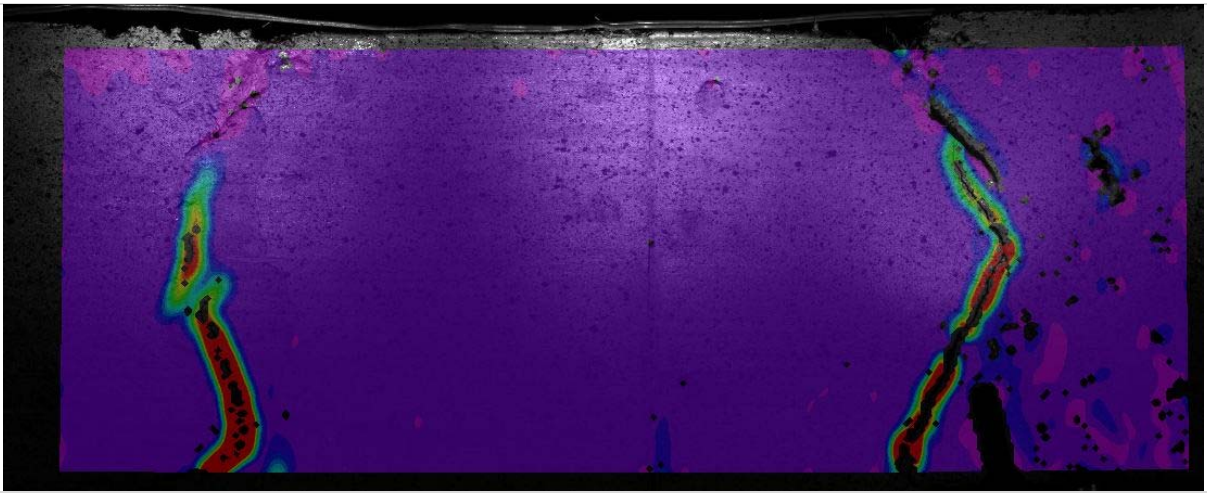

Strain (%) In Bars vs. Load (KN)

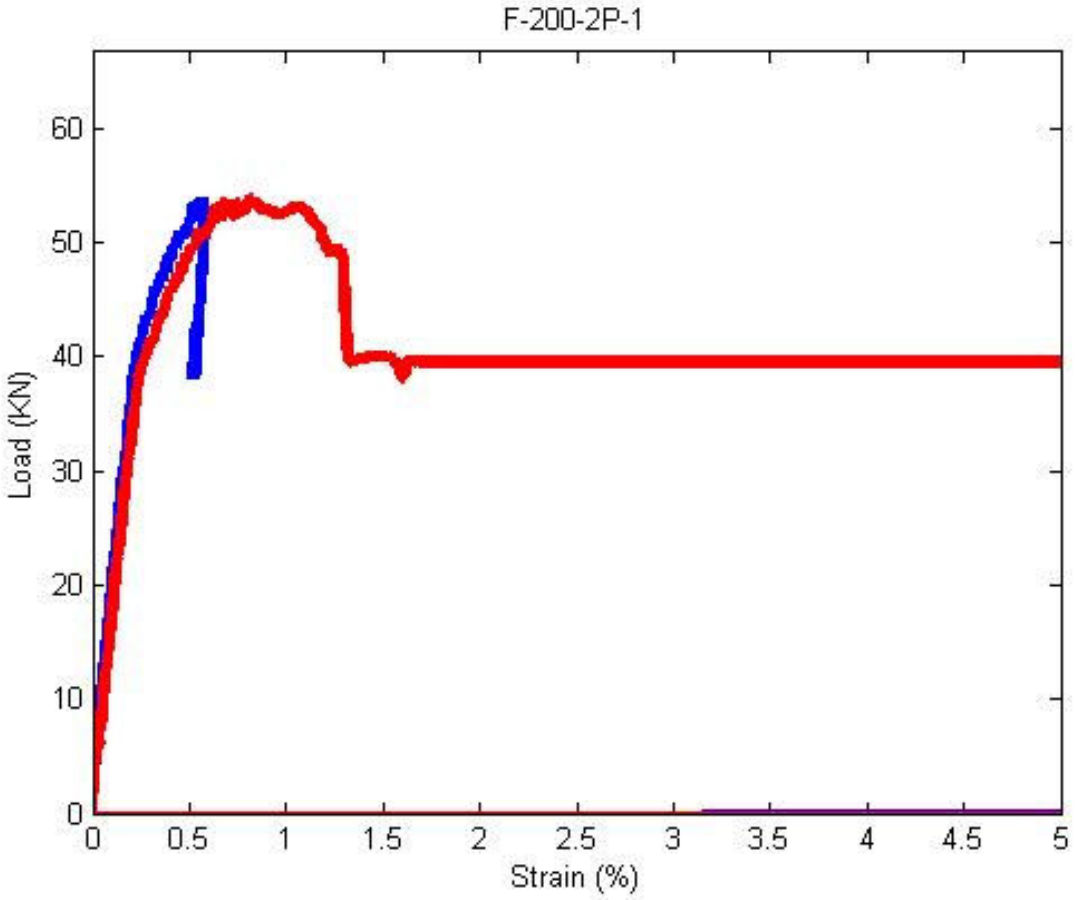

F-200-2P-2

Joint Width:	8 inches (200 mm)
Fiber Content (% vol.)	2%
Loading Scheme:	Pure Flexure

Prior to Load

At Peak Load

Strain Field (DIC)

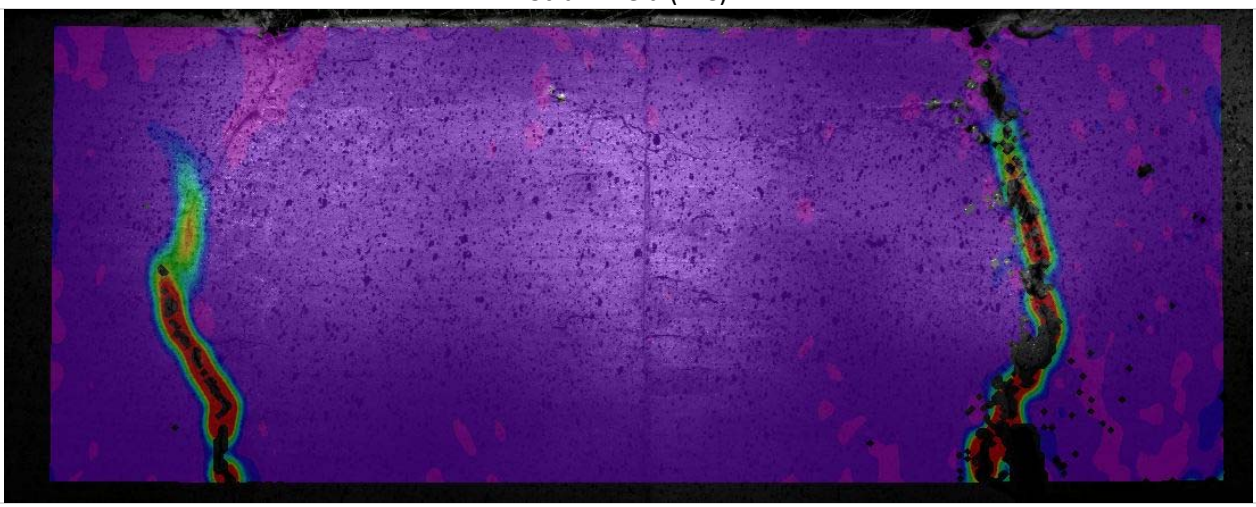

Strain (%) in Bars vs. Load (KN)

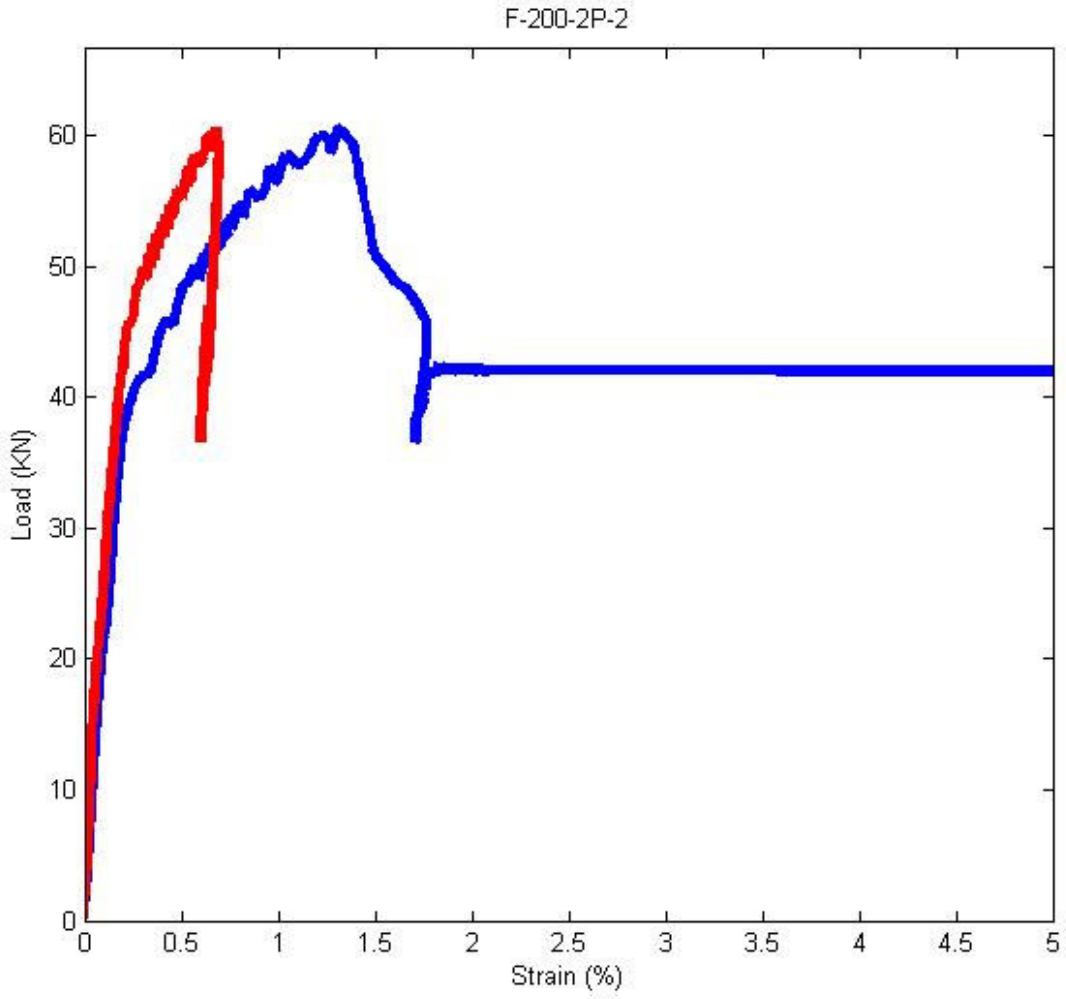

SF-100-1P-1	
Joint Width:	4 inches (100 mm)
Fiber Content (% vol.)	1%
Loading Scheme:	Combined Shear and Flexure

At Peak Load

Strain Field (DIC)

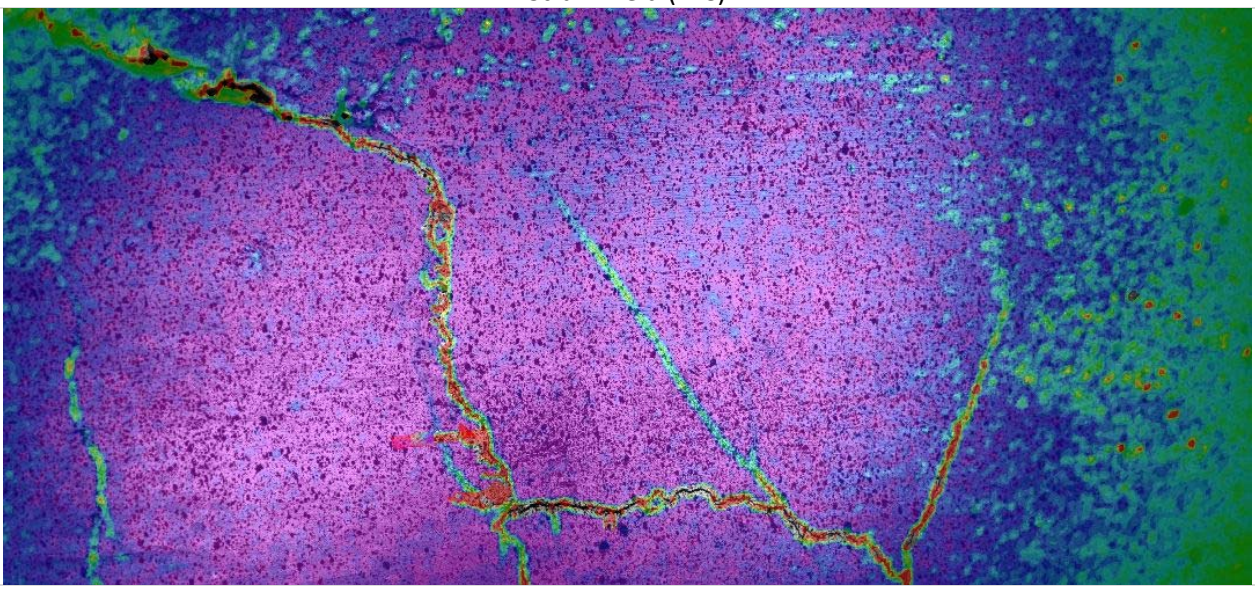

SF-100-1P-2	
Joint Width:	4 inches (100 mm)
Fiber Content (% vol.)	1%
Loading Scheme:	Combined Shear and Flexure

At Peak Load

Strain Field (DIC)

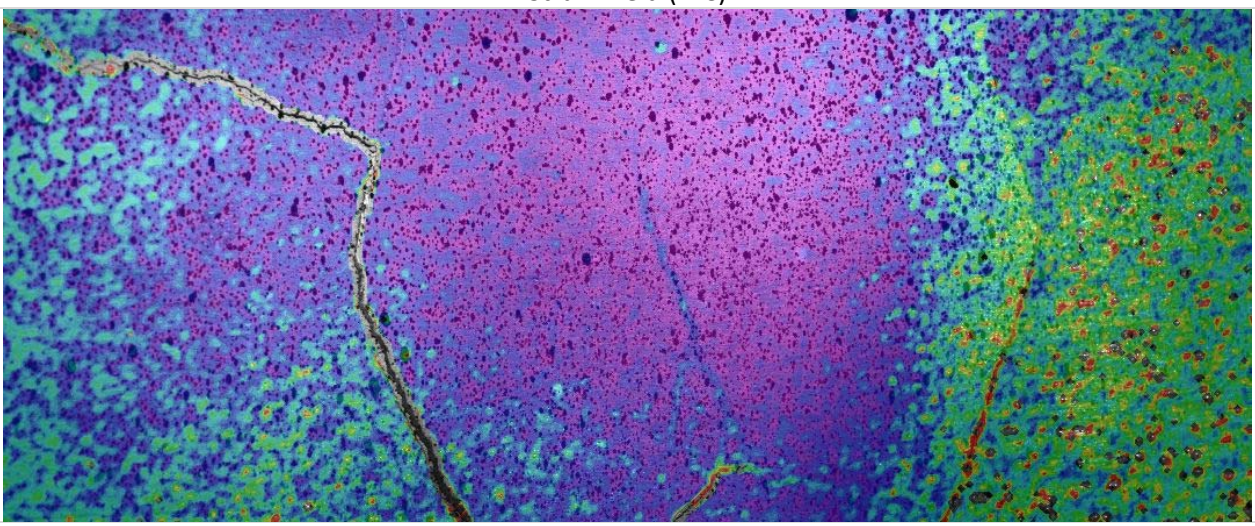

SF-100-2P-1	
Joint Width:	4 inches (100 mm)
Fiber Content (% vol.)	2%
Loading Scheme:	Combined Shear and Flexure

At Peak Load

Strain Field (DIC)

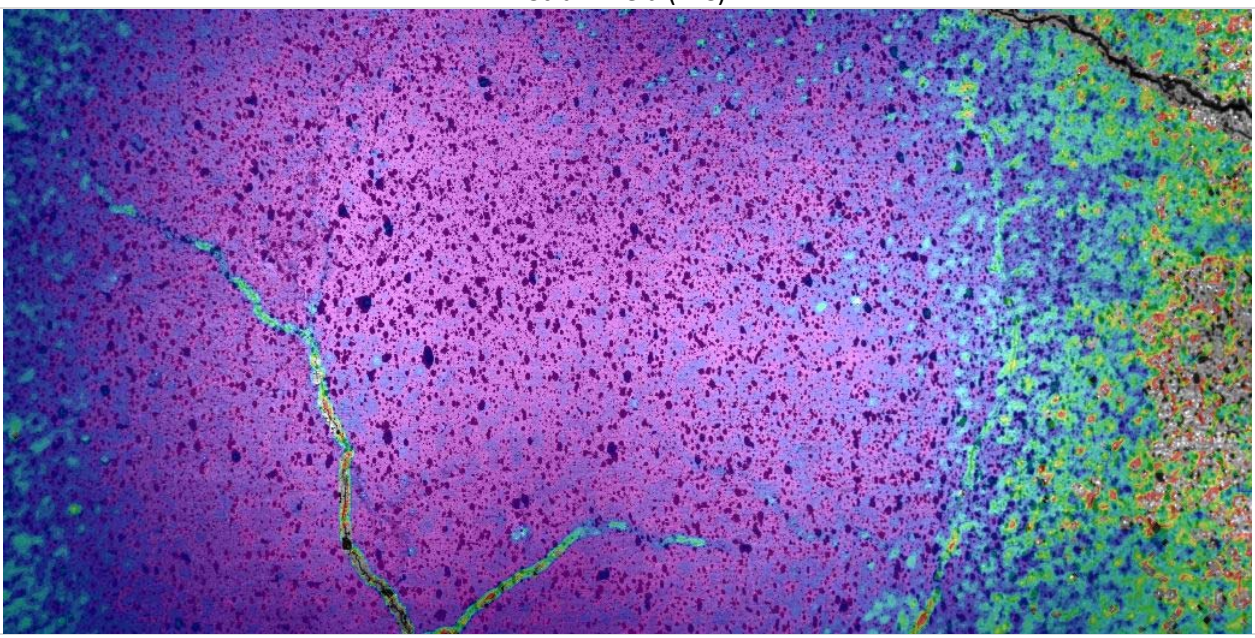

SF-100-2P-2	
Joint Width:	4 inches (100 mm)
Fiber Content (% vol.)	2%
Loading Scheme:	Combined Shear and Flexure
At Peak Load	
	
Strain Field (DIC)	
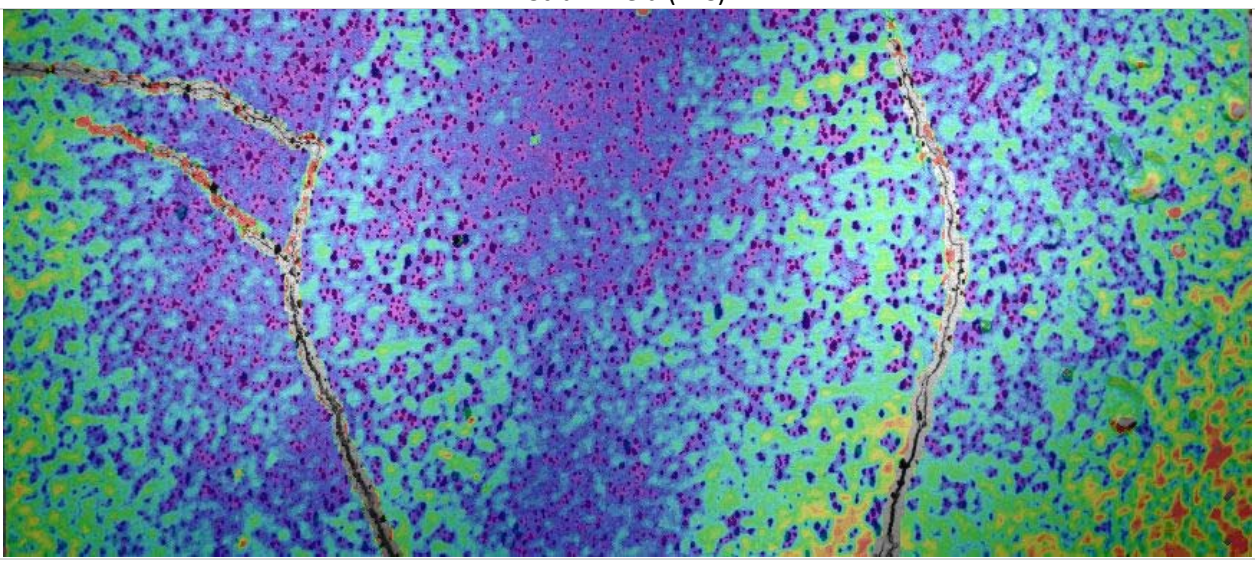	

Intentionally left blank

13. APPENDIX E – SPECIAL PROVISIONS

Special provisions were developed for one of the proposed UHPC blends. The provisions are necessary for MDOT to bid future UHPC projects. The approved provisions are listed in this Appendix.

MICHIGAN
DEPARTMENT OF TRANSPORTATION

SPECIAL PROVISION
FOR
MICHIGAN ULTRA HIGH PERFORMANCE CONCRETE (MI –UHPC) FOR FIELD CAST JOINTS

OFS:SCK 1 of 4 APPR:XXX:YYY:00-00-14

a. Description. This work consists of using Michigan Ultra High Performance Concrete (Mi-UHPC) for field casting of closure pours between precast components. The concrete mixture described in this special provision must be used at locations specified on the plans. All work must be in accordance with the standard specifications, except as modified herein.

b. Materials. The concrete mixture must contain the following materials per cubic yard:

Material	Weight [lb/yd^3]
Cement Blend	
Portland Type I	653
Slag Cement	653
Silica Sand	
Fine Sand[1]	407
Coarse Sand[2]	1629
Silica Fume	327
Water	277
High Range Water Reducer[3,4]	17.6[5]
Steel Fibers[5]	265

[1]US Silica F75
[2]US Silica F12
[3]AdvaCast 575
[4]High range water reducer is applied at the rate of 21.6 oz/cwt
[5]The steel fibers are 2% by volume.

Steel fibers – Steel fibers must be straight with a smooth surface and conform to ASTM A820, Type I fibers. They must have a diameter of 0.008 in and length of 0.75 in, both with a ±5% tolerance, and a minimum tensile strength of 285 ksi.

High Range Water Reducer – use AdvaCast 575. No substitutions are permitted without written approval of the Engineer.

c. Equipment. High shear paddle mixers with 0.5 cyd minimum capacity must be used. Paddle- or scraper-to-pan wall clearance must be small enough to prevent the material being mixed from adhering to the sidewalls. Pumping Mi-UHPC is not permitted.

d. Submittals. Submit the following to the Engineer, at least 21 days before placing for review and approval:

A. Material certifications and manufacturer's published product literature.

B. A quality control plan that must include, but is not limited to, the following:

(1) Mixing protocol.

(2) Casting procedure.

(3) Sampling and testing procedure.

(4) Curing procedure.

(5) Grinding procedure after field placement.

e. Pre-Pour Meeting. Prior to the initial placement of the Mi-UHPC, the Contractor must arrange for an onsite meeting with the Engineer and Construction Field Services. The objective of the meeting will be to clearly outline the procedures for mixing, transporting, finishing and curing of the Mi-UHPC, and to review the trial batch requirements.

f. Trial Batch. Perform one trial batch, a minimum of 21 days before concrete placement, to verify the mixture meets the requirements of this special provision. The trial batch must be attended by the Engineer and Construction Field Services.. The trial batch must be of sufficient size to complete the trial placement. Perform the trial batch under the same ambient conditions (e.g. time of day, weather, etc.) as anticipated during construction. Include documentation of ambient conditions at the time of the trial batch and anticipated ambient conditions at time of trial placement with the submittal to the Engineer.

Trial Placement: Construct a full scale trial batch mix and placement simulating a field cast closure pour full width between precast beams and of sufficient length to use at least the minimum mix capacity of the equipment, including quantities for sampling and testing. The trial placement must use the equipment and the same forming, casting, and curing procedures that will be used during construction. The trial placement must be witnessed by the Engineer and Construction Field Services.

Provide the results of temperature, slump, density (unit weight), 4-day compressive strength, and 7-day compressive strength testing. Each compressive strength test must be conducted according to subsection g.6 of this special provision. Submit the results of all tests above to the Engineer for review and approval a minimum of 10 calendar days prior to the use of the Mi-UHPC in the field .

To be considered a successful trial batch, the compressive strength must meet 12 ksi at 4 days, and 15 ksi at 7 days, and the slump flow must be within the range of 7 to 12 inches.

To be considered a successful trial placement, there must be no segregation of the Mi-UHPC and no visible voids when the forms are removed.

If the trial batch or trial placement does not meet these requirements, discard the material and repeat the trial batch and trial placement at no additional cost to the Department.

g. Construction.

1. Storage. Assure the proper storage of constituent materials, fibers, and additives as required by the manufacturer's specifications in order to protect materials against exposure to moisture and loss of physical and mechanical properties.

2. Temperature Limitations. Do not place concrete at ambient air temperatures below 40 degrees F, nor above 90 degrees F. The top surface of the concrete must be covered with insulating blankets, having a minimum R Value as specified in Table 706-1 of the Standard Specifications for Construction, when the air temperature is below 60 degrees F. Insulating blankets must meet the requirements of subsection 903.07.C of the Standard Specifications for Construction. Leave insulating blankets in place for a minimum 7 calendar days.

3. Mixing Protocol. The following mixing protocol must be followed:

A. Mix silica fume and all sand together for at least 7 minutes.

B. Add cement and mix together for at least another 7 minutes. Do not allow material to cake on the side of the mixer .

C. Add water and HRWR to the mixture and mix for a minimum of 10 minutes.

D. Perform the slump flow test according to subsection e.9 of this special provision. If the slump flow is between 7 and 12 inches, add the steel fibers into the mix. Do not incorporate any Mi-UHPC into the project with slump flow outside the stated range.

E. Mix the steel fibers and cementitious material for at least 5 minutes.

4. Forms: The forms must be water tight and coated to prevent absorption of water. The formwork must be resistant to the hydraulic pressure of the mix.

5. Quality Control. Submit a copy of all quality control records to the Engineer within 24 hours after the date of concrete placement covered by the record.

Use a flow table to measure the slump flow for each batch of Mi-UHPC. Conduct the slump flow test in accordance with ASTM C230/C230M without compacting and without moving or impacting the base plate. Record the slump flow for each batch in the QC records. The slump flow must be within the range of 7 to 12 in. Do not incorporate Mi-UHPC into the project with slump flow outside the stated range.

6. Compression Testing Requirements. Make three sets of compressive strength test samples for each day of placement. Each set consists of three 2x2 inch cubes. All test samples must be cured using the same method of curing as outlined in the quality control plan. The compressive strength tests must be conducted on a minimum of three 2x2 inch cube samples according to ASTM C109.

7. Casting Process: The fresh mix must not be allowed to flow farther than 24 inches during placement. Start the casting process at one end of the joint and proceed to the other end at a speed comparable to the flow speed of the fresh mix. Once the other end of the joint is reached, reverse the casting process and proceed in the other direction to cast another layer

of Mi-UHPC. Continue this process until the full depth of the joint has been cast. Vibrators may not be used.

Fill the joint 0.5 inch higher than the adjacent concrete to allow entrapped air to rise in this zone during curing.

8. Curing. Do not apply curing compound. The concrete surfaces must be continuously cured with wet burlap per subsection 706.03.N.1.b, except that the wet burlap must be applied immediately after casting.

9. Grinding. Grind the Mi-UHPC surface flush with the adjacent concrete surface within ±1/8 inch tolerances. Grinding of the Mi-UHPC surface can be performed after it has attained 12 ksi compressive strength. Suspend grinding operations if significant fiber pullout is observed. Do not resume grinding until approved by the Engineer.

h. Acceptance. The Engineer will sample the Mi-UHPC and test it for 4, 7, and 28 day compressive strength and table slump flow. If the Mi-UHPC achieves a minimum of 12 ksi at 4 days, 15 ksi at 7 days, the table slump flow is within 7 to 12 inches, and Mi-UHPC placement, segregation, and consolidation are acceptable, the Mi-UHPC for each representative placement will be accepted.

i. Measurement and Payment. The completed work, as described, will be measured and paid for at the contract unit price using the following pay item:

Pay Item	**Pay Unit**
Conc, Michigan Ultra High Performance	Cubic Yard

Conc, Michigan Ultra High Performance will be measured in cubic yards based on plan quantities. Payment for **Conc, Michigan Ultra High Performance** includes all labor, equipment, and materials required for the first trial batch, forming, furnishing, testing, placing, finishing, and curing the concrete according to this special provision. No additional compensation will be made for trial batches or trial placements that fail to meet the requirements of this special provision.